Alma Mater Studiorum · University of Bologna

School of Science
Department of Physics and Astronomy
Master Degree in Physics

Fracton phases: analytical description and simulations of their thermal behavior

Supervisor:
Prof. Elisa Ercolessi

Co-supervisor:
Dr. Sunny Pradhan

Submitted by:
Dario Rossi

Academic Year 2020/2021

Abstract

Many-body physics studies the collective behavior of systems with a large number of microscopic constituents. The interaction between the fundamental particles creates a common behavior within the system with emergent excitations exhibiting uncommon characteristics. In three spatial dimensions it has recently been found that a new kind of particles can exist characterized by a fractionalized mobility, being either immobile or mobile only along sub-dimensional spaces: *fractons*.
In this thesis I explore fracton phases focusing on their topological and thermal properties. Fractons can be explained as a generalization of usual topological particles with some fundamental differences, which make fracton order a new field on its own. Fracton models are studied first from the point of view of exactly solvable lattice spin models, focusing on the similarities and differences with usual topological models. Fracton phases are also described through the use of symmetric tensor gauge theory. This gives a theoretical background which is used to explore some possible phases at finite densities of fractons, like Fermi liquids and quantum Hall states.
The thermal properties of such systems are studied in detail through the use of numerical simulations relying on exact-diagonalization. Various correspondences with systems featuring quantum many-body scars are found, in particular with the PXP model. The non-thermal behavior of the models under study is justified by the fragmentation of the Hilbert space in a large number of separated sub-sectors, not related to symmetries of the model. Further, the range of the local Hamiltonian operators is found to be of fundamental relevance in the thermal properties of the system. For certain ranges it is observed that the models are not able to reach the thermal state at long times. Instead, increasing the length of interactions the system becomes ergodic, with the exception of a small number of special eigenstates which remain non-thermal.

Sommario

La fisica a molti corpi studia il comportamento collettivo di sistemi con un grande numero di componenti microscopici. L'interazione fra queste particelle dà luogo a un comportamento comune all'interno del sistema con eccitazioni emergenti dotate di caratteristiche non comuni. In tre dimensioni spaziali è stato scoperto recentemente che può esistere un nuovo tipo di particelle caratterizzate da una mobilità frazionata, in modo tale che esse siano o immobili o mobili solo all'interno di sottospazi sottodimensionali del sistema: i *fractoni*.
In questa tesi esploro le fasi fractoniche focalizzandomi sulle loro proprietà topologiche e termiche. I fractoni possono essere interpretati come una generalizzazione delle conosciute particelle topologiche ma con alcune differenze fondamentali, che fanno dell'ordine fractonico un nuovo campo di studio. I modelli fractonici vengono studiati prima dal punto di vista di modelli di spin su reticolo esattamente risolvibili, focalizzandosi su somiglianze e differenze con i noti modelli topologici. Le fasi fractoniche vengono anche descritte tramite l'uso della teoria di gauge con tensori simmetrici. Questo studio fornisce un background teorico che viene poi utilizzato per esplorare alcune possibili fasi a densità finita di fractoni, come i liquidi di Fermi e gli stati di Hall quantistico.
Le proprietà termiche di questi sistemi sono studiate in dettaglio tramite l'uso di simulazioni numeriche basate sulla diagonalizzazione esatta. Vengono trovate varie corrispondenze con sistemi dotati di "quantum many-body scars", in particolare con il modello PXP. Il comportamento non termico dei modelli studiati viene giustificato con la frammentazione dello stato di Hilbert in un gran numero di sottosettori separati e non associati con le simmetrie del modello. Inoltre, viene trovato che il raggio di interazione degli operatori Hamiltoniani locali è di importanza fondamentale per le proprietà termiche dei sistemi. Per alcuni raggi viene osservato che i modelli non sono in grado di raggiungere lo stato termico a tempi lunghi. Invece, aumentando il raggio delle interazioni il sistema diventa ergodico, ad eccezione di un piccolo numero di autostati speciali che rimangono non termici.

Contents

Introduction

Strongly interacting quantum states of matter have recently been subject of great interest since they exhibit novel and exciting characteristics which could lead the way to new applications of condensed matter systems. An interesting example is that of *Quantum Spin Liquids* (QSL) [1], a class of models consisting of highly-interacting spin systems which exhibit long-range entanglement in the ground state and an exotic excitation spectrum not smoothly connected to the non-interacting limit. The most famous example is Kitaev's Toric Code (TC) model [2], which has gapped electric and magnetic excitations which cannot be created locally and which are mutual semions, i.e. they exhibit anyonic statistic. The TC is the canonical example of a topological phase, in fact it has a 4-fold ground state degeneracy which cannot be lifted by any local operator.
Anyons in the TC are an example of emergent quasiparticles, excitations formed as a collective behavior of many-body systems. These quasi-particles can have many different properties not proper of any fundamental particle, such as anyonic statistical properties different both from fermions and bosons. Another example of quasi-particle is that of Laughlin excitations in Fractional Quantum Hall systems [3], which are characterized by carrying only a fraction of the elementary electric charge.
A new kind of quasi-particle was found recently in looking for constrained spin models. This excitation has the characteristic of having a fractionalized mobility, being either immobile or able to move only on sub-dimensional spaces. This new kind of excitation was named *fracton*. The subject of this thesis are indeed fracton phases [4, 5]. These where first found [6] by looking for solvable examples of many-body Hamiltonians of systems that, as the environment temperature decreases to absolute zero, are unable to reach their ground states. Later on they were found again by Haah [7] in looking for quantum stabilizer codes without string logical operators, i.e. solvable lattice models with fundamental excitations unable to move freely around the lattice. The purpose of this investigation was the research of quantum systems which could serve as recipients for quantum memories. Since the discovery of fracton phases it has been their major hypothesized application. But it was just with the work of Vijay, Haah and Fu [8] that these peculiar phases were identified as a new class of topological order, *fracton order*. Fracton topological order exhibits novel properties not shared with usual topological

order: a sub-extensive ground state degeneracy*, a particle content characterized by kinetic restrictions, featuring immobile or sub-dimensional excitations, and a duality to spin systems with sub-system symmetries [8, 9].
A breakthrough came with the work of Pretko [10] who recognized how to describe fracton phases through the use of gauge theory. Usually the gauge field degrees of freedom are taken to be the components of a vector field, like the usual vector potential of electromagnetism. Actually, there is no reason why the emergent gauge variable should not be a more complicated object like a generic rank-k tensor. However, it has been shown [11] that higher-form (antisymmetric tensors) gauge fields do not describe any new QSL in $3+1$ dimensions. Interestingly, it has been found that in the case of *symmetric* tensor gauge theories the panorama of possible stable theories in 3D is much richer. These symmetric gauge fields describe new stable gapless QSL in three dimensions. The new phases are similar to vector gauge theories regarding the gapless gauge modes but are significantly different in the particle structure, hosting excitations that are either immobile (the *fractons*) or mobile only along lower-dimensional subspaces. In this case the restrictions in the motion of fundamental particles emerge as generalized Gauss' laws imposing the conservation not just of charge but also of higher moments (like dipole moment).
The generalization of fracton phases to the framework of gauge theory has lead to many interesting phenomena involving fractons [12] and has pointed out the connection of these exotic particles to other fields of physics, like gravitation and elasticity [13, 14]. Nevertheless, the most active field of study involving these particles is centered around the thermal properties of these systems. The kinetic restrictions naturally lead to a slow relaxation process [15] which is characteristic of quantum glasses [16]. Because of these hints about the possible breaking of ergodicity in fracton models, the problem has been analyzed in deep. In particular, the thermal behavior of $1D$ spin chains respecting higher momentum conservation laws has been studied [17]. This is found to be in great analogy with recent experiments on Rydberg atoms [18]. The results are obtained through numerical simulations involving the dynamical evolution of the system and exact-diagonalization.
Let us go through the content of the chapters. First, in chapter 1 some exactly solvable models featuring topological order are analyzed. The TC is used as the prototypical example to show differences and similarities between systems with usual topological order and fracton order. In particular, we analyze in detail the X-Cube model in its particle sector to show the kinetic restrictions which make fracton models so peculiar. In chapter 2 we move on to the description of fracton phases through the use of symmetric tensor gauge theory, introducing a generalized theory of electromagnetism in analogy to usual vector $U(1)$ gauge theory. The issues on the stability of such theories are also taken in consideration. With the full set of generalized Maxwell equations we then mention

*In usual topological order the ground state degeneracy is a constant, which depends on topology.

some possible different phases at finite densities of fractons and fractonic dipoles that can appear. In particular, we analyze: (i) the microemulsion behavior of a finite density of fractons in $3D$, (ii) a finite density of fermionic dipoles in $3D$ exhibiting the characteristics of a Fermi liquid and (iii) the phase relative to a finite density of fermionic dipoles in $2D$ leading to a generalized quantum Hall effect on the boundaries.
In the second part of the thesis we change paradigm and, starting from the kinetic restrictions characteristic of fractonic particles, we study the dynamical behavior of such phases and their approach to equilibrium. In particular, in chapter 3 we review the Eigenstate Thermalization Hypothesis with its main consequences for thermal systems. Also, in this chapter the PXP model is introduced and studied in order to have a basis for comparison to refer to in the numerical simulations of the last chapter. The PXP model has been considered since it also features kinetic constraints and it has been found to host quantum many-body scars, which imply a difficulty of the system in reaching the thermal state. Finally, in chapter 4 the behavior of $1D$ spin chains featuring fractonic behavior through Hamiltonians conserving both charge and dipole moment has been studied in deep. Through numerical simulations, it is possible to observe that in some cases the system fails in thermalizing, thus showing non-ergodic behavior. This trend is observed to be strongly related to the range of interactions in the local Hamiltonian, with longer range systems showing a behavior reminiscent of many-body scars' systems, with a small number of non-thermal eigenstates violating the eigenstate thermalization hypothesis.

Chapter 1

Fracton spin models

Fracton models are a generalization of usual topological spin models, with the characteristic of having kinetic restrictions which limit the mobility of elementary charges. These models where first studied in [6] by looking at solvable models which fail in reaching the ground state when lowering the temperature to absolute zero. The same kind of excitations were found later [7] in looking for exactly solvable spin models without string logical operators which could move the particles around the lattice. Finally, these models have been categorized as a new state of matter [8] and dubbed fractons because of their intrinsic fractionalized mobility. Fracton models defined in exactly solvable lattice spin systems constitute the so-called gapped fracton phases. It has been just later with [10] that it was found these models could be described through the use of symmetric tensor gauge theory. These theories admit a gapless gauge field and thus are called gapless fracton phases. This field theoretic description gives a meaningful insight into fracton models and has lead to a deeper understanding of these exotic phases of matter. Let us mention that a way has been found [19, 20] to pass from a gapless to a gapped fracton theory through the breaking of the continuous symmetry of the former down to a discrete subgroup (Higgs mechanism), but it will not be considered in this thesis.
In this chapter we focus on gapped fracton phases and on their relationship with usual topological spin models. In particular, in Sec. 1.1 we will describe the Toric Code (TC) model as the prototypical example of topological spin system, emphasizing its gauge description and the topological properties. We will then use the TC to introduce the prototypical example of exactly solvable fracton spin model, the X-Cube model, in Sec. 1.2. We will see how the X-Cube model exhibits fundamentally different characteristics from usual topological systems, in particular in the particle content of the theory.

1.1 Toric Code

Topological Order is a new concept that describes quantum entanglement in many-body systems. To have an intuition about it we can use the description given in [21] using dancing rules. In symmetry breaking orders every elementary particle dances by itself, and they all dance in the same way (implying a long range order). A topological order instead is characterized by a global dance, where every particle is dancing with every other particle in a very organized way. In fact, all particles dance following a set of local rules trying to lower the energy of a local Hamiltonian and if all the particles follow these rules then they will form a global dancing pattern which correspond to the topological order.
In particular, quantum phases of matter are said to have topological order when they have (i) an excitation gap, (ii) exhibit degenerate ground states on topologically non-trivial manifolds (like the torus) that cannot be distinguished by any *local* measurement and (iii) support excitations that can be localized in space but cannot be created by local processes.
Let us focus on two dimensions and consider a square lattice which can possibly be embedded in an arbitrary 2-D surface. The simplest example consists in an $N \times N$ square lattice on which we can impose periodic boundary conditions (PBC) by wrapping it around the two-torus (T^2). Then let us denote the set of links in the lattice $\mathscr{L}$ and define on each link a bi-dimensional Hilbert space $\mathscr{H}_i$ so that the model's Hilbert space will be $\mathscr{H} = \bigotimes_{i\in\mathscr{L}} \mathscr{H}_i$. For clarity, in this lattice there are $2N^2$ links, N^2 vertices and N^2 plaquettes.

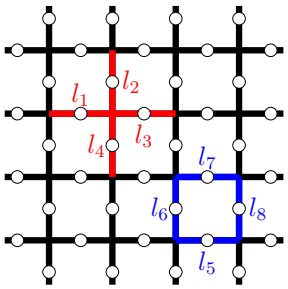

Figure 1.1: *Stabilizer operators of the Toric Code. Vertex operators (red links) consist in the four spins on the links touching the vertex. Plaquettes operators (blue links) instead involve the four spins on the links surrounding a plaquette.*

Consider now the operators in Fig. 1.1, the vertex one

$$A_v = \prod_{l\in star(v)} \sigma_l^x = \sigma_{l_1}^x \otimes \sigma_{l_2}^x \otimes \sigma_{l_3}^x \otimes \sigma_{l_4}^x \tag{1.1}$$

and the plaquette one

$$B_p = \prod_{l \in \partial p} \sigma_l^z = \sigma_{l_5}^z \otimes \sigma_{l_6}^z \otimes \sigma_{l_7}^z \otimes \sigma_{l_8}^z \tag{1.2}$$

where σ_l's are the usual Pauli operators acting on the link l. Operators A_v act non-trivially on the four spins around the vertex v, forming a star. Instead, the operators B_p act on the spins surrounding the plaquette p, i.e. the links defined on the boundary ∂_p of the plaquette. They are both local operators in the sense that they act non-trivially only on a small number of spins of the lattice. Pauli operators acting on different sites always commute while they respect their commutation relations when acting on the same link, i.e.

$$\{\sigma_l^x, \sigma_l^z\} = 0 \tag{1.3}$$

From these relations we see that the operators A_v and B_p always commute (both among themselves and between each other). This is clear since an A_v and a B_p always share either 0 or 2 links, as in Fig. 1.2.

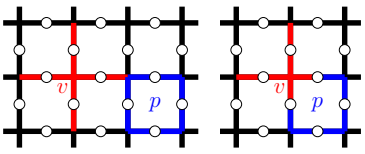

Figure 1.2: *Vertex (red links) and plaquette (blue links) operators always share either* 0 *(on the left) or* 2 *(on the right) links, thus they always commute.*

Also, since they are made of Pauli operators, they satisfy the relation $A_v^2 = B_p^2 = \mathbb{1}$. So, if we impose PBC on the lattice, by applying A_v, B_p on the whole lattice we see that

$$\prod_{v \in \mathscr{L}} A_v = \mathbb{1} = \prod_{p \in \mathscr{L}} B_p \tag{1.4}$$

Let us specify that $\mathscr{L}$ will denote the set of links, vertices or plaquettes of the lattice depending on the case, which will be clear from the context.
These are the only two non-trivial relations we can write for these operators, so the code will have dimension

$$2^{2N^2-(2N^2-2)} = 2^2 \tag{1.5}$$

which means that it encodes two logical qubits into $2N^2$ physical qubits. This is at the basis of the so-called error correcting codes [22], of which the TC is the prototypical example.

1.1.1 Ground State

Let us define now the Hamiltonian of our model as

$$\mathcal{H}_{TC} = -J_e \sum_{v \in \mathscr{L}} A_v - J_m \sum_{p \in \mathscr{L}} B_p \tag{1.6}$$

Since we saw that all terms commute, this Hamiltonian can be diagonalized in the basis of the eigenstates of the A_v, B_p operators, therefore it can be exactly solved (i.e. we can find the ground state (GS) and the excitations). To obtain the GS we need to maximize the eigenvalues of A_v, B_p (which can be ± 1 since the operators are nilpotent). Thus, we look for states such that

$$A_v \left|\psi_0\right\rangle = \left|\psi_0\right\rangle \quad \forall v \in \mathscr{L} \tag{1.7a}$$
$$B_p \left|\psi_0\right\rangle = \left|\psi_0\right\rangle \quad \forall p \in \mathscr{L} \tag{1.7b}$$

In this way the GS will have an energy $E_0 = -N^2(J_e + J_m)$. Equation (1.7b) is called *vortex free* condition and it means that the links of a generic plaquette are in one of the eight possible configurations reported in Fig. 1.3 where there are an even number of $|1\rangle$

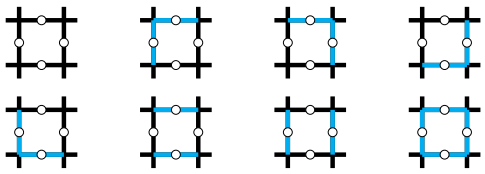

Figure 1.3: *The possible configurations of a single plaquette in the ground state are those involving an even number of* $|0\rangle$ *and* $|1\rangle$ *states. Black (blue) links represent the* $|0\rangle$ *(*$|1\rangle$*) states.*

(and $|0\rangle$) states. This because, by considering to work in the z-basis, B_p is made of σ_l^z and so the eigenvalues can be only ± 1. Then, we know that σ_l^x swaps the states, which means that A_v will swap all the links connected to that vertex. In this sense A_v can

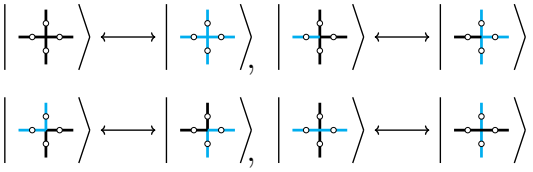

Figure 1.4: *Gauge equivalent configurations obtained by applying the vertex operator* A_v*.*

be understood as a local gauge transformation and states connected by A_v are gauge equivalent. Some examples are shown in Fig. 1.4.

Following these considerations we can find the exact form of the GS. From the vortex free condition

$$|\psi_0\rangle = \sum_{|s\rangle \; s.t. \; B_p|s\rangle=|s\rangle \forall p} t_s \, |s\rangle \tag{1.8}$$

(s is one of the eight possible configurations considered above), and from the condition (1.7a) we see that two configurations related by A_v have the same weight, so all t_s's are equal. Finally, we found that a GS of the Toric Code is an equal weight superposition of vortex free configurations.
More explicitly we can write the GS as

$$|\psi_0\rangle = \prod_{v \in \mathscr{L}} \frac{1}{\sqrt{2}} (\mathbb{1} + A_v) \otimes_{l \in \mathscr{L}} |0\rangle_l \tag{1.9}$$

By using the property $A_v(\mathbb{1} + A_v) = \mathbb{1} + A_v$, it is easy to check that condition (1.7a) is satisfied. Also the flux free condition is respected since $[A_v, B_p] = 0$ and $\sigma^z |0\rangle = |0\rangle$.
Let us now see how different local operators affect this GS. We can create local operators

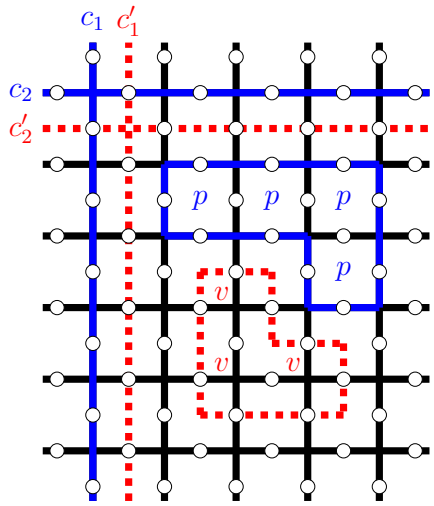

Figure 1.5: *Possible loop operators in the Toric Code. Contractible loops can be written as products of vertex/plaquette operators. Non-contractible loops distinguish the degenerate ground states.*

by taking products of $\sigma_l^{z/x}$ over closed paths in the direct/dual lattice as in Fig. 1.5. Indeed, the same A_v and B_p operators can be seen as loop operators of this kind over the simplest loops. It is easy to observe that such loop operators, if defined over contractible loops, are equivalent to products of A_v/B_p operators over the vertices/plaquettes contained in the loop, and so they do not modify the GS. We can thus consider the GS $|\psi_0\rangle$ as a *Loop Gas*, i.e. a state containing all possible combinations of loops in the lattice.

However, if we consider operators defined over non contractible loops (imposing PBC) of the torus, this identification no longer holds so in principle they can modify the GS. In fact, let us consider the two possible non contractible loops on the torus in the direct lattice (c_1 and c_2) and in the dual lattice (c_1' and c_2'), as reported in Fig. 1.5. The corresponding loop operators (called Wilson loops) are

$$Z(c_{1,2}) = \prod_{l \in c_{1,2}} \sigma_l^z \tag{1.10a}$$

$$X(c'_{1,2}) = \prod_{l \in c'_{1,2}} \sigma_l^x \tag{1.10b}$$

It is easy to check that $[X(c'_{1,2}), A_v] = 0$ and holds as well that $[Z(c_{1,2}), A_v] = 0$, since any A_v intersects the loops $c_{1,2}$ in either 0 or 2 sites. Consider now the action of $X(c_1')$ on the GS $|\psi_0\rangle$

$$X(c_1') |\psi_0\rangle = \prod_{v \in \mathscr{L}} \frac{1}{\sqrt{2}} (\mathbb{1} + A_v) \otimes_{l \notin c_1'} |0\rangle \otimes_{l \in c_1'} |1\rangle = |\psi_1\rangle \tag{1.11}$$

This is indeed still a GS because it is invariant under the action of A_v and of B_p (the latter coming from the fact that B_p acts trivially on plaquettes not crossed by c_1' and for those crossed, since c_1' is a loop in the dual lattice it will necessarily cross exactly 2 edges). Note that also $|\psi_1\rangle$ is a Loop Gas. We can proceed in the same manner for $|\psi_2\rangle = X(c_2') |\psi_0\rangle$ and $|\psi_{1,2}\rangle = X(c_1')X(c_2') |\psi_0\rangle$. Finally, we have in total 4 degenerate GS, which cannot be distinguished by any local parameter*. In general, the number of homotopically inequivalent non-contractible loops is what gives the so-called ground state degeneracy (GSD), which is GSD=4^g for a genus g surface [2].

1.1.2 Excitations

To talk about the excitations of the TC we need to brake some of the constraints (1.7) of the GS. Elementary excitations in fact consist of eigenstates of the Hamiltonian such that some A_v/B_p have changed their eigenvalue from $+1$ to -1. Consider for example the state in which a σ_l^z acts on the GS, as in Fig. 1.6,

$$|\psi_l^z\rangle = \mathbb{1} \otimes \cdots \otimes \sigma_l^z \otimes \mathbb{1} \ldots \mathbb{1} |\psi_0\rangle \tag{1.12}$$

The eigenvalue of A_{v_1} and of A_{v_2} (where v_1 and v_2 are the vertices touching l) is now -1, in fact

$$A_{v_{1/2}} |\psi_l^z\rangle = A_{v_{1/2}} \sigma_l^z |\psi_0\rangle = -\sigma_l^z A_{v_{1/2}} |\psi_0\rangle = - |\psi_l^z\rangle \tag{1.13}$$

*In fact operators over non-contractible loops are non-local.

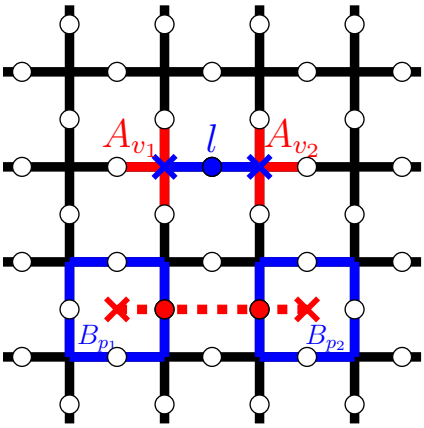

Figure 1.6: *Excitations in the TC. Above: two vertex excitations (charges) are created by the application of a σ^z on the link connecting them. Below: two plaquette excitations (fluxes) created by the application of two σ^x's on the dual-lattice path connecting the plaquettes.*

This means that the Pauli operator σ_l^z creates two excitations at the vertices v_1 and v_2. We can generalize this effect for a *string operator* of σ_l^z's along an open path in the direct lattice (called Wilson line): this will create two excitations, called *charges*, at the ends of the string. Charges will be denoted with e.
It is straightforward to generalize this procedure for σ_l^x's. By applying a string operator of σ_l^x's, taken over an open path on the dual lattice, results in a change of the eigenvalue of B_{p_1} and B_{p_2} on the two plaquettes at the end of the path, as shown in Fig. 1.6. These excitations are called *fluxes* and will be denoted with m.
In both cases the relevant part of the string operators creating the excitations are just the ends, not the "bulk". Let us now study deeper the excitations by finding their statistical properties and their fusion rules. It is easy to see that both charges and fluxes behave as $\mathbb{Z}_2$ charges: in fact by connecting the ends of two paths (and thus fusing excitations) of the same type they annihilate, i.e.

$$e \times e = 1 \qquad m \times m = 1 \tag{1.14}$$

There is also the possibility that a charge and a flux are created in the same place (the end points of the two string operators creating them are on the same link). This kind of excitation is called a *dyon*, denoted with ϵ

$$m \times e = e \times m = \epsilon \tag{1.15}$$

We can thus deduce the other non trivial fusion rules

$$\epsilon \times e = m \qquad \epsilon \times m = e \tag{1.16}$$

To see the statistical behavior of these excitations let us try to braid them. It is easy to see that by exchanging the positions of two e or two m the state remains the same

since we create a (contractible) loop (see Fig. 1.7), and as we know a loop leaves the state invariant because can be written in terms of A_v's or B_p's. In this way we see that

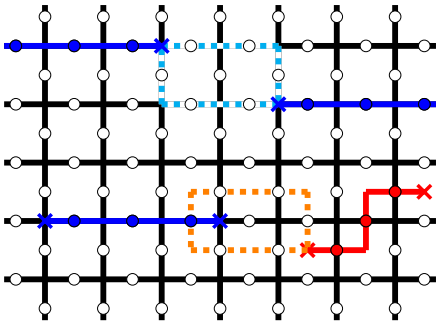

Figure 1.7: *Braiding of elementary excitations. Above: braiding of two charges. Below: braiding of a flux around a charge.*

e and m have a bosonic nature. Let us now try to take an m excitation around an e one and going back to the initial position. What we obtain is an additional minus sign to the final state coming from the fact that in one link the encircling path will have to cross the path of the e particle. We can thus conclude that e and m have non-trivial mutual statistics (called semionic mutual statistic) and behave as *Abelian anyons*, i.e. neither bosons nor fermions. Knowing this it is also possible to derive that dyons exhibit fermionic statistic [2].
Anyons are manifestations of the underlying topological order of the model. In fact, we can deduce that the GS is degenerate just by knowing that there are two particle types with -1 mutual statistics. Consider the operator Z winding an e particle around a non-contractible loop of the torus and annihilating it, and the operator X doing the same for an m particle on the other non-trivial loop. Simply by looking at the combination $Z^{-1}X^{-1}ZX = -1$ we see that there are two non commuting operators acting on the GS space, which means that it must have dimension bigger that one. Since there are four such operators (two particles over 2 non-contractible loops), we find again that GSD$= 4$.

1.1.3 Lattice gauge theory

The TC can be included into the more general framework of lattice gauge theory. This identification also explains the names assigned to the elementary excitations. A gauge theory implies a gauge symmetry which cannot be removed by any external perturbations, but we saw that the TC is stable to arbitrary local perturbations. To give a field theoretic interpretation we can consider the link labels z_l $(= \pm 1)$ to correspond to a $\mathbb{Z}_2$ vector potential, whereas σ_l^x corresponds to the electric field. Operators A_v, as mentioned before, are local gauge transformations while B_p is the magnetic flux across a plaquette p. The constraints (1.7a) mean that the state $|\psi\rangle$ is gauge invariant. It is possible to

violate the gauge invariance but it is energetically penalized. The Hamiltonian, which includes also the external perturbation, $\mathcal{H} = \mathcal{H}_{TC} + V$ (defined below), need not to obey the gauge symmetry. The constraints (1.7b) mean that the gauge field corresponds to a flat connection. Also these constraints can be broken with an energy cost. So, despite the absence of symmetry in $\mathcal{H}$, the system exhibits two conservation laws: electric and magnetic charges (fluxes), both modulo 2. By analogy with electromagnetism where the $U(1)$ gauge invariance yields the electric charge conservation, there should be a $\mathbb{Z}_2$ symmetry for electric charges and another $\mathbb{Z}_2$ symmetry for magnetic fluxes.
In order to see this symmetry we have to use redundancy, i.e. add unphysical degrees of freedom. First, let us consider the Hamiltonian

$$\mathcal{H} = \mathcal{H}_{TC} + V = -J_e \sum_{v \in \mathscr{L}} A_v - J_m \sum_{p \in \mathscr{L}} B_p - h_z \sum_{l \in \mathscr{L}} \sigma_l^z - h_x \sum_{l \in \mathscr{L}} \sigma_l^x \tag{1.17}$$

where the last two terms are couplings with external fields. Now we add some new variables: $\tau_v^x = \pm 1$ on each vertex and $\mu_p^z = \pm 1$ on the plaquettes. In this way we define a bigger Hilbert space given by $\mathscr{H}_{big} = \mathscr{H}_0 \otimes \mathscr{H}_\tau \otimes \mathscr{H}_\mu$. We want to map uniquely the physical states $|\psi\rangle$ into the enlarged space, and we do it by taking, for physical states, $\tau_v^x = A_v$ and $\mu_p^x = B_p$, so that $|\psi\rangle \leftrightarrow |\Psi(\psi)\rangle$. Now, let us rewrite the Hamiltonian in the enlarged space in such a way that the action on physical states remains the same, i.e. such that $\langle\Psi(\psi)|\,\tilde{\mathcal{H}}\,|\Psi(\psi)\rangle = \langle\psi|\,\mathcal{H}\,|\psi\rangle$,

$$\tilde{\mathcal{H}} = \mathcal{H}_{TC} - h_z \sum_{\langle uv \rangle} \tau_u^z \sigma_{uv}^z \tau_v^z - h_x \sum_{\langle pq \rangle} \mu_p^z \sigma_{pq}^x \mu_q^z \tag{1.18}$$

where σ_{uv} is the Pauli operator acting on the link between the nearby vertices u and v and σ_{pq} acts on the link between the two touching plaquettes p and q.
Finally, by using the constraints for the physical space ($\tau_v^x = A_v$ and $\mu_p^x = B_p$) we can rewrite

$$\mathcal{H}_{TC} = -J_e \sum_{v \in \mathscr{L}} \tau_v^x - J_m \sum_{p \in \mathscr{L}} \mu_p^x \tag{1.19}$$

In this way we have that $\tilde{\mathcal{H}}$ is gauge invariant and the generators of the local symmetry are $\mu_p^x B_p$ and $\tau_v^x A_v$. In fact, σ_{uv}^z changes the values of A_u and A_v, so in $\tilde{\mathcal{H}}$ we use the term $\tau_u^z \sigma_{uv}^z \tau_v^z$ so that the symmetry under $\tau_v^x A_v$ is respected. A minus sign at each vertex is given by the action of σ_{uv}^z and another instead arrives from the anti-commutation between τ_v^x and τ_v^z. The same holds for the second term.
The ground state for small h_z and h_x has an emergent symmetry. When $h_x = h_z = 0$ both A_v and B_p (or equivalently τ_v^x and μ_p^x) separately commute with $\tilde{\mathcal{H}}$. Since the GS for $\vec{h} = (h_x, h_z) = 0$ is unique up to global degeneracies which depend upon the geometry, and is separated by a gap from the excited states, it retains this structure to all orders in perturbation theory.

Viewed as a standard $\mathbb{Z}_2$ gauge theory, the protected topological degeneracy of the GS is physically familiar as the protected degeneracy associated with the choice of flux threading the $2g$ holes of a genus g surface.

1.2 X-Cube model

Let us now pass to the prototypical example of fracton phases: the X-Cube model [8]. The defining characteristic of fracton phases is that the elementary excitations exhibit restricted mobility, i.e. they are either immobile or can move only in certain directions (sub-dimensional particles). Instead, composites of elementary excitations are mobile particles so that the former can be viewed as having *fractionalized mobility* (from this their name). There are two types of fracton topological orders:

- *Type I* fracton phases have fracton excitations appearing at corners of membrane operators[†] and composites of fractons are only mobile along sub-dimensional subsystems. An example is the X-Cube model;
- *Type II* fracton phases have fracton excitations that appear at corners of fractal operators[‡], all excitations are localized and there are no mobile topological quasiparticles. An example is the Haah cubic model [7].

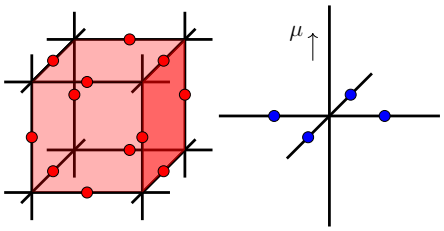

Figure 1.8: *Stabilizer operators of the X-Cube model. The red (blue) dots on the links represent the σ_x (σ_z) Pauli operators.*

We will analyze in particular the X-Cube model underlying its connections with the TC and its excitations.
The X-Cube model is a 3-D lattice spin model: take the cubic lattice ($\mathscr{C}$) and put spins

[†]Membrane operators consist of $\sigma_{x,z}$ operators acting on the links of rectangular shaped regions. See Fig. 1.9 for an example.

[‡]Fractal operators are equivalent to membrane operators with the only difference being that they have support on a fractal region of space. See Fig. 5 in Ref. [4] for an example.

on the links. Consider the following local operators represented in Fig. 1.8

$$B_c = \prod_{l \in \partial c} \sigma_l^x \tag{1.20a}$$

$$A_v^\mu = \prod_{l \in star(v), l \perp \mu} \sigma_l^z, \qquad \mu = x, y, z \tag{1.20b}$$

where in B_c the product is taken over the (twelve) links surrounding the cube c, while in A_v^μ over the (four) links touching the vertex v and lying on the plane orthogonal to the direction μ, as shown in Fig. 1.8. The Hamiltonian is then defined as

$$\mathcal{H}_{XC} = -K_m \sum_{c \in \mathscr{C}} B_c - K_e \sum_{v \in \mathscr{C}, \mu = x,y,z} A_v^\mu \tag{1.21}$$

It is easy to see that B_c / A_v^μ always commute (both among themselves and between each other). It is clear since an A_v^μ and a B_c always share either 0 or 2 links. Also, since they are made of Pauli operators, they also satisfy $(A_v^\mu)^2 = B_c^2 = \mathbb{1}$. This means that, as for the TC, the model is exactly solvable and the Hamiltonian can be diagonalized in the basis of the eigenstates of these (local) operators. The GS will be the state where all the eigenvalues are $+1$.

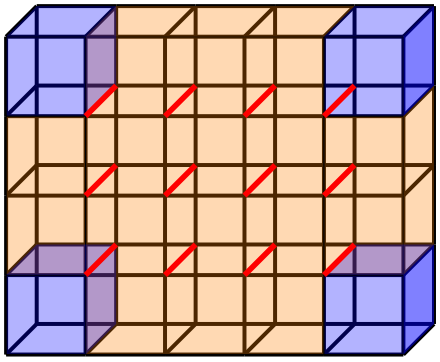

Figure 1.9: *Membrane operators of σ^z's create fracton excitations (blue cubes) at the corners of the membrane (highlighted in faint orange).*

Further, it is possible to show (and we will see it later) that in this model, for an $L \times L \times L$ cubic lattice with PBC on the three-torus T^3, the ground state degeneracy (GSD) is exponential in linear system size and in particular $\log_2(GSD) = 6L - 3$. These degenerate GS cannot be distinguished by any local measurements, so the model is topologically ordered.
The X-Cube model has two types of elementary excitations. The first are the immobile fracton excitations, which resides on the cubes with $B_c = -1$. Note that acting on a link with a σ_l^z creates four fracton excitations on the cubes touching the link. This means

that four separated fractons can be created at the corners of a membrane operator, as in Fig. 1.9, which is a product of σ_l^z's over a rectangular region. This explains why these excitations are immobile: in order to move one of them, two additional fractons must be created.
The second kind of excitations are 1-D particles residing on vertices where $A_v^x = A_v^y = -1$ and $A_v^z = 1$, for example, as in Fig. 1.10. In this case these excitations are created by acting with a string of σ_l^x's and reside at the ends of this string. They can move only in one direction (parallel to x,y or z, in this example z), since in order to make a corner they should emit two other particles, which cost energy.
An important characteristic of TC's excitations was that an anyon of type "a" can be detected remotely by acting with an encircling loop of "b"-type string operator. There exist an analogous process in the X-Cube model and to see it clearly we have to look at the connection with the TC.

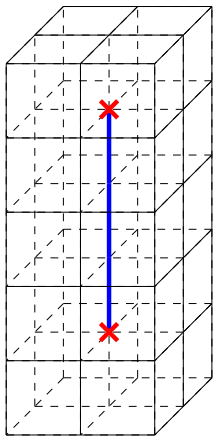

Figure 1.10: *Line of σ_z operators (blue line) creating two excitations (red crosses) on the vertices at their ends. Note that in these vertices the value of the vertex operator parallel to the line (A_v^z in this case) will be $+1$. Instead, the other two vertex operators, A_v^y and A_v^x, will have one link with a σ_z acted upon, thus an eigenvalue -1.*

1.2.1 X-Cube from stacks of Toric Codes

The X-Cube model can be obtained by the strong coupling limit of three intersecting stacks of 2-D Toric Codes [23]. To see how, let us consider three stacks of TCs in the three spatial directions. This results in having two spins on each link of the cubic lattice, participating each to the TC of one plane (the two planes containing the link). For example a link in the x direction is contained both in a xy and in a xz plane.

For a plane $\mathcal{P}$ the TC Hamiltonian is

$$\mathcal{H}_{\mathcal{P}}^{TC} = -\sum_{v\in\mathcal{P}} A_v^{o(\mathcal{P})} - \sum_{p\in\mathcal{P}} B_p \tag{1.22}$$

where we have the usual vertex and plaquette operators of the TC. This time however we change the role of σ_l^x and σ_l^z, in order to maintain the general conventions, and call $\sigma_l^x = X_l$ and $\sigma_l^z = Z_l$

$$A_v^{o(\mathcal{P})} = \prod_{l\in star(v), l\in\mathcal{P}} Z_l \tag{1.23a}$$

$$B_p = \prod_{l\in\partial p} X_l^{o(\mathcal{P})} \tag{1.23b}$$

Then, we couple together the spins residing on the same link and this results in the Hamiltonian

$$\mathcal{H} = \sum_{\mathcal{P}\in\mathscr{C}} \mathcal{H}_{\mathcal{P}}^{TC} - J_z \sum_l Z_l^{\mu_1} Z_l^{\mu_2} \tag{1.24}$$

We chose a ZZ coupling with $J_z > 0$, where $\mu_{1,2}$ are the two orthogonal directions to the link. We see that for $J_z = 0$ the various TCs are decoupled. The X-Cube model is obtained by taking the limit $J_z \to \infty$ and treating $\sum_{\mathcal{P}\in\mathscr{C}} \mathcal{H}_{\mathcal{P}}^{TC}$ as a perturbation. Using Brillouin-Wigner perturbation theory, it is possible to obtain the X-Cube Hamiltonian at sixth order [23]

$$\mathcal{H}_{XC} = -K_m \sum_{c\in\mathscr{C}} \tilde{B}_c - K_e \sum_{v\in\mathscr{C},\mu=x,y,z} \tilde{A}_v^{\mu} \tag{1.25}$$

where

$$\tilde{A}_v^{\mu} = \prod_{l\in star(v), l\perp\mu} \tilde{Z}_l \tag{1.26a}$$

$$\tilde{B}_c = \prod_{l\in\partial c} \tilde{X}_l \tag{1.26b}$$

$\tilde{Z}_l$ and $\tilde{X}_l$ are obtained by considering the GS without perturbation, i.e. any spin configuration, in z-basis, satisfying the constraint $Z_l^{\mu_1} = Z_l^{\mu_2}$, which means that

$$\tilde{Z}_l = Z_l^{\mu_1} = Z_l^{\mu_2} \tag{1.27a}$$

$$\tilde{X}_l = X_l^{\mu_1} X_l^{\mu_2} \tag{1.27b}$$

The vertex term of $\mathcal{H}_{\mathcal{P}}^{TC}$ contributes at first order ad gives the vertex term in the X-Cube Hamiltonian (in fact the projection to the GS simply replaces Z_l^{μ} with $\tilde{Z}_l$). Instead, the cube term in $\mathcal{H}_{XC}$ is a product of six B_p's where each such operator (made of X_l's)

anticommutes with the coupling term on the four links of the perimeter of p. To get a non trivial operator we have to get a product of B_p's over plaquettes forming a closed surface and the simplest such structure is a cube with six faces (this is why we have to arrive to sixth order in perturbation theory). It is also possible to prove that no other terms arise between first and sixth order.

1.2.2 Excitations and fusion rules

We can recover the properties of the excitations of the X-Cube model from the decoupled TCs by the condensation of extended 1-D objects called p-strings.
As we saw above, the J_z term does not commute with B_p, and acting with it on the GS creates TC's $m_{\mathcal{P}}$-particles. In fact, acting with $Z_l^{\mu_1} Z_l^{\mu_2}$ creates four $m_{\mathcal{P}}$ particles (two pairs) in the plaquettes surrounding l. Considering $m_{\mathcal{P}}$ as fluxes, let us represent them as line segments, at the center of plaquettes, normal to the plane where they reside. Joining the four segments of these excitations we form a so-called (closed) p-string, as shown in Fig. 1.11. It is immediate to see that it can be bigger by considering an operator made

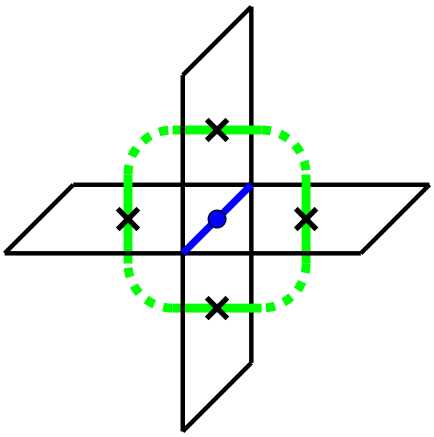

Figure 1.11: *Representation of a closed p-string (green). This is obtained connecting the axes orthogonal to the plaquettes touched by the link on which the term $Z_l^{\mu_1} Z_l^{\mu_2}$ acts upon, as explained in the text.*

of a collection of $Z_l^{\mu_1} Z_l^{\mu_2}$ on links orthogonal to a rectangular membrane. Increasing J_z from 0, at some point we expect to induce a condensation[§] of the p-strings created by the interaction. This condensation can be proved to confine individual $e_{\mathcal{P}}$ excitations, while bound pairs of $e_{\mathcal{P}}$ particles on intersecting planes survive this process. This phenomenon is given by the fact that isolated excitations have non-trivial braiding phase with p-strings, while coupled pairs $e_{\mathcal{P}_v} e_{\mathcal{Q}_v} = \tilde{e}_\mu^v$ do. $\mathcal{P}$ and $\mathcal{Q}$ represent the planes on which

[§]By condensation is meant that the great number of p-strings created by the interaction will inevitably come close to each other thus forming larger strings, eventually containing all the lattice.

the TC charges reside, and v is the specific vertex of the plane. These excitations can move in 1-D in the direction of the intersection of the two planes (μ). These are the 1-D particles we found before and are called, in similarity with the TC, electric excitations. Using the well known fusion rules of TC's $e_{\mathcal{P}}$ (see (1.14)), we can find the analogs for $\tilde{e}$

$$\tilde{e}^v_\mu \times \tilde{e}^v_\nu = \begin{cases} \tilde{e}^v_{o(\mu,\nu)} & \mu \neq \nu \\ 1 & \mu = \nu \end{cases} \tag{1.28}$$

Also, recall that $m_{\mathcal{P}}$ particles in TC are created at the ends of m-string operators, $S_m(\gamma) = \prod_{l\in\gamma} Z^z_l$, with γ path (dual) on xy plane, in this example. Take now a stack of $m_{\mathcal{P}}$ particles in the z direction, they form an open p-string. The coupling term $Z^{\mu_1}_l Z^{\mu_2}_l$ on the string moves it around but does not change the endpoints. This because the coupling creates loops of p-strings, which means that it cannot change the flux through any given cube. Upon condensation ($J_z \to \infty$) the bulk disappears but the endpoints remain: these are the 0-dimensional (immobile) magnetic excitations found in the X-Cube model, which reside in the cubes, and we will call them $\tilde{m}_c$. From the fusion rules for the TC (1.14) we see that also $\tilde{m}_c$ behave in the same way, i.e.

$$\tilde{m}_c \times \tilde{m}_c = 1 \tag{1.29}$$

The operator $M_\sigma = \prod_{l\in\sigma} Z^z_l$, where σ is a rectangular membrane and the links l cut it transversely, can be viewed as a stack of m-strings with each string creating two $m_{\mathcal{P}}$ particles on opposite sites of the membrane. M_σ creates four fracton excitations at its corners, in fact for $J_z \to \infty$ we have $M_\sigma \to \tilde{M}_\sigma = \prod_{l\in\sigma} \tilde{Z}_l$.
It is instructive to look at the case where there is a single layer, so that $M_\sigma = S_m(\gamma)$. In this case we can define an m-string operator in the X-Cube model by $\tilde{S}_m(\gamma) = \prod_{l\in\gamma} \tilde{Z}_l$, where γ lies in one plane, and it creates two $\tilde{m}_c$ fracton excitations at each end. This means that TC $m_{\mathcal{P}}$ particles survive in the X-Cube model as bound states of two $\tilde{m}_c$ fractons.
Since we derived $\tilde{e}^v_\mu$ and $\tilde{m}_c$ from the TC's e and m, it is clear that any statistical process involving only one of the two types will be trivial. Taking a rectangular prism with faces σ_1, σ_2, σ_3 and σ_4 (excluding the faces say in the xy plane) the membrane operator $\tilde{M}_{prism} = \tilde{M}_{\sigma_1} \dots \tilde{M}_{\sigma_4}$ does not create any excitation since it is possible to see that they cancel out. Instead, what it does is to count the number of total $\tilde{e}_x$ and $\tilde{e}_y$ excitations inside the prism (modulo 2). We can see this by the fact that

$$\tilde{M}_{prism} = \prod_{v\in prism} A^z_v \tag{1.30}$$

and $A^z_v = -1$ on states with $\tilde{e}_x$ or $\tilde{e}_y$ excitations. In this way we see that we have an analogous process for remote detection of defects as we had in the TC, but this time instead of loop operators we have to consider membrane operators over closed surfaces.

1.2.3 Ground state degeneracy

To evaluate the GSD we will consider the X-Cube model on an $L \times L \times L$ cubic lattice wrapped around the 3-torus T^3. This is the same as considering that each TC (each plane) in the model has T^2 topology. To evaluate the GSD we will follow a non rigorous approach relating this GS with the single GS's of the TC, but turns out that also in this way the result obtained is exact.
To find the GSD we have to count the number of independent logical operators in our theory: in the TC we are on T^2 so, considering for example m particles, there are two non-contractible loops (c_1' and c_2' in Fig. 1.5) and so two string operators ($X(c_1')$ and $X(c_2')$) threading m particles around the torus. Further they are linearly independent, which means that they form a complete set of independent, commuting logical operators and their eigenvalues completely label the GS, which has degeneracy $(GSD)_{TC} = 2^2 = 4$. In the X-Cube model on T^3 analogously we count the number of distinct ways we can thread the magnetic membranes $\tilde{M}_\sigma$ through non contractible loops. A generic $\tilde{M}_\sigma$ can be constructed from a stack of $\tilde{S}_m(\gamma)$ with γ a non-contractible loop in one plane, so in a T^2 torus. Each plane has two such paths so they all contribute as 2^2 to the GSD. Since there are L planes in each of the three directions we count $6L$ logical operators. However these are not all linearly independent, as can be seen by considering that, for all $\mu \neq \nu$

$$\prod_{0 \leq n < L} \tilde{S}_m(\gamma^\nu_{o(\mu,n)}) = \prod_{0 \leq n < L} \tilde{S}_m(\gamma^\mu_{o(\nu,n)}) = M_{\mu\nu} \tag{1.31}$$

where $\gamma^\nu_{o(\mu,n)}$ is a path on the plane (μ, n) (plane orthogonal to μ with μ-component equal to n) passing around a non contractible loop in the $\nu \neq \mu$ direction. So, $M_{\mu\nu}$ is a membrane operator where σ covers the hole $\mu\nu$ plane. Since this equality holds $\forall \mu \neq \nu$ we have three such relations in the X-Cube model, which means that $\log_2(GSD_{XC}) = 6L-3$. This result has been proven exactly fo L even [8]. In principle we could have missed additional logical operators independent from the ones listed above, but it turns out this is not the case. The exponential growth of the GSD is a defining characteristic of fracton models and distinguishes them from usual topological models, like the TC, where instead the GSD is constant in system size.

1.2.4 Lattice gauge theory

As for the TC, also the X-Cube model can be included into the broader class of lattice gauge theories, but this time in a peculiar way. That is why we call it a *generalized* lattice gauge theory. This generalization is useful in order to find new fracton models. Fracton models can be obtained as quantum dual of d-dimensional systems that possess *subsystem symmetries*. This refers to a symmetry over a subspace of the system with dimension $0 < d_s < d$, where d is the system's dimension. A subsystem symmetry is something between a local and a global symmetry, a mid-step that yields new intriguing

features.
In particular, to obtain the X-Cube model let us consider a cubic lattice with spins (denoted by τ) on the vertices and Hamiltonian given by the sum of the products of the four spins around each plaquette

$$\mathcal{H}_{spin} = \sum_p T_p^z \tag{1.32}$$

where $T_p^z = \tau_1^z \tau_2^z \tau_3^z \tau_4^z$. This model has a subsystem symmetry in the sense that it is invariant under a spin flip $\tau \to -\tau$ over any plane of the lattice. It is called the *plaquette Ising model*.
We have now to promote this sub-system symmetry to a local (gauge) symmetry and to do it we turn again to redundancy (as for the TC in Sec. 1.1.3). Let us first add a transverse field to allow the spins (τ) to have quantum fluctuations. Then we add additional Ising spins σ at the *center* of each multi-spin interaction, in this case in the faces' centers. Finally, we introduce a minimal coupling between σ and τ spins, so that we arrive to

$$\mathcal{H} = -t \sum_p \sigma_p^z T_p^z - h \sum_v \tau_v^x \tag{1.33}$$

We call σ the *nexus* field and it is a natural generalization of a gauge field in a conventional lattice gauge theory. Applying the standard gauging procedure by introducing a gauge field on the links would have resulted into a Hamiltonian with conventional $\mathbb{Z}_2$ topological order.
Now the subsystem symmetry of the spin system has been promoted to a local spin-flip symmetry. In fact, τ_v^x anti-commutes with the first term of $\mathcal{H}$, so we can compensate by acting with the nexus field σ_p^x on the twelve faces which have v as a vertex. In this way the operator

$$G_v = \tau_v^x B_v \tag{1.34}$$

where

$$B_v = \prod_{p \text{ s.t. } v \text{ touch } p} \sigma_p^x \tag{1.35}$$

is a local symmetry of the Hamiltonian, i.e. $[G_v, \mathcal{H}] = 0$. Note that in the dual lattice, nexus fields reside on the links and the operators appearing in B_v are the links of the cube centered in v. Finally, we include also the transverse field for the nexus field, $-J \sum_p \sigma_p^x$. The condition $G_v |\psi\rangle = |\psi\rangle$ on the Hilbert space amounts to a generalized Gauss' law. B_v is called nexus charge operator. We can now chose a particular gauge in order to eliminate the fields τ

$$\tau_v^x |\psi\rangle = B_v |\psi\rangle \tag{1.36}$$

Further, since each τ_v^z operator now commutes with $\mathcal{H}$ we can just focus on the sector where $\tau_v^z = 1$. Thus, we obtain

$$\mathcal{H} = -t \sum_p \sigma_p^z - h \sum_v B_v - J \sum_p \sigma_p^x = -t \sum_{\tilde{l}} \sigma_{\tilde{l}}^z - h \sum_{\tilde{c}} B_{\tilde{c}} - J \sum_{\tilde{l}} \sigma_{\tilde{l}}^x \tag{1.37}$$

where the $\sim$ indicates the dual lattice.
Finally, for $t/h \ll 0$ we can identify an effective Hamiltonian [8]

$$\mathcal{H}_{eff} = -t \sum_{\tilde{v},\mu} A_{\tilde{v}}^{(\mu)} - h \sum_{\tilde{c}} B_{\tilde{c}} - J \sum_{\tilde{l}} \sigma_{\tilde{l}}^x \tag{1.38}$$

where the operators $A_{\tilde{v}}^{(\mu)}$ are determined in perturbation theory as the simplest product of σ^z's near a (dual) lattice vertex that commute with the nexus charge, i.e. $[A_{\tilde{v}}^{(\mu)}, B_{\tilde{c}}] = 0$. In this way we obtain the standard star operators of the X-Cube model. $A_{\tilde{v}}^{(\mu)}$ operators provide the natural generalization of the flux in a lattice gauge theory.
This shows how the X-Cube model can be obtained as the dual of a spin-system with subsystem symmetry. This property is a general feature of fracton phases, holding also for type-II models [9] where the subsystem symmetries have fractal support.

Chapter 2

Tensor gauge theory and fractons

Let us now move on to the description of fracton phases using tensor gauge theory. First, in Sec. 2.1 we review the description of usual vector $U(1)$ gauge theory. Then, in Sec. 2.2 we study the case of symmetric rank-2 $U(1)$ tensor gauge theory, which effectively describes gapless fracton models. Of the various possible theories, the case of scalar elementary particles is analyzed, dubbed Scalar Charge Theory (SCT). Particular emphasis is given to the stability of SCT (Sec. 2.2.4) and to the interactions mediated by the gauge field (Sec. 2.2.3).
In the second part of the chapter, Sec. 2.3, we review the theoretical progress achieved through the tensor gauge theory description of fracton phases. In particular, we analyze some possible phases of matter which can arise when considering a finite density of fractons and/or of other non-trivial excitations, like the dipolar bound states.

2.1 Vector U(1) gauge theory

Let us start by considering the quantized lattice version of electromagnetism [1, 10], which represents an example of $U(1)$ vector gauge theory. This theory on a three dimensional lattice hosts a Coulomb phase with a gapless photon mode with two polarizations as in Maxwell theory and gapped electric and magnetic excitations, where magnetic monopoles arise as a consequence of the compactness of the gauge field. Note that in order to have just the two ± 1 polarizations of the photon, it is necessary that the gauge field A is compact and that the theory is defined on a lattice [24]. As in the TC, excitations are non local, signaling the presence of highly entangled states.
We take the degrees of freedom to be those of a vector field $A_i(x, y, z)$, where to keep track of all degrees of freedom and avoid confusion, we denote with $i = x, y, z$ the spatial directions, and with (x, y, z) the coordinates of a site in the lattice of spacing a. Considering the theory to be compact ($U(1)$) this field will satisfy $A_i \sim A_i + 2\pi$. The only gauge transformation possible for a vector field is that of adding the derivative of a

scalar function

$$A_i \to A_i + \partial_i \alpha \tag{2.1}$$

where ∂_i is the lattice derivative, like for example

$$\partial_x A_x(x,y,z) = \frac{1}{a}(A_x(x+a,y,z) - A_x(x,y,z)) \tag{2.2}$$

with a the length of a link in the lattice.
Since the field is compact each component of the gauge field is a $O(2)$ quantum rotor [25], and its canonical conjugate E_i will be the corresponding angular momentum, quantized to take integer values. The gauge transformation is better understood in terms of the electric field, which yields the so-called Gauss' law

$$\partial_i E^i = 0 \tag{2.3}$$

In a concrete lattice model, let us consider for simplicity the cubic lattice, both A^i and E^i are taken to live on the links. The corresponding Hamiltonian of the system will be given by

$$\mathcal{H} = \frac{1}{2} g \sum_{\text{links}} E^2 - \sum_{\text{plaquettes}} \cos\left(B^2\right) \tag{2.4}$$

where $B_i = \epsilon_{ijk}\partial^j A^k$ is the magnetic field and the cosine is taken in order to respect the compactness of the gauge field. The magnetic field is defined in this way since it is the simplest combination of derivatives of the gauge field which commutes with the gauge transformation. Also, since it is formed by mixed derivatives* of the gauge field, the magnetic field is naturally taken to live on the plaquettes of the lattice.
Let us now consider the different possible values of g in (2.4). This parameter represents the energy content of the theory. In particular, for small g, i.e. at low energies, the cosine can be expanded around its minimum yielding

$$\mathcal{H} \sim \int \frac{1}{2} g E^2 + \frac{1}{2} B^2 \tag{2.5}$$

which is the usual Hamiltonian for electromagnetism. Here the Gauss' law is taken to be automatically satisfied, but if we consider not just the low energy sector we have also to include terms which impose the Gauss' law as an energy constraint. In particular, violations of the Gauss' law will be interpreted as particle states of the theory, or charges. These charges will exist as gapped excitations of the system and will have an energy penalty in the Hamiltonian

$$\mathcal{H} = \frac{1}{2} g \sum_{\text{links}} E^2 - \sum_{\text{plaquettes}} \cos\left(B^2\right) + U \sum_{\text{vertices}} (\partial_i E^i)^2 + \cdots \tag{2.6}$$

*The terms in the magnetic field will be of the kind $\partial_i A_j$ with $i \neq j$.

Note that charges naturally live on vertices of the lattice as they correspond to first derivatives of the electric field. The $\cdots$ terms represent the part which do not commute with the gauge constraint and whose role is that of dictating the dynamics of the charges. The effect of breaking the gauge invariance in the pure gauge theory is simply to introduce excitations above a gap in the theory, but the stability is unaffected.
This theory possesses a gapless photon mode with linear dispersion relation and two polarizations. If we consider the large g limit, we see that the electric term dominates, effectively disordering the magnetic cosine term, and the system picks up a gap of order g. This corresponds to the so called confined phase [1].
There is an inherent self-duality in this theory, manifested in the fact that we can describe it both with electric charges or magnetic monopoles. This duality helps us establish that the theory is stable against instanton proliferation [26], since magnetic monopoles behave exactly as their electric counterparts. However, this is the case only in three dimensions since in $2D$ the magnetic monopoles are instantons, not excitations with a well defined energy. This tells us that in $2D$ the $U(1)$ gauge theory is totally destroyed and is not stable against confinement.

2.2 Tensor U(1) gauge theory

Let us now pass to the main topic of this chapter, which is Tensor Gauge Theory (TGT). In the continuum, the idea is that there is no actual reason to restrict ourself to only vector gauge fields and that growing with the rank of the field new phases could be possible. The first step could be that of considering higher differential forms. However, antisymmetric tensor theories do not lead to new stable phases in $3+1$ dimensions and in the discrete case they turn out to be simply dual descriptions of usual one-forms. Thus, in order to find new stable phases we restrict our-self to symmetric tensors, in particular of rank-2 [10]. Symmetric gauge fields are reminiscent of gravity and in fact they were first studied in this field [27, 28]. What has been found is that these symmetric gauge fields lead to a new class of stable gapless spin liquids. Further, these are effectively distinct theories since, while the gauge modes are similar to the rank-1 case, the particle content is completely different, hosting excitations with kinetic restrictions.
Increasing the rank of the gauge field raises also the number of admitted gauge transformations [27]. Let us take the gauge field to be a symmetric $U(1)$-valued rank-2 tensor $A_{ij}, \quad i,j = x,y,z$, with canonical conjugate E_{ij} representing a generalized electric field, such that

$$[A_{ij}(\vec{r}), E_{kl}(\vec{s})] = \frac{i}{2}\delta_{\vec{r},\vec{s}}(\delta_{ik}\delta_{jl} + \delta_{il}\delta_{jk}) \tag{2.7}$$

where $\vec{r}, \vec{s}$ represent positions in the (continuous) space.
As in Sec. 2.1, each component of the gauge field is a $O(2)$ quantum rotor (the field is compact) with the corresponding electric field tensor component which serves as the

angular momentum, and so is quantized to integer values.
There are three possible kinds of transformations for a symmetric rank 2 gauge field [27]

$$A_{ij} \to A_{ij} + \partial_i \partial_j \alpha \tag{2.8a}$$
$$A_{ij} \to A_{ij} + \partial_i \alpha_j + \partial_j \alpha_i \tag{2.8b}$$
$$A_{ij} \to A_{ij} + \delta_{ij} \alpha \tag{2.8c}$$

which can be imposed also one on top of the other. Here we will focus on the first one (2.8a), which implies, in terms of the electric field, the generalized Gauss' law

$$\partial_i \partial_j E^{ij} = 0 \tag{2.9}$$

This holds for the low energy sector. Considering the possibility of charges in our theory we see that these will be scalars, defined by $\partial_i \partial_j E^{ij} = \rho$ and this gives the name to the theory: *Scalar Charge Theory* (SCT) [10].
This theory can be proven to be stable in $3D$ as the magnetic monopoles are gapped excitations while it is confined in $2D$ because of instantons proliferation as in classical electromagnetic theory. We will discuss this issue in sec. 2.2.4.
SCT posses a gapless gauge mode with five polarizations which propagate normally. This can be seen by the fact that the gauge field has 6 degrees of freedom, and one of these is removed by the Gauss' law, remaining with five independent polarizations of the gauge mode. The linear dispersion relation comes from the number of derivatives in the magnetic field, which in this theory reads

$$B_{ij} = \epsilon_{ilm} \partial^l A^m_j \tag{2.10}$$

This in the equations of motion yields a linear dispersion. Note that it would be possible to define a symmetrized version of the magnetic field, but this would end up to be fine tuned as one of the gauge modes is tuned to have exactly flat dispersion. This non-symmetric field describes the point at which all gauge modes have the same velocity.
The main difference from the vector gauge theory seen in the section above lies in the particle content. In fact, this Gauss' law implies higher momentum conservation laws which restrict the mobility of single charges. In particular, we have as before the local conservation of charge

$$\int \rho = \int \partial_i \partial_j E^{ij} = \oint \partial_j E^{ij} = const. \tag{2.11}$$

where in the last step we used the fact that it is an integration over the boundary. Further, Gauss' law also enforces the conservation of dipole moment, since

$$\int \vec{x} \rho = \int x^k \partial_i \partial_j E^{ij} = \oint \left[x^k \partial_j E^{ij} - E^{ki} \right] = const. \tag{2.12}$$

where we integrated by parts and then considered the second term as a total derivative in order to evaluate it at the boundary.
Note that for a closed manifold we need to introduce a branch-cut for $\vec{x}$ away from the charges of the theory. Instead for an open manifold this simply implies the conservation of dipole moment in the bulk.
This additional conservation law forbids elementary charges from moving at all, since any single charge changes the dipole moment by moving. These immobile excitations are dubbed *fractons*. Further, we see that dipole bound states of fractons can move freely without breaking any conservation law.
In the following we will study in deep SCT. First of all we will see in Sec. 2.2.1 how to concretely define it on the lattice. Then, we will see how the emergent gauge structure can arise by imposing the gauge principle starting from global conservation of charge and dipole moment (Sec. 2.2.2). This approach will give us an explicit coupling to matter. Following, in Sec. 2.2.3 the emergent generalized electromagnetism of fractons and dipoles of the theory is studied, exploiting its generalized Maxwell's laws. Finally, the matter of stability of the theory against confinement is considered in Sec. 2.2.4, pointing out the phenomenon of electrostatic confinement.

2.2.1 Lattice model

Scalar charge theory can be put on the lattice as follows [13, 28]. The natural place

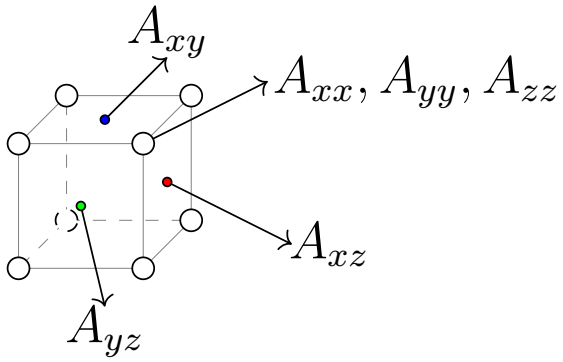

Figure 2.1: *Positions of the gauge fields in Scalar Charge Theory.*

to put the six gauge degrees of freedom is to split them in diagonal and non-diagonal components. The diagonal ones naturally live on the vertices of the cubic lattice, while the non-diagonal ones on the faces of the corresponding plane: A_{xx}, A_{yy} and A_{zz} on each vertex and A_{xy} on the faces of the xy plane and so on, as in Fig. 2.1. This is clear if we think about the most simple rank-two object: a second derivative $\partial_i \partial_j \lambda$. With λ placed on the vertices of the lattice, the first derivatives $\partial_i \lambda$ will naturally live on the

links in the i-th direction. Thus, diagonal second derivatives will reside on vertices while mixed second derivatives will lie on the faces of the corresponding plane. The same argument holds also for the components of the electromagnetic field E_{ij}. Finally, the resulting lattice model has three rotors on each site and one on each face of the cubic lattice. The rotors at sites are not all identical since at the level of the Hamiltonian the A_{xx} component will have interaction prevalently in the x direction and so on, in a quite similar way to p orbitals on atoms in a cubic lattice environment[†].
Now, let us construct the Hamiltonian of the model. First of all, this Hamiltonian will contain an energetic penalty term for the violation of the Gauss' law, which we can write as

$$\mathcal{H}_U = U(\partial_i \partial_j E^{ij})^2 \tag{2.13}$$

where all the derivatives are intended as lattice derivatives. Let us see an example for clarity

$$\partial_x \partial_x E^{xx}(x,y,z) = \frac{1}{a^2}(E^{xx}(x+a,y,z) + E^{xx}(x-a,y,z) - 2E^{xx}(x,y,z)) \tag{2.14}$$

For the other terms we have to consider the mostly relevant gauge invariant terms. The lowest energy term for the electric field is

$$\mathcal{H}_E = \frac{J}{2} E_{ij} E^{ij} \tag{2.15}$$

As in electromagnetism we have to find some magnetic field which has to be gauge invariant and with the lowest number of derivatives. In the case of SCT it is given by (2.10), thus we can include in the Hamiltonian a term of the form

$$\mathcal{H}_B \propto -\sum_{ij} \cos(B_{ij}) \approx -1 + \frac{1}{2} B_{ij} B^{ij} \tag{2.16}$$

The cosine is needed in order to respect the compactness of the gauge field. The full Hamiltonian thus reads

$$\mathcal{H} = \frac{J}{2} E_{ij} E^{ij} + \frac{K}{2} B_{ij} B^{ij} + U(\partial_i \partial_j E^{ij})^2 + \cdots \tag{2.17}$$

Here the $\cdots$ terms represent the part that do not commute with the gauge constraint and so is irrelevant to the low energy theory. Nevertheless, they represent the piece of Hamiltonian governing the dynamics of the massive charges. Consider for example the operator $\exp(iA_{yz})$ which is a raising operator increasing E_{yz} by one. This operator is not

[†]This gives a hint that p-orbitals may be central in looking for experimental realizations of fractonic phases.

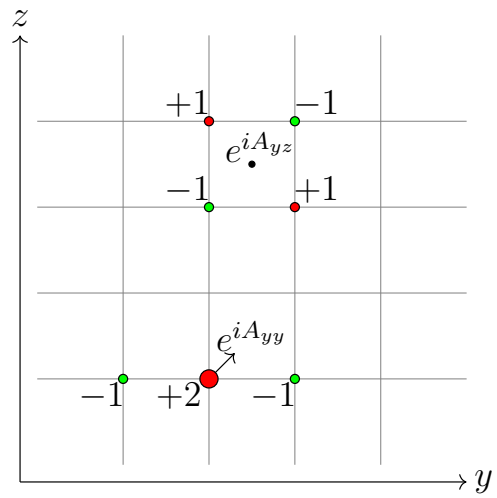

Figure 2.2: *Admissible configurations in SCT. They are both quadrupolar configurations. The one above acts as a hopping parameter for a dipole in a direction orthogonal to the dipole's one. The configuration below instead acts as a longitudinal hopping operator, making the dipole a fully mobile particle.*

gauge invariant and takes us out of the pure gauge sector, in fact it creates additional particles. The same holds for the diagonal components. These charge configurations must nevertheless respect the Gauss' constraint, so they have to be quadrupolar configurations of charges, as reported in Fig. 2.2. These operators show that indeed the elementary particles are fractons, while dipolar bound states, which are still non-trivial configurations of charges since no local operator can create them without energy cost, are fully mobile.
Let us rename the charge at site $\vec{r}$ as $n_{\vec{r}}$ so that

$$\partial_i \partial_j E^{ij}(\vec{r}) = n_{\vec{r}} \tag{2.18}$$

We can describe matter degrees of freedom by defining on each lattice site an $O(2)$-quantum rotor variables θ with number n, satisfying the relation

$$\left[\theta(\vec{r}), n(\vec{r'})\right] = i\delta_{\vec{r},\vec{r'}} \tag{2.19}$$

These will couple to the gauge field, resulting in an Hamiltonian of the form

$$\mathcal{H} = \sum_{\vec{r}} \left[\frac{J}{2} E_{ij} E^{ij} + \frac{K}{2} B_{ij} B^{ij} + U n_{\vec{r}}^2 - V \sum_{i \leq j} \cos(\partial_i \partial_j \theta - A_{ij}) \right] \tag{2.20}$$

The form of the coupling between the gauge field and the matter field depends on the gauge structure of the theory and the requirement of gauge invariance of the Hamiltonian

[19, 20]. In this case we have the gauge transformations

$$A_{ij} \to A_{ij} + \partial_i \partial_j \alpha \tag{2.21a}$$
$$\theta \to \theta + \alpha \tag{2.21b}$$

The representation of gauge and matter fields in terms of quantum rotors helps in the characterization of the different phases in the theory [25]. It is known that quantum rotors have a paramagnetic phase when the kinetic term is prevalent and a ferromagnetic phase when the coupling between the rotor is more relevant. In the paramagnetic phase there are $N = 2$ different excitations while in the ferromagnetic phase the $O(2)$ symmetry is broken and remains just $N-1 = 1$ gapless mode. In this case we already took the limit for the ordered phase when asking to work in the low energy sector and expanding the $\cos(B_{ij})$-term in the Hamiltonian. This has lead us to a theory with a gapless, linearly dispersing photon mode with five polarizations and a gapped charge sector.

2.2.2 Gauge principle

A way to find the gauge symmetry of the SCT is that of starting from a theory of ungauged fractons which respects global conservation of charge and dipole moment. Then, by requiring that this symmetry holds locally, i.e. it is a gauge symmetry, it is possible to see that this requires the coupling to a symmetric tensor gauge field [29].
The first step is that of writing a theory for ungauged $U(1)$ fractons. Let us consider a matter field Φ and the corresponding charge density $\rho = \Phi^\dagger \Phi$. In order for the charge to be conserved globally we need the action to be invariant under a global phase rotation

$$\Phi \to \exp(i\alpha)\Phi \tag{2.22}$$

with α constant. Further, in order for the theory to globally conserve dipole moment we also need to ask that the action be invariant under a linearly varying phase rotation

$$\Phi \to \exp\left(i\vec{\lambda} \cdot \vec{x}\right)\Phi \tag{2.23}$$

with $\vec{\lambda}$ constant. Overall, we are asking the theory to be invariant under a phase rotation $\alpha(x)$ at most linear in x. We need to look for operators which transform in a nice way under this rotation, like $O \to e^{in\alpha}O$ for integer n. While the field Φ is transforms in this way and so is covariant, its derivatives are not. In fact, the lowest order covariant operator is given by two fields, explicitly

$$\Phi \partial_i \partial_j \Phi - \partial_i \Phi \partial_j \Phi \tag{2.24}$$

Using this, we can construct the Lagrangian for our theory, which reads

$$\begin{aligned} \mathcal{L} =& |\partial_t \Phi|^2 - m^2 |\Phi|^2 - k \left(\Phi \partial_i \partial_j \Phi - \partial_i \Phi \partial_j \Phi\right) \left(\Phi^* \partial^i \partial^j \Phi^* - \partial^i \Phi^* \partial^j \Phi^*\right) - \\ & - k' \left[\Phi^{*2} (\Phi \partial^2 \Phi - \partial_i \Phi \partial^i \Phi) + c.c.\right] \end{aligned} \tag{2.25}$$

where $\partial^2 = \partial_i \partial^i$ and summation over same indexes is implied. Here we also added a term with a time derivative and a mass term, which have no interplay with the spatially dependent phase rotation. Rotational invariance has been assumed throughout.
Before gauging the theory let us note its shape: in fact, it is already not Gaussian, since it contains fourth powers of Φ in its action. This non-Gaussian behavior reflects the fact that fractons have an intrinsic ability to interact with each other, also in the absence of a mediating gauge field, as we will see in Sec. 2.3.1.
Let us now apply the gauge principle and try to pass from global to local conservation laws. The action will have to be invariant under a generic phase rotation $\alpha(x)$ with arbitrary dependence. We have to construct covariant objects, and this can be achieved by the coupling with a gauge field transforming in an adequate way. In particular, we can construct a covariant derivative

$$D_{ij}\Phi^2 = \Phi\partial_i\partial_j\Phi - \partial_i\Phi\partial_j\Phi - iA_{ij}\Phi^2 \tag{2.26}$$

where the gauge field A transforms as $A_{ij} \to A_{ij} + \partial_i\partial_j\alpha$. Further, if we allow α to also have arbitrary time dependence we need to include another gauge field in order to define a covariant time derivative

$$D_t\Phi = (\partial_t - i\psi)\Phi \tag{2.27}$$

with the field ψ transforming as $\psi \to \psi + \partial_t\alpha$. Before putting all this inside the new action of the theory, we need to look at which gauge invariant objects we can construct starting just from the gauge fields, like electric and magnetic field in usual electromagnetism. In this case the electric field tensor takes the form $E_{ij} = \partial_t A_{ij} - \partial_i\partial_j\psi$ and the magnetic field tensor $B_{ij} = \epsilon_{ikl}\partial^k A^l{}_j$. Finally, the Lagrangian of the gauged theory reads

$$\mathcal{L} = |D_t\Phi|^2 - m^2|\Phi|^2 - k|D_{ij}\Phi^2|^2 - k'(\Phi^{*2}D_i^i\Phi^2 + c.c.) + E_{ij}E^{ij} - B_{ij}B^{ij} \tag{2.28}$$

The k and k' terms represent the interaction of the matter field with the gauge field, while the last two terms represent the gauge field sector of the theory. In this way we obtained also an explicit coupling to matter. This route of developing gauge invariant theories may lead the way for defining generalization also to non-Abelian fracton theories.

2.2.3 Generalized Electromagnetism

As we have seen, SCT in some ways remains very similar to vector gauge theory but the principal differences arise in the particle content of the theory. In order to study systems at a finite density of fractons and/or of dipole moments it is necessary to develop an analogue of Maxwell laws for this higher rank gauge theory. In fact, also this theory exhibits an emergent electromagnetism, but of a more exotic form [30].
Let us first see the form that the electrostatic field must take. Consider an isolated charge q at position r. The Gauss' law will have the form

$$\partial_i\partial_j E^{ij} = q\delta^{(3)}(r) \tag{2.29}$$

Let us start by the assumption that the electric field *i*) has to be symmetric, *ii*) depends only on rotationally invariant objects and *iii*) scales as q/r. The last point can be justified by Fourier transforming the Gauss' law (2.29)

$$\tilde{E} \sim \frac{q}{k^2} \tag{2.30}$$

and then transforming back to obtain the electric field

$$\begin{aligned} E \sim \int d^3k \exp\left(i\vec{k}\cdot\vec{r}\right)\tilde{E} &\sim q\int dk \int d\theta \sin(\theta)\exp(ikr\cos(\theta)) \\ &\sim q\int dk \frac{\sin(kr)}{kr} \sim \frac{q}{r} \end{aligned} \tag{2.31}$$

With these assumptions, the most general form of the electric field is

$$E^{ij} = q\left(\alpha\frac{\delta^{ij}}{r} + \beta\frac{r^i r^j}{r^3}\right) \tag{2.32}$$

Imposing that it has to satisfy the Gauss' law we obtain the constraint $\beta - \alpha = 1/4\pi$. Differently from standard electromagnetism, the electric field is not completely fixed by Gauss' law and rotational invariance. In order to completely specify it we need to take into account the magnetic field $B^{ij} = \epsilon^{ikl}\partial_k A_l{}^j$. The equation governing its evolution is

$$\partial_t B^{ij} = \epsilon^{ikl}\partial_k \partial_t A_l{}^j = \epsilon^{ikl}\partial_k E_l{}^j \tag{2.33}$$

By asking for a magnetostatic solution $\partial_t B^{ij} = 0$ we obtain the constraint $\alpha = -\beta$ and the static electric field generated by a point charge in the origin can be written as

$$E^{ij}_{\text{mono}} = \frac{q}{8\pi}\left(\frac{r^i r^j}{r^3} - \frac{\delta^{ij}}{r}\right) \tag{2.34}$$

In order to obtain the electric field generated by a more complicated set of charges we can just invoke the superposition principle. In particular, a configuration which will be very useful is that of a dipole moment p^k centered at the origin, which will generate an electric field $-p^k\partial_k E^{ij}_{q=1}$ explicitly given by

$$E^{ij}_{\text{dip}} = -\frac{1}{8\pi}\left(\frac{\delta^{ij}(p\cdot r)}{r^3} + \frac{p^i r^j + r^i p^j}{r^3} - 3\frac{r^i r^j (p\cdot r)}{r^5}\right) \tag{2.35}$$

Let us now pass to a potential formulation. From the magnetostatic condition we see that we can write the electric field as $\partial_i\lambda_j$, but for its symmetry this also means that $\epsilon_{ijk}\partial_j\lambda_k = 0$. So, we can in turn write λ as the derivative of a scalar potential ϕ, resulting in

$$E_{ij} = \partial_i\partial_j\phi \tag{2.36}$$

Gauss' law assumes the form

$$(\partial^2)^2\phi = q\delta^{(3)}(r) \tag{2.37}$$

By dimensional analysis we see that the potential field ϕ scales as r, so the only possibility is $\phi = Cr$. By imposing Gauss' law we find that $C = -q/8\pi$. Using again the superposition principle we can also obtain the potential for a dipole configuration

$$\phi_{\text{mono}} = -\frac{qr}{8\pi} \tag{2.38a}$$

$$\phi_{\text{dip}} = \frac{p \cdot r}{8\pi r} \tag{2.38b}$$

As in electromagnetism this potential can be used to evaluate the energy stored in the electric field of a static charge configuration

$$\epsilon = \frac{1}{2}\int E^{ij}E_{ij} = \frac{1}{2}\int \rho\phi \tag{2.39}$$

Thus, the potential represents the energy associated with a particle at a particular location. Even if fractons do not posses a conventional sense of forces (because of the restricted mobility), they admit a potential energy. Importantly, since ϕ grows linearly, separating a group of fractons requires an energy linear in the separation, but their restricted mobility stabilizes them against collapsing and thus being confined, as we will see in Sec. 2.2.4.

We now want to introduce a concept of force in order to see how charges behave in the presence of an electric field. We know that fundamental charges (fractons) are strictly immobile, so they do not respond at all to electromagnetic fields. Nevertheless there are still dipoles, which are fully mobile nontrivial excitations. This tells us that dipoles will serve as test particles for this treatment, and we ask what are the effects of the fields on this effective particle. Drawing intuition from the lattice model seen above (Sec. 2.2.1) we see that a dipole p^i responds to a magnetic field as a conventional charged particle responds to an ordinary electromagnetic field, with an effective vector potential given by $A^j_{\text{eff}} = -\hat{p}_i A^{ij}$ and an effective magnetic field[‡] $B^i_{\text{eff}} = -B^{ij}\hat{p}_j$. The corresponding effective electric field is $E^i_{\text{eff}} = -\hat{p}^i E^{ij}$, and the generalized Lorentz force on a dipole p^i moving at velocity v^i is given by

$$F^j = -p_i(E^{ij} + \epsilon^{jlk}v_l B_k{}^i) \tag{2.40}$$

From this, we can evaluate for example the work to move a dipole and this would lead us to the potential energy of a dipole derived above. Another interesting thing to do is to evaluate the force applied by a dipole on another one with same magnitude and direction. Using (2.35) and assuming a static electric charge distribution, the force on a dipole at location r^i due to an identical dipole at the origin is given by

$$F^j = \frac{1}{8\pi}\left(\frac{2p^j(p\cdot r)}{r^3} + \frac{p^2 r^j}{r^3} - 3\frac{(p\cdot r)^2 r^j}{r^5}\right) \tag{2.41}$$

[‡]Note that B^{ij} is non-symmetric, so it is important to keep track of which index is contracted.

Let us consider the radial component of this force

$$F^j \hat{r}_j = \frac{1}{8\pi}\left(-\frac{(p\cdot r)^2}{r^4}+\frac{p^2}{r^2}\right) = \frac{p^2\sin^2(\theta)}{8\pi r^2} \tag{2.42}$$

where θ is the angle between the dipoles' directions and their relative position.
From this expression we can deduce that for like dipoles (dipoles with the same direction) the radial force is always repulsive while for oppositely directed dipoles there will be an additional minus sign and so an always attractive force. Further, this force vanishes when dipoles line-up along a line ($\theta = 0$). This corresponds to a minimum for like dipoles and a maximum for opposite dipoles, meaning that like dipoles will tend to arrange themselves end to end while opposite dipoles prefer to lie side by side.
It remains to talk about steady current flows. Since fundamental charges are fractons, they have no sense of current. We need to define an object which describes the motion of dipoles. This work is done naturally by a symmetric tensor J_{ij} since microscopically the motion of an i directed dipole in the j direction has to be the same as a j directed dipole in the i direction (see Fig. 2.3 for an example). We can see this also by the fact

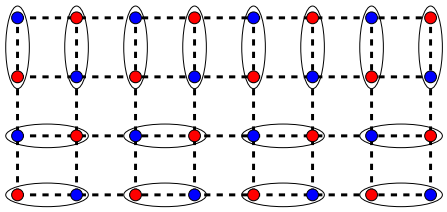

Figure 2.3: *Current of dipoles has to be described by a symmetric tensor since stacked configurations of charges like the one in the figure can be interpreted in different ways. For example here it could be both a current of x or y-oriented dipoles.*

that in the action of SCT a source term enters, as in the one-form theory, coupled to the gauge field as $A_{ij}J^{ij}$ and would not be sensitive to any anti-symmetric components. The Hamiltonian reads

$$\mathcal{H} \propto \int \frac{1}{2}E_{ij}E^{ij} + \frac{1}{2}B_{ij}B^{ij} + A_{ij}J^{ij} \tag{2.43}$$

and the equations of motion for E_{ij} yield the generalized Ampere equation

$$\frac{1}{2}\left(\epsilon^{imn}\partial_m B_n^{\ j} + \epsilon^{jmn}\partial_m B_n^{\ i}\right) = -J^{ij} - \partial_t E^{ij} \tag{2.44}$$

This can be seen as a fundamental definition of the currents J^{ij}: as the charge density ρ represented a violation of Gauss' law and so a deviation from the pure gauge theory, here J^{ij} represents a deviation of Ampere's law from pure gauge theory. From Ampere's law we can derive the generalized continuity equation

$$\partial_t \rho + \partial_i \partial_j J^{ij} = 0 \tag{2.45}$$

J^{ij} represents the rate of multi-body hopping processes, instead of the single body analogue for usual continuity equations. It is possible to derive an analog of Biot-Savart law where a steady current produces a magnetic field [30]

$$B^{ij} = -\frac{1}{6\pi}\int dr' J^i_{\ k}(r')\epsilon^{ikl}\frac{(r-r')_l}{|r-r'|^3} \tag{2.46}$$

The scaling of this law is the same as for electromagnetism, where the magnetic field produced by a current in a wire decays as $1/r$ away from it. So, while electric fields of static charges are hugely energetically costly, magnetic fields of steady currents are in line with standard electromagnetism.
It is possible to go on and describe also all the magnetic sector of this theory, which will be different from the electric sector because of the lack of electromagnetic duality of the theory [30]. All together we can summarize the Maxwell laws for SCT as

$$\partial_i\partial_j E^{ij} = \rho \tag{2.47a}$$

$$\frac{1}{2}\left(\epsilon^{imn}\partial_m B_n^{\ j} + \epsilon^{jmn}\partial_m B_n^{\ i}\right) = -J^{ij} - \partial_t E^{ij} \tag{2.47b}$$

$$\partial_i B^{ij} = \tilde{\rho}^j \tag{2.47c}$$

$$\epsilon^{imn}\partial_m E_n^{\ j} = \partial_t B^{ij} + \tilde{J}^{ij} \tag{2.47d}$$

2.2.4 Electromagnetic duality and stability

Usual compact rank-1 $U(1)$ gauge theory exhibits a duality between electric and magnetic charges. Magnetic monopoles arise from the compactness of the gauge field. In fact, the form of the magnetic field $B_i = \epsilon_{ijk}\partial^j A^k$ seems to automatically obey $\partial_i B^i = 0$. But since A_i is only defined modulo 2π, in general there can be

$$\partial_i B^i = 2\pi n \tag{2.48}$$

for integer n. Such defects correspond to magnetic charges of strength n. The properties of these charges are the same as for the electric charges, in a manifestation of electromagnetic duality. In fact, it is possible to construct the theory by changing the role of electric and magnetic sectors. By means of the Gauss' law $\partial_i E^i = 0$ we can write the electric field as the rotor of a compact dual vector gauge field $\tilde{A}_i$ as

$$E_i = \epsilon_{ijk}\partial^j \tilde{A}^k \tag{2.49}$$

In terms of this variable the electric and magnetic field have simply exchanged places, giving a dual formulation of the theory. This also tells us that magnetic defects are excitations and not instantons, thus the theory is stable. In general, a theory with such electromagnetic duality will not suffer from confinement due to proliferation of instantons

[26]. However, this is not the case for SCT. In fact, in this theory the magnetic field has the non-symmetric form given by (2.10). Despite the lack of self-duality, due to the compactness of the gauge field A_{ij}, the theory has magnetic charges, denoted by f_i, given by

$$\partial_i B^{ij} = 2\pi f^j \tag{2.50}$$

It is possible to show that these are two-dimensional vector particles which can move only in directions orthogonal to their charge vector. This can be easily seen by observing that

$$\int \vec{x}\cdot\vec{f} = \int \frac{1}{2\pi} x_i \partial_j B^{ji} = \frac{1}{2\pi}\oint x_i B^i - \frac{1}{2\pi}\int B^i{}_i = const. \tag{2.51}$$

due to the tracelessness of B. Thus, since magnetic defects are point like excitations with well defined energy and structure, SCT is stable against confinement by instanton proliferation.

Nevertheless, the form of the electrostatic energy of fractons (2.38a), which grows with the separation between fractons, is not ideal since it implies that the energy stored in the electric field of an isolated fracton is actually infinite. Also, a linear potential between two fractons implies that there is an attractive force independent of the distance always seeking to recombine the particles into the vacuum, meaning that they never become independent and are thus confined. However, in this case fractons have an electric field which dies as $1/r$ and so at large distances they do not feel each other. This means that the large energy associated with separating particles does not arise by the interaction with the electric field of the other particle, but from the energy needed to create their individual electrostatic fields. These two concepts usually coincide but here instead the immobility of fractons makes the notion of force not well defined, since there is no sense in which one fracton can do work to move a particle against the field.

Thus, fractons experience this milder form of confinement, dubbed *electrostatic confinement*, which is only felt in the large energy cost needed to create well separated fractons. In fact, the gauge field does not acquire a gap like in traditional Polyakov confinement [26] and after creating the particle there will be no restoring force seeking to recombine it into the vacuum. The only effect will be that of inhibiting fractons from being created by thermal fluctuations, since they are too energetically costly.

In concluding the description of SCT let us note that in our construction of Sec. 2.2.1 electric dipoles are bosonic particles. In fact, we can exchange two dipoles without having any sign popping out. The same holds for the magnetic monopoles, which are given by (2.50). Despite all these trivial statistics, a magnetic vector charge and a parallel coplanar electric dipole have mutual π statistics. To show this it is easier to wind the dipole around the monopole, as in Fig. 2.4. The effective magnetic field felt by the dipole p^i will be $B^i_{\text{eff}} = -p_j B^{ij}$. By the definition of magnetic monopole, the effective magnetic field seen by the dipole will respect $\partial_i B^i_{\text{eff}} = -2\pi\,(p\cdot f)$. Let us take the dipole and the monopole to have the same unit strength. When they are parallel $\partial_i B^i_{\text{eff}} = -2\pi$, so the

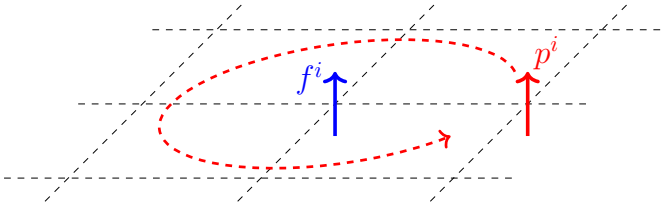

Figure 2.4: *Braiding of an electric dipole around a coplanar magnetic monopole in Scalar Charge Theory.*

dipole sees the magnetic vector as a unit monopole of its effective magnetic field. This means that a surface enclosing the magnetic vector will see a -2π flux of the effective magnetic field for the dipole. When the dipole is wound around the vector in their plane of mutual motion, we can conclude by symmetry that the enclosed flux is precisely half of the total, i.e. $-\pi$. Thus, when an electric dipole is wound around a magnetic vector charge within their mutual plane of motion, the wave-function of the system picks up a factor $e^{-i\pi} = -1$. Concluding, an electric dipole moment and a coplanar parallel magnetic vector are mutual semions (anyons) and together they form a fermion. It looks strange to find particles having non-standard statistical properties in more than 2 dimensions, but in this case it happens because of the kinetic restrictions.

2.3 Finite densities of fractons

Let us move on to a review of the progress in the field of fracton phases at finite densities. First of all, the mechanism by which fractons move in the vicinity of other fractons by the emission of a "virtual" dipole is analyzed in Sec. 2.3.1. This mechanism is shown to lead to a microemulsion behavior when in the presence of a finite density of fractons. Then, in Sec. 2.3.2 the behavior of a finite density of fermionic dipoles in $3D$ is studied which exhibit characteristics of usual Fermi-Landau liquid theory but with some interesting developments. Further, the problem of stability in $2D$ is tackled in order to study the presence of quantum Hall states of dipoles. In Sec. 2.3.3 the stability of $2D$ fracton phases with the addition of a generalized Chern-Simons term is studied while in Sec. 2.3.4 the phase obtained by considering a $2D$ gas of fermionic dipoles is analyzed. This latter is shown to yield a generalized form of the usual quantum Hall effect.

2.3.1 Self-interaction between fractons

In the presence of finite densities of fractons, new possibilities for the interactions emerge. In fact, even though fractons are immobile excitations, they can move by exchanging a dipole moment virtual particle with another fracton nearby. This exchange mechanism makes them mobile only when in vicinity of other fractons. In particular, the propagation

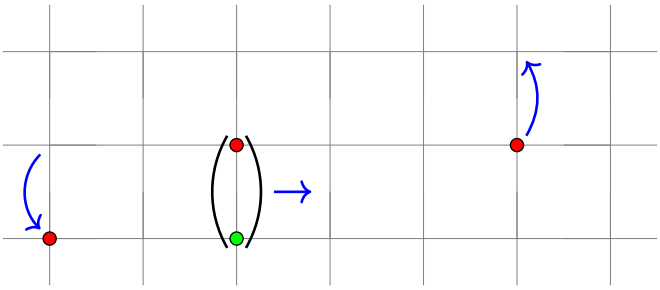

Figure 2.5: *Dipole exchange interaction between fractons. This interaction does not involve the gauge field.*

speed drops as the separation increases, making this interaction an effective attraction (see Fig. 2.5). The normal logic of attraction is in some way changed in this context. In fact, here the motion is not intrinsic to the body which feels some sort of forces by other particles. In this case motion is inherently a cooperative effect: as fractons approach each other they do not increase their velocity because of the effect of a force per se, rather they are increasing each other's mobility through a more rapid exchange of dipole particles. This is a phenomenon reminiscent of gravity [13] since the mobility of the charges depends by the configuration of matter in the system. Also, the exchange of a dipole amounts to the exchange of a center of mass information, since in gravitational systems the center of mass is always conserved.
The characteristic interaction between fractons will thus be proportional to their density and it is possible to show that it is short ranged, in general of the form [13]

$$V(r) \sim -V_0 e^{-Mr} \tag{2.52}$$

where M is the energy gap of the dipoles which permit this interaction. In the case where dipoles are gapless, this interaction falls off as a power law, becoming long ranged. The case where dipoles are massless can occur in a complex theory of gravity where non-linearity and gauge invariance can combine to guarantee the existence of such gapless dipoles, but this issue goes beyond the scope of this thesis [28, 31].
Note that while like-charged fractons effectively attract each other, oppositely charged fractons do not repulse. In fact, always by conservation of dipole moment, they simply have to move in the same direction upon exchange of a dipole. Thus, oppositely charged dipoles cannot attract or repel each other, just maintain a fixed distance.
Let us now consider the case of a finite density of fractons in $3D$ [12]. As we have seen these excitations exhibit a short-ranged attraction through the exchange of a virtual dipole moment. The form of this interaction is given by (2.52). Further, depending on the theory under consideration, they will have another form of interaction mediated by the gauge mode. In the case of SCT this is given by (2.38a) but in general the potential

could be given by a long-range repulsion of the form

$$V_{lr}(r) = V_1 r^n \tag{2.53}$$

The competition of these two interactions leads to the phenomenon of microemulsion [32]. At short scales the attraction will dominate forming clusters of fractons which will behave as droplets in a phase dominated by long-range repulsion forming a Wigner crystal [33] of such fracton clusters. If the repulsion is increased than the clusters will become smaller till the point of being formed by just one fracton each and the system becomes a Wigner crystal of individual fractons. Instead, if the attraction is increased the clusters will collapse into a single big cluster.
It is possible to show that microemulsion physics, with finite size clusters emulsed in a Wigner crystal of clusters, is obtained only for repulsive potentials whit $0 > n > -3$ [12]. In the case of SCT the form of the interaction has $n = 1$ meaning that the repulsion dominates and the resulting phase will feature fractons which are spaced apart as much as possible.

2.3.2 Dipolar Fermi liquids

Let us now consider the case of a finite density only of dipolar bound states, remaining in 3 dimensions. As we saw above, dipoles in SCT are freely moving excitations which interact between each other according to (2.38b). In the following discussion we will assume dipoles to have a minimal size, i.e. that dipole moment is quantized, and also that dipoles are fermions. This last assumption is in contrast to the lattice model described before, where dipoles were bosons. However, in principle nothing prevents dipoles from exhibiting fermionic statistic. At the moment there is no lattice model which describes such excitations, but there are several arguments which indicate that fermionic dipoles should be realizable. For example, we will show in Sec. 2.3.3 that θ-terms can be added to SCT and have the effect of attaching dipole moments to the magnetic monopoles of the theory. This phenomenon of flux attachment can produce the same effect as in Maxwell theory, where magnetic monopoles become fermions. In this way, by adding an appropriate θ term, it should be possible to convert dipoles into fermions.
Fermionic dipoles have phases of matter directly analogous to conventional electronic phases. The simplest configuration of the system is that where dipoles form a Fermi surface [3]. Here dipoles are interacting, so in order to justify the existence of a stable Fermi liquid it is necessary to look in detail at the interaction between dipoles. The easiest system to consider is that where are present only dipoles oriented in a certain direction. By the conservation of dipole moment we know that these dipoles cannot change their direction and their interaction has the form

$$V(r) = \frac{p^2 \sin^2(\theta)}{8\pi r} \tag{2.54}$$

As we saw above, this interaction for like dipoles is always repulsive and vanishes when dipoles are disposed along a line. The scaling of this interaction is exactly that of a Coulomb interaction between electrons, so we can treat it as an anisotropic Coulomb force. This suggests that as in usual Fermi liquid theory, dipoles will be able to screen each other.

This screening can be seen through an electrostatic calculation [34]. We consider a Fermi surface of dipoles all oriented in the same direction and then add a test dipole. The potential energy felt by a dipole will be $p^i\partial_i\phi$, with ϕ being the perturbing potential. The induced dipole moment density will be $-p^j(gp^i\partial_i\phi)$ with g the density of states of dipoles at the Fermi surface. Then we can write a self consistency equation for the potential

$$\phi(r) = \phi_{\text{bare}}(r) - \int dr'(gp^i\partial_i\phi(r'))\frac{p^j(r_j - r'_j)}{8\pi|r - r'|} \tag{2.55}$$

Integrating by parts and taking the Fourier transform we can solve for the potential $\phi(k)$ which results

$$\phi(k) = -i\frac{pk_p}{k_\perp^4 + gp^2k_p^2} \tag{2.56}$$

where k_p is the component of k^i in the p^i direction and $k_\perp$ the orthogonal projection. We can then derive the inter-particle potential energy between dipoles $V = p^i\partial_i\phi$ which has the form the form

$$V(k) = \frac{(pk_p)^2}{k_\perp^4 + gp^2k_p^2} \tag{2.57}$$

Thus, we see that the effect of the screening is that of reducing the interaction to a short-ranged repulsion between dipoles. Then, the usual aspects of Fermi liquid theory will carry over unaffected. There will be a discontinuity in the occupation number at a Fermi surface in momentum space. The dipole moment is now serving simply as an additional quantum number. Nevertheless, the anisotropy of the dipoles' interaction has the result of modifying the shape of the Fermi surface since equal dipoles will tend to arrange themselves more densely in the direction of their dipole moment.

In such Fermi liquid of dipoles it is interesting to study what happens to fractons. Even though they are no longer at finite density, they can still appear as excitations of the system. As we saw above, bare fractons have an interaction potential energy which scales linearly in the distance. In the case of a finite density of dipoles something interesting happens, namely that this interaction gets screened by the dipoles and becomes logarithmic in the distance.

The way to see this screening behavior is similar to the procedure employed in the previous electrostatic calculation. We take a Fermi surface of dipoles, put a perturbing fracton and see how things change. The potential energy of a fracton is given by (2.38a) and the dipoles will still have an induced dipole moment density given by $-p^j(gp^i\partial_i\phi)$.

So, the self consistency equation (2.55) is modified into

$$\phi(r) = -\frac{qr}{8\pi} - \frac{gp^i p^j}{8\pi} \int dr' \phi(r') \left(\frac{\delta_{ij}}{|r-r'|} - \frac{(r_i - r'_i)(r_j - r'_j)}{|r-r'|^3} \right) \tag{2.58}$$

Now the procedure is the same as before: by Fourier transforming we obtain $\phi(k)$, we solve the equation to find it and then we Fourier transform back to coordinate space. The result is [12]

$$\phi(r) = \int \frac{dk_p d^2 k_\perp}{(2\pi)^3} \frac{q}{k_\perp^4 + gp^2 k_p^2} e^{i(k_p r_p + k_\perp \cdot r_\perp)} \tag{2.59}$$

We can evaluate it in the two directions orthogonal and longitudinal to the dipole moment direction. First, putting $r_p = 0$ we get

$$\phi(r_\perp) = \frac{q}{4\pi\sqrt{gp^2}} \log(r_\perp) \tag{2.60}$$

Taking instead $r_\perp = 0$ yields

$$\phi(r_p) = \frac{q}{16\sqrt{gp^2}} \log(r_p) \tag{2.61}$$

Thus, the presence on a dipolar Fermi surface can eliminate the issues of electrostatic confinement and allows fractons to be separated more easily. Still, the energy cost to create an isolated fracton scales as $\log(L)$, where L is the system size, and this is reminiscent of vortexes in two-dimensional superfluids [35]. Similarly to superfluids it is natural to expect that fractons will proliferate above a certain critical temperature. The free energy associated with a fracton will take the form

$$F \sim \left(\frac{1}{\sqrt{g}} - T \right) \log(L) \tag{2.62}$$

and so fractons will proliferate when this becomes negative, i.e. above the critical temperature

$$T_c \sim \frac{1}{\sqrt{g}} \tag{2.63}$$

Below this temperature fractons will exist mostly in bound states, like dipoles. Above the transition they will be able to unbind and behave independently like in a BKT transition. This transition destroys the Fermi surface and, since the temperature is finite, fractons lose their immobility becoming able to move around the system, even if very slowly, thus resulting in a trivial phase.

2.3.3 Generalized Chern-Simons theory

Let us now change the dimensionality and consider a $2D$ system with a finite density of dipoles [12, 36]. Since dipoles are taken to be fermions, we expect to see a phenomenon reminiscent of quantum Hall states, with chiral edge states. First of all, we ask weather or not our fractonic tensor gauge theories can be stable in 2 spatial dimensions, since as we saw above in Sec. 2.2.4 instanton proliferation is expected to destroy the phase. Nevertheless, as in usual electromagnetism, the theory can be made stable by the addition of a suitable Chern-Simons term which prevents the gapless gauge modes to be confined in $2D$.
First of all we need a Lagrangian formulation of the theory. This can be obtained starting from the low energy Hamiltonian. The partition function of the system can be written as

$$\mathcal{Z} \propto \int \mathcal{D}A\mathcal{D}E\delta(\partial_i\partial_j E^{ij}) e^{i\int (E_{ij}\dot{A}^{ij} - \mathcal{H})} \tag{2.64}$$

We can introduce one Lagrange multiplier ϕ in order to enforce Gauss' law as $\delta(\partial_i\partial_j E^{ij}) \sim \int \mathcal{D}\phi e^{-i\int \phi\partial_i\partial_j E^{ij}}$. Then, integrating by parts two times this term, we can integrate out the field E_{ij} resulting into

$$\mathcal{Z} \propto \int \mathcal{D}A\mathcal{D}\phi e^{i\int \left(\frac{1}{2}\left(\dot{A}_{ij} - \partial_i\partial_j\phi\right)^2 - \frac{1}{2}B_{ij}B^{ij}\right)} \tag{2.65}$$

Coupling the field also with charges results into the Lagrangian

$$\mathcal{L}\left[A_{ij}, \phi\right] = \frac{1}{2}\left(\dot{A}_{ij} - \partial_i\partial_j\phi\right)^2 - \frac{1}{2}B_{ij}B^{ij} - \phi\rho - A_{ij}J^{ij} \tag{2.66}$$

for charge density ρ and current density J^{ij}.
Now we can introduce a so-called θ-term as in usual electromagnetic theory, where it takes the form $\vec{E}\cdot\vec{B}$. This term has to be gauge invariant and will turn out to be a solely boundary term, since it can be written as a total derivative. Further, it will have the effect of attaching charge to fluxes. For SCT, charges are scalars while magnetic excitations are vectors. So, the most natural form of combining charges in this theory is attaching an electric dipole moment to a magnetic vector. This additional term assumes a similar form to electromagnetism as

$$\begin{aligned} S_\theta =& \frac{\theta}{4\pi^2}\int \left(\dot{A}_{ij} - \partial_i\partial_j\phi\right)\epsilon^{iab}\partial_a A_b^{\ j} \\ =& \frac{\theta}{4\pi^2}\int \partial_a\left(\frac{1}{2}\epsilon^{iab}\dot{A}_{ij}A_b^{\ j} + \partial_j\phi\epsilon^{iab}\partial_i A_b^{\ j}\right) - \frac{1}{2}\partial_t\left(\epsilon^{iab}\partial_a A_{ij}A_b^{\ j}\right) \end{aligned} \tag{2.67}$$

Introducing this term, the total action of the system becomes

$$S = \int \left(E^{ij} + \frac{\theta}{4\pi^2}B^{ij}\right)\left(\dot{A}_{ij} - \partial_i\partial_j\phi\right) - \frac{1}{2}E^2 - \frac{1}{2}B^2 \tag{2.68}$$

Since it can be written as a total derivative it will not have any effect on the low energy gauge mode in the bulk, but instead it leads to a Chern-Simons term on a boundary between the system and an external region with $\theta = 0$. Integrating by parts the ϕ term two times and integrating out ϕ, which is a Lagrange multiplier, from the path integral yields the gauge constraint given by

$$\partial_i \partial_j E^{ij} = -\frac{\theta}{4\pi^2} \partial_i \partial_j B^{ij} \tag{2.69}$$

This can be re-written in terms of the charges $\partial_i \partial_j E^{ij} = \rho$ and $\partial_i B^{ij} = 2\pi f^j$ as

$$\rho = -\frac{\theta}{2\pi} \partial_i f^i + n \tag{2.70}$$

The above relation shows that the effect of this θ-term is that of attaching fractonic electric charges to the endpoints of the magnetic charge vectors. It is like a dipole is attached to each magnetic vector, as anticipated above. Since electric charges are costly to create, this term will favor configurations where groups of magnetic vectors line up in string arrangements.

Let us now look at the periodicity of θ. It seems that at $\theta = 2\pi$ we have returned to the starting point, but we have to consider also the statistic of particles. In this case, by noting that two parallel vector and dipole moments have mutual π statistic (see the end of Sec. 2.2.4), together they will form a fermion. This means that θ will be 4π periodic.

Let us now study the boundary terms which arise as a consequence of the Chern-Simons action. Consider a spatial boundary with normal oriented in the z-direction. The action (2.67) will take the form

$$S_\partial = \frac{\theta}{4\pi^2} \int_\partial \left(\frac{1}{2} \epsilon^{bi} \dot{A}_{ij} A_b^{\ j} + \partial_j \phi \epsilon^{bi} \partial_i A_b^{\ j} \right) \tag{2.71}$$

where ϵ^{ij} is the 2-dimensional Levi-Civita symbol. Let us note that the A_{zz} component of the gauge field is no more present in the boundary theory, but there are still terms $\propto \partial_z$. It is thus useful to introduce the decomposition

$$\begin{cases} A_{ij} = a_{ij} & \text{for } i,j = x,y \\ A_{iz} = \lambda_i & \text{for } i = x,y \end{cases} \tag{2.72}$$

In the action (2.71) ϕ and $\partial_z \phi$ can be varied independently so they act as Lagrange multipliers from which we can deduce the equations of motion

$$\frac{\delta S}{\delta \phi} = 0 \quad \Longrightarrow \quad -\frac{\theta}{4\pi^2} \epsilon^{bi} \partial_i \partial_j a_b^{\ j} = 0 \tag{2.73a}$$

$$\frac{\delta S}{\delta \partial_z \phi} = 0 \quad \Longrightarrow \quad \frac{\theta}{4\pi^2} \epsilon^{bi} \partial_i \lambda_b = 0 \tag{2.73b}$$

The remaining dynamical term instead reads

$$S_{\text{dyn}} = \frac{\theta}{4\pi^2}\int_\partial \frac{1}{2}\epsilon^{bi}\left(\dot{a}_{ij}a_b^{\ j} + \dot{\lambda}_i\lambda_b\right) \tag{2.74}$$

We note that it is convenient to separate the gauge field into a trace and a traceless symmetric part as $a_{ij} = \tilde{a}_{ij} + \gamma\delta_{ij}$. In this way the trace disappears from (2.74) and the constraints (2.73a). The remaining theory is now decoupled in λ_i and $\tilde{a}^{ij}$.
The λ part is a standard Chern-Simons theory where charges have no restriction in motion. Instead, the $\tilde{a}$ theory is more subtle: it is a chiral generalized Chern-Simons theory described by the action

$$S_{\text{dyn}} = \frac{\theta}{8\pi^2}\int \epsilon^{bi}\dot{\tilde{a}}_{ij}\tilde{a}_b^{\ j} \tag{2.75}$$

leading to the equations of motion

$$-\frac{\theta}{4\pi^2}\epsilon^{bi}\partial_i\partial_j\tilde{a}_b^{\ j} = 0 \tag{2.76}$$

The two components of $\tilde{a}$ form a conjugate pair. This implies that the one constraint we have, (2.76), is enough to fix the theory, thus not leaving any local degree of freedom. Allowing for the appropriate gauge charges coupled to the field, the conserved charge $\rho = \epsilon^{bi}\partial_i\partial_j\tilde{a}_b^{\ j}$ has conserved dipole moment, thus yielding a chiral 2-dimensional stable fracton phase.
Finally, we can verify the presence of an energy gap, and thus the stability of the theory, by considering the regularized theory in 2-dimensions. In this case, since we are looking at the theory for $\tilde{a}_{ij}$, which is traceless, we need to include a Maxwell term appropriate to *traceless* scalar charge theory [10]

$$\begin{aligned} S = \int \frac{1}{2e^2}\left(\left(\dot{\tilde{a}}_{ij} - \left(\partial_i\partial_j - \frac{1}{2}\delta_{ij}\partial^2\right)\phi\right)^2 - \left(\epsilon^{ij}\partial_j\partial^k\tilde{a}_{ik}\right)^2\right) + \\ + \frac{\theta}{8\pi^2}\left(\epsilon^{bi}\dot{\tilde{a}}_{ij}\tilde{a}_b^{\ j} - 2\phi\epsilon^{bi}\partial_i\partial_j\tilde{a}_b^{\ j}\right) \end{aligned} \tag{2.77}$$

The Euler-Lagrange equations of motion for this action yield $\frac{1}{e^2}\dot{E} \propto \theta E$ and so an energy gap scaling as $\Delta \sim \theta e^2$. This means that at low energy the theory is gapped, so the Chern-Simons term is capable of fully gaping the traceless scalar charge theory, yielding a stable 2-dimensional phase of matter.

2.3.4 Quantum Hall states of dipoles

Summarizing, in Sec. 2.3.3 we found that the Chern-Simons term can stabilize SCT in $2D$, and results in a completely gapped phase, with the low energy physics of this phase

described by a traceless symmetric rank-2 field $\tilde{a}_{ij}$ (2.77). This is a generalized version of Chern-Simons theory, which usually contains vector gauge fields. As in the more usual theory also in this generalized version the coefficient θ is quantized in units of 2π

$$\theta = 2\pi k, \qquad k \in \mathbb{Z} \tag{2.78}$$

Let us now look at the particle content of the theory. The ϕ constraint imposes in the low energy sector

$$-\frac{k}{2\pi}\epsilon^{bi}\partial_i\partial_j\tilde{a}_b^{\ j} = 0 \tag{2.79}$$

or in general, allowing for charges, $-\frac{k}{2\pi}\epsilon^{bi}\partial_i\partial_j\tilde{a}_b^{\ j} = \rho$. From this we can establish the conservation laws

$$\int \rho = \text{const.} \tag{2.80a}$$

$$\int \vec{x}\rho = \text{const.} \tag{2.80b}$$

$$\int x^2\rho = \text{const.} \tag{2.80c}$$

We see that there is an additional conservation law with respect to usual SCT. This is due to the fact that the gauge field now is traceless. Dipoles are no longer completely mobile particles, but are restricted to move only in the direction orthogonal to their dipole moment. This restriction in motion arises naturally also due to the fact that there has been a flux attachment caused by the Chern-Simons term, in fact

$$\rho = \frac{k}{2\pi}\partial_i\tilde{B}^j \tag{2.81}$$

Remembering now that magnetic vectors are restricted to move orthogonally to their direction, dipoles simply inherit this restriction since to each of them is attached a magnetic flux $2\pi/k$.
By coupling this theory with a current J^{ij} the Hall response of the system will be [12]

$$\langle J^{ij}\rangle = -\frac{\delta S}{\delta\tilde{a}_{ij}} = \frac{k}{8\pi^2}\left(\epsilon^{ib}\dot{\tilde{a}}_b^{\ j}\epsilon^{jb}\dot{\tilde{a}}_b^{\ i}\right) = \frac{\theta}{8\pi^2}\left(\epsilon^{ib}E_b^{\ j} + \epsilon^{jb}E_b^{\ i}\right) \tag{2.82}$$

So, the conductivity tensor will be given by

$$\sigma^{ijkl} = \frac{\theta}{8\pi^2}\left(\epsilon^{ik}\delta^{jl} + \epsilon^{jk}\delta^{il}\right) \tag{2.83}$$

Differently from the Hall effect of a state of electrons, where the current is due to the response to an externally applied electromagnetic field, here there is no such external

field. In fact, here the conductivity is due to the response of the system to the internal emergent tensor electric field E_{ij}.
The integer k has the natural interpretation as the number of filled Landau levels occupied by the mobile dipoles. Hence, this phase corresponds to an emergent integer quantum Hall phase of dipoles. Differently from Chern-Simons theory, here there is no fractionalization of charge or change in the statistics. Instead, dipoles undergo a fractionalization of motion, being allowed to move only in $1D$ orthogonally to their dipole vector.
The description of the case where in (2.78) k takes non-integer values, thus the fractional quantum Hall effect analogue for fractons, has been developed in [12] along with the description of the resulting edge modes.

Chapter 3

Ergodicity-breaking and scar states

The restricted mobility of fractonic excitations naturally points to the subject of the thermalization of such phases. This is also the most interesting and important application of these exotic particles, and the first reason they have been studied so much. It is known that topological phases in two dimensions possess a logical subspace into which information may be encoded and that this subspace is immune to local perturbations. Nevertheless, this is possible only exactly at zero temperature, since thermal fluctuations destroy the state. Fracton phases are much more robust from this point of view because of the kinetic restrictions.
In order to study the thermal properties of fracton models, in Sec. 3.1 we describe the behavior of quantum ergodic systems through the *eigenstate thermalization hypothesis*, focusing of the observable quantities which characterize these systems such as entanglement entropy and level spacing statistics. Then, systems exhibiting a weak breaking of ergodicity, dubbed quantum many-body scars, are introduced and studied in deep in Sec. 3.2. Finally, in Sec. 3.3 we study the thermalization behavior of the X-Cube model in contact with a thermal bath to show that it exhibits a slow relaxation to a thermal state, in a way analogue to quantum glasses.

3.1 Eigenstate Thermalization Hypothesis

Thermalization and dynamical properties of quantum systems are topics which have attracted a wider attention in recent years due to the novel possible experimental verifications. It has recently become possible to simulate quantum systems (almost) completely decoupled from the environment and to observe their long-time behavior. We know that in classical systems the ergodic hypothesis assures us of the destiny of every chaotic model: it will thermalize and become independent of the initial conditions. In quantum systems the matter of thermalization and ergodicity is a bit more subtle. In fact, the ergodic hypothesis relies on the phase space description of a classical system: over a long

period of time the trajectory of an ergodic model will access all the phase space and the time spent in each region will be proportional to its volume. Time averages can then be taken to be equal to ensemble averages. In the quantum case there is not such a thing as the phase space trajectory, so the definition of an ergodic system needs to be formulated in a different manner.
It is believed that quantum thermalization is controlled by the properties of the system's many-body eigenstates, which evaluated on physical observables result in thermal expectation values. The Eigenstate Thermalization Hypothesis (ETH) [37–39] explains the microscopic mechanism of thermalization in isolated quantum systems considering the properties of the system's eigenstates. First we need to define what we mean by thermalization. A generic initial non-equilibrium state $|\psi(t_i)\rangle$ can in general be expanded over a basis of many-body eigenstates $\{|s\rangle\}$ as

$$|\psi(t_i)\rangle = \sum_s A_s |s\rangle \tag{3.1}$$

with the probability to find the state in an eigenstate $|s\rangle$ being $p_s = |A_s|^2$. An intuitive definition of thermalization is that at long times, independently from the initial state, the system's observables reach values given by the Gibbs' micro-canonical ensemble. Thus, the infinite-time expectation value of any physical observable $\hat{O}$ will be given by

$$\langle \hat{O} \rangle_\infty = \lim_{T\to\infty} \frac{1}{T} \int_0^T \langle \psi(t)| \hat{O} |\psi(t)\rangle \, dt = \sum_s p_s \langle s| \hat{O} |s\rangle \tag{3.2}$$

where only diagonal terms appear, since off-diagonal ones oscillate and therefore average out. Since the terms p_s are fixed by initial conditions, a natural way to assure this behavior at long times is to assume that the individual expectation values $\langle s| \hat{O} |s\rangle$ behave micro-canonically. This is the core of ETH: in ergodic systems individual many-body eigenstates have thermal observables, identical to micro-canonical ensemble values. This means that for an ergodic system, even if the initial state is an eigenstate, the subsystems will behave as if the rest of the system is a heat bath, and will explore all possible configurations (as classical ergodic systems). In this sense thermalization and ergodicity coincide, thus we will use them interchangeably. Also, asking that eigenstates follow the thermal expectation values of physical observables means that if we consider a set of eigenstates $\{|\epsilon_k\rangle\}$ and an observable $\hat{\mathcal{O}}$ then

- The diagonal elements $O_k = \langle \epsilon_k| \hat{\mathcal{O}} |\epsilon_k\rangle$ will vary slowly. In particular,

  $$\Delta_k = O_{k+1} - O_k \tag{3.3}$$

  will be exponentially small in system size.

- The off diagonal elements instead will simply be exponentially small, because of the loss of correlation in the thermal state.

ETH thus implies that the time average of a physical observable is a function of energy only and that it is independent of initial conditions, in agreement with the microcanonical ensemble.
ETH has many implications on the structure of the eigenstates and on the behavior of some observables. In particular, let us consider the entanglement properties of the thermal eigenstates. Considering a small subsystem ω the expectation values of all observables will be thermal. This implies that the reduced density matrix $\rho_\omega = \mathrm{Tr}_{\Omega\setminus\omega} |s\rangle \langle s|$ is also thermal. This leads us to the conclusion that the entanglement entropy of ω in state $|s\rangle$ will be given by the von Neumann (thermal) entropy [40]

$$S_\omega = -\operatorname{Tr} \rho_\omega \log \rho_\omega = S_{th} \tag{3.4}$$

Finally, highly excited eigenstates will have entanglement entropy following a volume-law, i.e. scaling proportionally to the volume of the subsystem ω.
Another characteristic is the strong sensitivity of ergodic eigenstates to external perturbations of the Hamiltonian. This can be observed from the effect it has on the level spacing distribution of the energy spectrum. Consider a set of ordered eigenvalues ϵ_i such that $\epsilon_i \leq \epsilon_{i+1}$ for $i = 1, \dots n$. Then the level spacings are defined as

$$s_i = (\epsilon_{i+1} - \epsilon_i)/\langle s \rangle \tag{3.5}$$

where $\langle s \rangle$ is the mean spacing value.
It is known that systems which thermalize follow a Wigner-Dyson distribution of level spacings, characteristic of random matrix ensembles [41]. This is a consequence of the strong sensitivity to external perturbations which causes level repulsion.

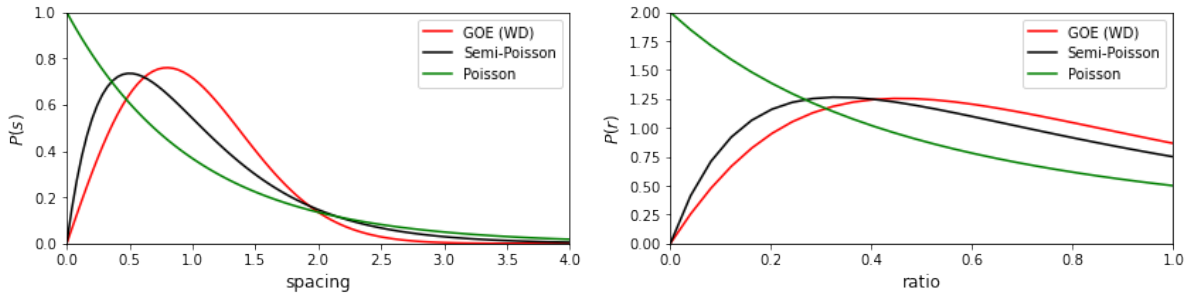

Figure 3.1: *Left panel: Probability distributions characterizing level spacing statistics in quantum systems. Right panel: Same probability distributions for consecutive spacing ratios.*

The Wigner-Dyson distribution is obtained through random matrix theory, by considering orthogonal (Gaussian Orthogonal Ensemble) or unitary (Gaussian Unitary Ensemble) matrices with entries which are Gaussian distributed with mean 0 and variance σ. It is used the GOE or the GUE if the systems respects or not time reversal symmetry

respectively. The probability distribution of spacings does not have a closed form but is very similar to the Wigner Surmise [41]

$$P(s) = A_\beta s^\beta \exp\left(-B_\beta s^2\right) \tag{3.6}$$

where $\beta = 1, 2$ refers to GOE and GUE respectively. The coefficients A_β and B_β are obtained by normalizing the distribution. The level repulsion can be seen by observing that the probability of having energy separation ω goes to zero for $\omega \to 0$. Also, at large energy separations the distribution decays in a Gaussian manner.
Differently, non-ergodic systems like integrable systems and many-body localized (MBL) phases, have been shown to follow a Poisson distribution of level spacings [39]. This was first conjectured by Berry and Tabor [42] for quantum systems with an integrable classical counterpart but holds for any non-ergodic system, like MBL. The distribution of level spacings in this case takes the form

$$P(s) = \exp(-s) \tag{3.7}$$

This is very different from Wigner-Dyson distribution in that there is no level repulsion in this case.
Another case to take into consideration is a middle step between Wigner-Dyson and Poisson, the so called Semi-Poisson distribution [43], which is likely to appear in systems exhibiting a milder form of ergodicity breaking, as in many body-scars that we will see below. The form of the distribution is given by

$$P(s) = 4s \exp(-2s) \tag{3.8}$$

and is reported in Fig. 3.1 along with the others.
A quantity which is usually considered instead of the level spacings are the level ratios

$$r_n = \frac{min(s_n, s_{n-1})}{max(s_n, s_{n-1})} \tag{3.9}$$

and their mean value

$$\langle r \rangle = \frac{1}{\mathcal{N}} \sum_n r_n \tag{3.10}$$

since spacing ratios have the advantage of not requiring unfolding [44] since they are independent of the local density of states [41]. These mean values are characteristic of the single distributions and are

$$\langle r \rangle_{WD} = 0.536 \tag{3.11}$$

for the WD,

$$\langle r \rangle_{P} = 0.386 \tag{3.12}$$

for Poisson and

$$\langle r \rangle_{SP} = 0.5 \tag{3.13}$$

for the Semi-Poisson [44].

3.2 Quantum many-body scars

As anticipated above, two main examples where the ETH does not hold are integrable systems and many-body localized phases (MBL). These non-ergodic systems are said to break ETH strongly, since all eigenstates have expectation values of physical operators not following the micro-canonical ensemble. What has been found recently is that there are systems which behave in an intermediate manner.
In a recent experiment on quantum simulators based on Rydberg atoms [18] it has been observed a peculiar dynamical behavior of the system which in a quench experiment, depending on the initial conditions, has been shown to fail in thermalizing. This anomalous behavior has been referred to as a weak breaking of ergodicity, since the initial states leading to a non thermal behavior represent a small fraction of all the states. These have been named *quantum many body scars* (QMBS)[45] in analogy to the weak breaking of ergodicity of a classical single particle inside a stadium billiard [46]. These scars are eigenstates which are present also in the highly excited energy spectrum of the system. Here ETH is said to be violated weakly since the anomalous eigenstates constitute a vanishing fraction of the Hilbert space and they are immersed in a sea of thermalizing eigenstates.
Let us first examine the model describing the Rydberg chain in Sec. 3.2.1. Following, we will see that many systems exhibiting QMBS have been found with a common characteristic being the presence of a subspace which is decoupled from the rest of the energy spectrum and which is not attributed to a symmetry of the system. We review the known mechanisms leading to weak ergodicity breaking in Sec. 3.2.2. Finally, in Sec. 3.2.3 we will see how to obtain scar states from modifications of "every-day" familiar models.

3.2.1 PXP model

The chain of Rydberg atoms can be effectively characterized as a PXP model [47]: each atom of the chain can be either in the ground state or in an excited state and, when subject to a microwave field, each atom can oscillate between the two configurations, but not freely. In fact, there is a constraint due to the fact that two excited atoms repel each other: this repulsion can be tuned to affect only nearest neighboring sites implementing the so-called Rydberg blockade [48]. This kinetic restriction implies that only atoms neighboring with ground state ones can flip to the excited state. Let us define the excited states to be $|\bullet\rangle$ and the ground states $|\circ\rangle$. In the exact limit, this system is described by the following spin-1/2 Hamiltonian

$$H_{PXP} = \sum_i P_{i-1} X_i P_{i+1} \tag{3.14}$$

where the X_i operator flips the i-th spin only if the two projectors are satisfied. These can be written as $P_i = |\circ\rangle_i \langle\circ|_i = (1 - Z_i)/2$. Due to the presence of projectors the

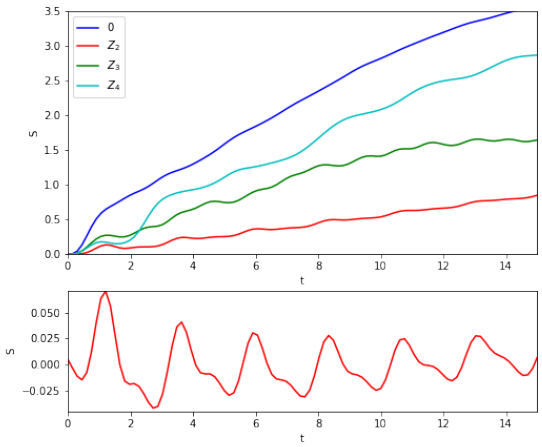

Figure 3.2: *Upper panel: Half-chain entanglement entropy evolution in time starting from different initial states. In particular are considered the state* $|0\rangle$, $|\mathbb{Z}_2\rangle$, $|\mathbb{Z}_3\rangle$ *and* $|\mathbb{Z}_4\rangle$. *We can see that the slope of the curve depends strongly on the initial conditions. Lower panel: by removing the linearly growing part from the* $|\mathbb{Z}_2\rangle$*-slope it is possible to observe periodic revivals persisting at long times.*

Hilbert space of the model acquires a non-trivial local constraint: configurations with two consecutive excited atoms are prohibited. It is possible to show [47] that the constrained Hilbert space of this model grows as the Fibonacci sequence. In particular, for a chain of length L with open boundary conditions the Hilbert space dimension will scale as $d \sim F_{L+2}$, with F_n the n^{th} Fibonacci number. For this reason the PXP model is often referred to also as the Fibonacci model.
The system described by (3.14) possess a particle-hole symmetry. The operator $\mathcal{P} = \prod_i Z_i$ anticommutes with the Hamiltonian, so every eigenstate $|\psi\rangle$ with energy E has symmetric partner $\mathcal{P}|\psi\rangle$ of energy $-E$. Also, the system has spatial inversion symmetry mapping $i \to L - i + 1$.
What has been observed in the experiment on Rydberg atoms is that the relaxation under unitary dynamics strongly depends on the initial configuration of the system: for almost all initial sates the system ends up thermalizing at long times, while for some particular states this behavior is lost. One of the non-thermalizing initial states that have been found is the Néel state $|\mathbb{Z}_2\rangle = |\circ \bullet \circ \bullet \circ \bullet \ldots\rangle$ and its partner $|\mathbb{Z}_2'\rangle = |\bullet \circ \bullet \circ \bullet \circ \ldots\rangle$.
It is possible to numerically simulate the system using exact diagonalization. In Fig. 3.2 we show the time evolution of the half-chain entanglement entropy for different initial states. To obtain these data was used the library QuSpin [49] with a chain of length $L = 19$ and open boundary conditions. It is possible to observe that the entanglement entropy grows linearly in time, as expected for ergodic systems. Nevertheless, the slope

of the curve depends on the initial states* and for Néel initial state it undergoes periodic oscillations. Special states like $|\mathbb{Z}_2\rangle$ can be distinguished through their entanglement properties as can be observed from Fig. 3.3. In fact, entanglement entropy should follow

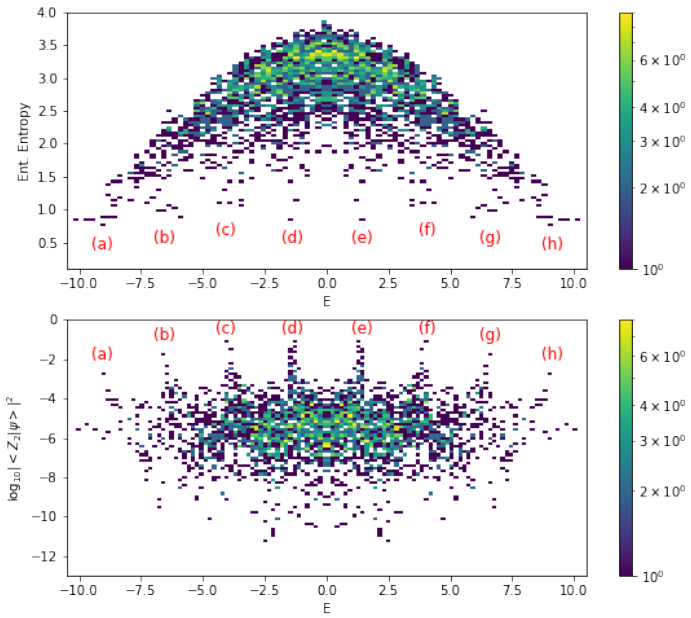

Figure 3.3: *Upper panel: Half-chain entanglement entropy evaluated for all eigenstates of an $L = 18$ PXP chain with open boundary conditions. The colors indicate the number of states lying in every singular bin, with the legend given by the lateral color-bar. Lower panel: overlap of eigenstates with the Néel state $|\mathbb{Z}_2\rangle$, with overlap defined by $\log_{10} |\langle \mathbb{Z}_2|\psi\rangle|^2$. States with high overlap with the Néel state form towers which coincide with low entanglement states in the upper panel.*

a volume law for thermal eigenstates while special states exhibit a sub-thermal amount of entanglement. We can also see that these states define bands of non-thermal eigenstates, characterized by having large overlap with the Néel state, also plotted in 3.3.
Finally, it is possible to show that the model is non-integrable by calculating the level spacing distribution. In order to do so we compute the energy level spacings and the ratios over consecutive spacings. These are plotted in Fig. 3.4 which shows also the

*With $|\mathbb{Z}_k\rangle$ we refer to states with period k: $|\ldots \underbrace{\bullet\circ\circ\cdots\circ}_{k} \ldots\rangle$.

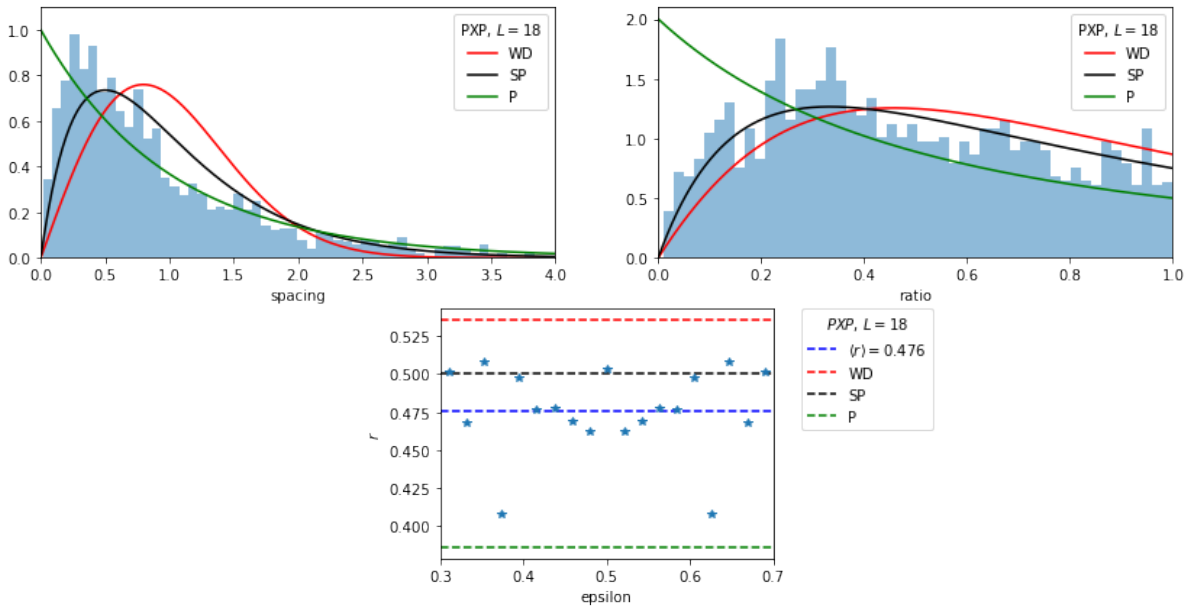

Figure 3.4: *Upper left panel: energy level spacing distribution. Upper right panel: ratio of consecutive spacings distribution. Bottom panel: Consecutive levels' ratios r plotted in function of the normalized energy ϵ with 20 steps. In all graphs was considered the central part of the spectrum $\epsilon \in [0.3, 0.7]$ and are also shown the values expected from WD, SP and P distributions.*

ratios plotted as a function of the normalized spectrum [50]

$$\epsilon_n = \frac{E_n - E_{min}}{E_{max} - E_{min}} \tag{3.15}$$

The statistic of the energy levels is approximately distributed close to the Semi-Poisson prediction, which is expected for systems weakly violating ETH.
The energy levels statistics together with the linear growth of entanglement rule out the integrability-based explanation of the non-ergodic dynamics of the system. In fact, for an integrable system we would expect a Poisson distribution of level spacings.

3.2.2 Mechanisms of weak ergodicity breaking

The mechanisms by which weak breaking of ergodicity may arise have in common the fact that the Hilbert space factors into two almost separated subspaces not related to any global symmetry of the full Hamiltonian

$$\mathcal{H} \approx \mathcal{H}_{scar} \bigoplus \mathcal{H}_{thermal} \tag{3.16}$$

Here $\mathcal{H}_{scar}$ contains all eigenstates violating ETH and is decoupled from the thermalizing subspace.

There are three mechanisms found so far [45] that explain this decoupled subspace: spectrum generating algebra, Krylov restricted thermalization and projector embedding.

- The first mechanism is the so-called *spectrum generating algebra*. The family of excited non thermalizing eigenstates is constructed by means of a local operator and allows to exactly construct scar eigenstates, which can physically be interpreted as quasi-particle condensates built on top of the system's ground state. The spectrum generating algebra is defined by a local operator $\hat{Q}$ satisfying the relation

$$\left(\left[H, \hat{Q}^\dagger\right] - \omega \hat{Q}^\dagger\right) W = 0 \tag{3.17}$$

  where W is a linear subspace of the full Hilbert space left invariant under the action of $\hat{Q}^\dagger$ and ω is an energy scale characterizing the operator $\hat{Q}$ and the corresponding subspace W. In QMBS W is not the full Hilbert space and $\hat{Q}^\dagger$ is *not* associated to any symmetry. Then, starting from an eigenstate $|\psi_0\rangle$ with energy E we can build a tower of states $\left(\hat{Q}^\dagger\right)^n |\psi_0\rangle$ which are all eigenstates with energy $E + n\omega$. These are candidates for QMBS.

- The spectrum generating algebra relies on the notion of the operator $\hat{Q}$ which is usually difficult to find, thus we can rely on another mechanism to realize exactly embedded subspaces, which is the *Krylov restricted thermalization* construction. For arbitrary Hamiltonian H and state of the Hilbert space $|\psi_0\rangle$, the Krylov subspace is defined as

$$\mathcal{K} = span\left\{|\psi_0\rangle, H|\psi_0\rangle, H^2|\psi_0\rangle, \dots\right\} \tag{3.18}$$

  A case of particular interest is when $\mathcal{K}$ is finite, i.e. for some n, $H^n|\psi_0\rangle = 0$. This causes a dynamical fracture of the Hilbert space since the Schrodinger dynamics realized starting from a state $|\psi\rangle \in \mathcal{K}$ remains in that subspace at any later time. Krylov subspaces occur in models of the fractional quantum Hall effect in a quasi-one dimensional limit and in models of bosons with constrained hopping on optical lattices. More generally Krylov fracture is present in models which feature a conservation of dipole moment, like fracton models [17], as we will show in the next Chapter.

- At last, there is the mechanism of *projector embedding*, which consists in incorporating an arbitrary subspace into the spectrum of a thermalizing system. This can be achieved via the projection embedding procedure: starting from a set of non-thermalizing states $|\psi\rangle$ it is assumed that these are annihilated by some local projectors $P_i|\psi\rangle = 0$. Next, by considering a lattice Hamiltonian of the form

$$H = \sum P_i h_i P_i + H' \tag{3.19}$$

where h_i are arbitrary operators with support on a finite number of sites around i and $[H', P_i] = 0$. Then, it is straightforward to show that $[H, \sum_i P_i] = 0$ and so that H takes the block diagonal form of eq. (3.16). Physical mechanisms such as geometrical frustration in correlated materials can implement the projector embedding. Also, it is particularly useful for various topologically ordered lattice models, which are themselves defined in terms of projectors [51]. Deformations of such models, including the toric code and X-Cube, can be used to embed scar states, as will be done in the next section.

3.2.3 More on topological scar states

Violation of ETH can be detected from some indicators: (i) sub-volume law scaling of for the entanglement entropy of eigenstates, (ii) emergent local integrals of motion in non-integrable systems and (iii) oscillations in the expectation value of suitably chosen local observables under the unitary time evolution. Analytical progress in quantum many body scars is difficult because of the non-integrability of the models. On the other hand, numerical techniques to obtain highly excited states rely mostly on exact-diagonalization. Thus, these are limited by the reachable system sizes, which are often too small to have an extrapolation of the thermodynamic limit. This is why studies on ETH-violating systems are mostly focused on $1D$ models.
In this section we will derive scar states by suitably modifying exactly solvable models. First of all consider a general local Hamiltonian [51]

$$H(\beta) = \sum_s \alpha_s \mathcal{Q}_s(\beta) \tag{3.20}$$

where the operators $\mathcal{Q}_s$ are Hermitian, positive semi-definite and local. Let us consider these operators to be parameterized by a parameter β. The index s labels a bounded region of space the operator acts non-trivially on (it could be for example the plaquettes of a square lattice). These operators are built so as to share a common null state $|\Psi(\beta)\rangle$, i.e. such that

$$\mathcal{Q}_s(\beta)\,|\Psi(\beta)\rangle = 0, \qquad \forall s \tag{3.21}$$

If all couplings α_s are positive, then $|\Psi(\beta)\rangle$ is the ground state of the Hamiltonian since the $\mathcal{Q}_s$ operators are positive-semidefinite. In contrast, if the couplings take both positive and negative values, this is not guaranteed. $|\Psi(\beta)\rangle$ is still an eigenstate with energy 0 and even when it is a highly energy eigenstate it is atypical since it displays an area entanglement entropy law, being a ground state for a different local Hamiltonian, namely $\tilde{H}(\beta) = \sum_s |\alpha_s| \mathcal{Q}_s(\beta)$. This tells us that $|\Psi(\beta)\rangle$ is a scar state, if $H(\beta)$ is non-integrable.
To obtain scar states the underlying idea is that of deforming exactly solvable spin models in order to break integrability while retaining the $E = 0$ scar state. In this way it is

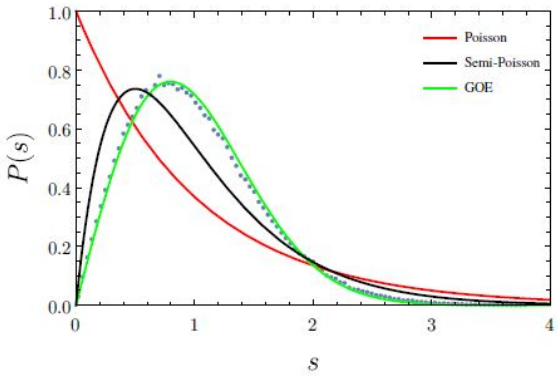

Figure 3.5: *Consecutive level spacings for the* $1D$ *Hamiltonian defined in* (3.22)*. Figure taken from [51].*

possible to construct scar states in any dimension.
Let us start with the topologically trivial example of a $1D$ spin-1/2 chain on a ring of length L. The local Hamiltonian under consideration has the form (3.20) with

$$\alpha_s = (\alpha + (-1)^s), \qquad \mathcal{Q}_s(\beta) = e^{-\beta(Z_{s-1}Z_s + Z_sZ_{s+1})} + X_s \tag{3.22}$$

where $\beta \geq 0$ and $0 < |\alpha| < 1$. Here s labels the sites of the chain.
For $\beta = 0$ this reduces to a paramagnetic chain in a Zeeman field, which is integrable. However, for $\beta \neq 0$ the operators on nearest-neighbor sites no longer commute, indicating that the Hamiltonian is no longer integrable. This can be confirmed by numerically [51] studying the distribution of consecutive energy level spacings which turn out to match the Wigner-Dyson distribution, thus supporting this claim. The spacings are plotted in Fig. 3.5.
One can then verify that the state

$$|scar(\beta)\rangle = G(\beta) \bigotimes_i |+\rangle_i^x \tag{3.23}$$

where $|+\rangle_i^x$ is the state such that $X_i\,|+\rangle_i^x = +1\;|+\rangle_i^x$ and $G(\beta) = exp\left(\frac{\beta}{2}\sum_s Z_sZ_{s+1}\right)$ is annihilated by $\mathcal{Q}_s$ for all s. So, as seen above, $|scar(\beta)\rangle$ is the ground state of the local Hamiltonian $\tilde{H}(\beta) = \sum_s |\alpha_s|\mathcal{Q}_s(\beta)$.
This kind of construction can be used to obtain scar states in many other non-trivial models. An interesting example is that of scar states arising in a deformation of the SPT cluster model in $1D$ (see App. A). Let us consider a spin-1/2 ring of $2L$ sites described by the Hamiltonian $H_{1D} = H_1 + H_2$ where

$$H_a = \sum_{j \in sublattice\ a} \alpha_{j,a}\mathcal{Q}_{j,a}, \qquad a = 1, 2 \tag{3.24}$$

and

$$\alpha_{j,a} = \alpha + (-1)^{\frac{j-a}{2}} \tag{3.25a}$$

$$\mathcal{Q}_{j,a} = \exp(-\beta_a (X_{j-1} + X_{j+1})) - Z_{j-1} X_j Z j + 1 \tag{3.25b}$$

The ring is divided into even and odd sites. For any value of $\beta_a \geq 0$ it holds that $[H_1, H_2] = 0$. The special case for $\beta_1 = \beta_2 = 0$ is an exactly solvable model whose ground state is exactly the gapped symmetry protected topological cluster state. This model has topological properties originated from the zero energy modes localized at the ends of an open chain when open boundary conditions are considered. The symmetry protecting these edge states is a $\mathbb{Z}_2 \times \mathbb{Z}_2$ symmetry. The ground state is gapped, so even for small values of β_1, β_2 it remains so. The zero energy state at non-vanishing β's is given by

$$|scar\rangle^{1D} = G_1^{1D} G_2^{1D} |+, \ldots, +\rangle \tag{3.26}$$

where the state of all +'s is the ground state at $\beta_a = 0$ and the operators G_a^{1D} are defined in analogy to the previous example

$$G_a^{1D} = \exp\left(\frac{\beta_a}{2} \sum_{j \in sublattice\ a} X_{j-1}\right) \tag{3.27}$$

In order to establish that these are actually scar states, we need to show that the model now is non-integrable. It is possible to do so by mapping the model to the topologically trivial one introduced above [51]. Thus, the $1D$ symmetry protected topological scar state defined in eq. (3.26) is an exceptional state in the spectrum of a non-integrable Hamiltonian $H_1 + H_2$.

Let us pass to $2D$ and consider a modification of the Toric Code (TC) model seen in Sec. 1.1. The Hamiltonian we consider is given by two separate commuting parts $\tilde{H}_{TC} = H_1 + H_2$ where

$$H_1 = \sum_v \alpha_v \left[\exp\left(-\beta_1 \sum_{s \in v \cap \mathcal{P}_1} Z_s\right) - A_v\right] \tag{3.28a}$$

$$H_2 = \sum_p \alpha_p \left[\exp\left(-\beta_2 \sum_{s \in p \cap \mathcal{P}_2} X_s\right) - B_p\right] \tag{3.28b}$$

With v we refer to vertices and with p to plaquettes in the square lattice, while A_v and B_p are defined as in equation (1.1) and (1.2) respectively. For $\beta = 0$ we recover the usual Toric Code model described in section 1.1. At $\beta \neq 0$ the model is a bit more complicated. In order to understand the form of the Hamiltonian we need to split the square lattice into two sub-lattices defined by the vertices and plaquettes respectively, as in Fig. 3.6. Then, the paths $\mathcal{P}_1$ and $\mathcal{P}_2$ are non-crossing paths defined on the two

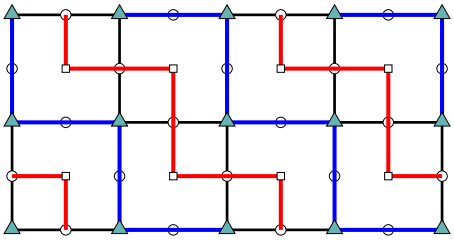

Figure 3.6: *Example of non-intersecting paths covering the square lattice. Periodic boundary conditions are assumed. The red path crosses all plaquettes' centers ($\mathcal{P}_2$ in eq. (3.28b)) while the blue path crosses all the vertices ($\mathcal{P}_1$ in eq. (3.28a)).*

different sub-lattices, such that together they cover all the spins on the links of the lattice. There are many possible such paths, an example is reported in Fig. 3.6.
The above construction guarantees that the two Hamiltonian terms commute with each other. Finally, it is possible to show that the spectrum of H_1 is the same as that of (3.24) for a path $\mathcal{P}_1$ of length L [51]. Thus, the level statistics will also be the same, and the numerical evidences of non-integrability carry over. We can now proceed to look for the exact form of the scar states. To do so we can introduce an orthogonal basis $|\lambda\rangle$ labeled by the $2^{2N_xN_y-2}$-dimensional vector λ taking the eigenvalues of the distinct vertex and plaquette operators. The factor of 2^2 left out is due to the ground state degeneracy of the TC, thus we can complete the basis of the Hilbert space by using the eigenstates $|\omega\rangle$ with additional eigenvalues ω_x and ω_y labeling the the non-local operators distinguishing between the degenerate ground states[†]. The scar states will be four, one for each topological sector, and will all have energy $E = 0$

$$\left|scar^{2D};\omega\right\rangle = G_1^{2D}G_2^{2D}\left|+,\ldots,+;\omega\right\rangle \tag{3.29}$$

where again

$$G_a^{2D} = \exp\left(\frac{\beta_a}{2}\sum_{i\in\mathcal{P}_a} Z_i(X_i)\right) \tag{3.30}$$

Until now we have seen how to construct scar state in 1 and 2 dimensions. It is possible to extend this construction also to three dimensions by following the same steps. In particular, let us see how to do so for the X-Cube model introduced in Sec. 1.2. In fracton phases the ground state degeneracy scales exponentially in linear system size, thus we will have a set of $3D$ scar states with the same exponential degeneracy. Again, we define the Hamiltonian as the sum of two terms $\tilde{H}_{TC} = H_1 + H_2$ where the terms are

[†]These are the operators defined in Sec. 1.1.1

given by

$$H_1 = \sum_v \alpha_v \left[\exp\left(-\beta_1 \sum_{i \in v \cup \mathcal{P}_1} Z_i \right) - A_s \right] \tag{3.31a}$$

$$H_2 = \sum_c \alpha_c \left[\exp\left(-\beta_2 \sum_{i \in c \cup \mathcal{P}_2} X_i \right) - B_c \right] \tag{3.31b}$$

Here, v labels the vertices and c the cubes of the simple cubic lattice. The operators A_v and B_c are the vertex and cubic operators of the X-Cube model as defined in eqs. (1.20). For $\beta_1 = \beta_2 = 0$ the model reduces to the usual X-Cube model up to a constant. The coefficients α are defined as $\alpha_{v(c)} = \alpha + (-1)^{\rho_{v(c)}}$ where, similarly to the TC construction, $\rho_v(c)$ is equal to 0 on one sub-lattice and 1 on the other one. The two sub-lattices are the ones defined by the sites of the cubic lattice (the vertices) and by the cube centers (the dual lattice). Again, the paths $\mathcal{P}_1$ and $\mathcal{P}_2$ are defined on the respective sub-lattices in order to not cross each other and cover all the links of the cubic lattice (on which are defined the spins). These conditions again guarantee that $[H_1, H_2] = 0$ for any $\beta_{1(2)}$. As above, we can construct a basis in order to build the scar states of this model. The Hilbert space has overall dimension 2^{3L^3} for a cubic lattice of linear size L. We can store the eigenvalues of the independent star and cube operators in a vector λ which will have dimension $3L^3 - 6L + 3$, because of the extensive degeneracy of ground states studied in Sec. 1.2.3. Then, we can complete this basis by adding the topological quantum numbers ζ. This means that the number of scar states that are eigenstates of $\tilde{H}_{XC}$ with energy $E = 0$ grows sub-extensively in system size, and are given by

$$\left| scar^{3D}; \zeta \right\rangle = G_1^{3D} G_2^{3D} \left| +, \ldots, +; \zeta \right\rangle \tag{3.32}$$

where

$$G_a^{3D} = \exp\left(\frac{\beta_a}{2} \sum_{i \in \mathcal{P}_a} Z_i(X_i) \right). \tag{3.33}$$

3.3 Glassy behavior of fracton models

In this section we look at the thermal behavior of fracton models in $3D$ [15] and we will see that these models naturally exhibit problems in thermalizing. In fact, the lack of line-like operators inevitably imposes kinetic restrictions on the excitations, resulting in a long thermalization process. Let us use as example the X-Cube model treated in Sec. 1.2. First, recall that fracton phases arise in exactly solvable lattice spin models in three spatial dimensions and exhibit a sub-leading topological ground state degeneracy when considering periodic boundary conditions. The key concept is that there does not exist a local line-like operator that can create a pair of fractons and thus move them around

the system without energy cost, differently from the Toric Code. The operators in the X-Cube model instead create the excitations at the corners of membrane-like operators (see Fig. 1.9). Let us rewrite the Hamiltonian of the X-Cube for convenience as

$$\mathcal{H}_{XC} = -\sum_{c}\prod_{l\in\partial c}\sigma_l^x - \sum_{v,\mu}\prod_{l\in star(v), l\perp\mu}\sigma_l^z \tag{3.34}$$

Let us define the different possible kinds of excitations in this model. First of all there are fractons, excitations created at the corners of membrane like operators (made of σ_z's), where the eigenvalue of cubic operators is flipped from $+1$ to -1. These are immobile particles, since in order to move them two additional charges must be created. Let us denote fractons $e^{(0)}$ because of the 0-dimensional mobility. If instead we consider a bound pair of fractons we obtain a so-called dipole. This is free to move by the repeated application of local membrane-like operators. In fact, a straight Wilson line of σ_z's creates a pair of fractons at each end of the line. With this operator it is possible to move these bound pairs in the 2 directions orthogonal to their orientation, so we will call them $e^{(2)}$. Finally, there are additional dimension-1 excitations created on the vertices at the end of a Wilson line of σ_x's, which we will refer to as $m^{(1)}$. Also, we will refer to the four fracton composites created by the application of a single σ_z, as the topologically neutral sector since these can be created and annihilated simply by the application of Pauli operators. Since this composite is fully mobile without any restriction in motion we will call it $e^{(3)}$. Consequently, $e^{(1)}$ and $e^{(2)}$ will be the topologically charged sector.
Let us consider the X-Cube model in the presence of external transversal Λ and longitudinal λ fields

$$H = -J\sum_{c} B_c - \sum_{v,\mu} A_v^\mu + \Lambda\sum_{l}\sigma_{z,i} + \lambda\sum_{l}\sigma_{x,i} \tag{3.35}$$

Since the operators A_v^μ and B_c are commuting projectors, the coefficient J only sets the energy scale between the e and m excitations (created respectively by B and A operators). Let us take $J = 1$ and the transverse field $\Lambda \ll 1$ in order to stay into the

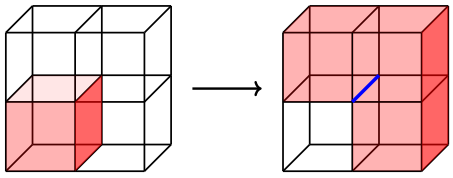

Figure 3.7: *A fracton can be transformed into a configuration of fracton + dipole by the application of a σ_z.*

fracton phase. Also we take $\lambda = 0$. Thus, we will consider the third term of eq. (3.35) as a small perturbation. In this way the m particles are not allowed to hop and we can focus on the dynamics of the other excitations.

Each fracton ($e^{(1)}$) hop is accompanied by the creation of two additional fractons, thus has an energy cost (gap) of $W = 4$. In this way, a fracton can move by the creation of an $e^{(2)}$ (Fig. 3.7) which then can move to infinity without energy cost, thus changing the particle content. To understand the relaxation of the fracton sector we have to consider $e^{(2)}$'s and $e^{(3)}$'s as thermal baths for the fractons since rearrangements within these sectors allow the system to come back on energy shell after each hop.
Let us consider first the system at equilibrium at some temperature T. The energy scale in the topological sector is the energy W associated to the cost of a fracton hop. Each of the three species is gapped, with the gap given by $W/2$, W and $2W$ for creating a single $e^{(1)}$, $e^{(2)}$ and $e^{(3)}$ respectively. Further, $e^{(3)}$ and $e^{(2)}$ are topologically neutral, with fractons carrying a $\mathbb{Z}_2$ charge. This implies that the species cannot be tuned independently, rather the equilibrium temperature uniquely determines their density to[‡]

$$n_f \sim e^{-\frac{W}{2T}} \tag{3.36a}$$

$$n_b \sim e^{-\frac{W}{T}} \tag{3.36b}$$

$$n_c \sim e^{-\frac{2W}{T}} \tag{3.36c}$$

We can see by the form of the perturbation σ_z that the only processes exchanging energy between the different sectors are those with conserved total $\mathbb{Z}_2$ charge on each row and column of the cubic lattice. Each process will be suppressed with increasing number of Λ perturbations, thus only processes with low number of interactions will be relevant. The maximum energy the bath can provide is $\tilde{\Lambda} = \min(\Lambda, T)$ so the bath must be probed $n \sim W/\tilde{\Lambda}$ times for the fractons to borrow enough energy to perform a single hop. Thus, the relaxation rate in the charge sector will be given by

$$\Gamma \sim n_f e^{-n} \sim n_f e^{-W/\tilde{\Lambda}} \tag{3.37}$$

which is exponentially slow in n. We need to take in consideration also the hopping mechanism analyzed in Sec. 2.3.1, where a fracton can move mediated by the presence of a nearby dipole, or $e^{(2)}$ in this case. This process will depend on the density of these excitations, so the rate will be given by

$$\Gamma \sim n_f n_b \sim n_f e^{-W/T} \tag{3.38}$$

The faster process will dominate the relaxation, so it will be the rate (3.38). If we analyze this behavior, we see that it is in contrast with typical gapped phases, where the relaxation displays Arrhenius law $\Gamma_A \sim n \sim e^{-\Delta/T}$ with n the density of charge carriers

[‡]We will refer to $e^{(2)}$'s as bosons (b), in distinction with $e^{(1)}$'s which are fractons (f). $e^{(3)}$'s are still bosons but are of no use now because of their big energy cost, as explained in the text. When needed, we will refer to them as composites (c).

and Δ the energy gap. In our case, in addition to the exponential suppression due to the fracton density, we have an additional slowing term related to the restricted mobility of the excitations.
Let us now consider the non-equilibrium dynamics of our model prepared in the ground state and in contact with a (low) finite temperature bath composed of $e^{(2)}$'s and $e^{(3)}$'s. The initial temperatures of the various sectors are taken such that $T_i^0 \ll \Lambda$ for $i = f, b, c$. Also, let us assume that the temperatures of $e^{(2)}$'s and $e^{(3)}$'s coincide so that we can study the equilibration of fractons with the bath. Fractons are initially prepared at low temperature $T_f^{(0)} \ll T_{b,c}^{(0)}$, since we care about fractons prepared in their ground state. Let us consider only the most relevant processes, i.e. those involving only two-body on-shell interactions between the fracton sector and boson sector. In fact, $e^{(3)}$'s are not relevant because they are at the same temperature of the bosons and cost more energy. The dominant processes will be: (i) boson + boson $\rightleftarrows$ 4 fractons, (ii) boson + boson $\rightleftarrows$ boson + 2 fractons and (iii) boson + fracton $\rightleftarrows$ 3 fractons. The processes are shown in Fig. 3.8. All these channels occur at second order in Λ and their rates are controlled by

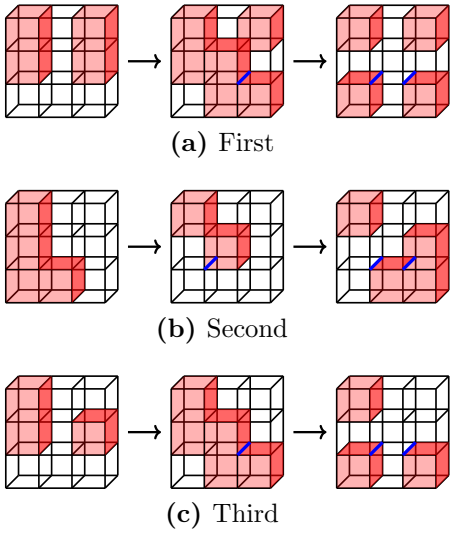

(a) First

(b) Second

(c) Third

Figure 3.8: *Most relevant mechanisms for exchange of energy between fracton and boson sectors. They are all at second order in perturbations* Λ *since two applications of* σ_z *are needed.*

the densities of the excitations involved. We can thus establish a balance between the thermal and charged sectors as[§]

$$\frac{dE_f}{dt} = \Lambda^2(3n_b^2 + n_b n_f - n_b n_f^2 - n_f^3 - 2n_f^4) = -\frac{dE_b}{dt} \tag{3.39}$$

[§]For example, the rate of the first channel is $\Gamma \sim \frac{\Lambda^2}{W} n_b^2$ and since the bath lends an energy of $2W$ for this process, $dE_b/dt \sim -2W\Gamma = -2\Lambda^2 n_b$.

We need now to determine the heat capacities which will be exponentially small due to the gappness of the various species, $C_i \sim n_i,\ i = f, b, c$. In particular, we expect that

$$E_f \sim \frac{W}{2} n_f \quad \longrightarrow \quad C_f \sim \frac{W^2}{4T_f^2} e^{-\frac{W}{2T_f}} \tag{3.40a}$$

$$E_b \sim W n_b \quad \longrightarrow \quad C_b \sim \frac{W^2}{T_b^2} e^{-\frac{W}{T_b}} \tag{3.40b}$$

The balance between fracton and boson sector then leads to the rate equations

$$\frac{dT_b}{dt} = -\frac{\Lambda^2 T_b^2}{W^2} \left(3n_b + n_f - n_f^2 - n_f^3/n_b - 2n_f^4/n_b\right) \tag{3.41a}$$

$$\frac{dT_f}{dt} = \frac{4\Lambda^2 T_f^2}{W^2} \left(3n_b^2/n_f + n_b - n_b n_f - n_f^2 - 2n_f^3\right) \tag{3.41b}$$

These relations can be studied analytically [15]. In particular, in the regime for $T_f \sim 0$, when fractons are initially in the ground space at vanishing energy density, we have that $T_f^{(0)} \ll T_b^{(0)}$. Thus

$$T_f(t) = -\frac{W/2}{\log\left(\frac{6\Lambda^2}{W} t + k\right) - \frac{2W}{T_b^{(0)}}} \tag{3.42}$$

with $k = \exp\left(\frac{2W}{T_b^{(0)}} - \frac{W}{2T_f^{(0)}}\right)$, and

$$T_b(t) = \frac{W}{\log\left(\frac{3\Lambda^2}{W} t + e^{W/T_b^{(0)}}\right)} \tag{3.43}$$

These results imply that the fractons heat logarithmically slow and the bath inversely cools logarithmically. An important characteristic is that this behavior persists until fractons are close to equilibration, which takes an exponentially long time

$$0 \leq t \lesssim t* = \frac{W}{6\Lambda^2} \exp\left(\frac{W}{T_b^{(0)}}\right) \tag{3.44}$$

This is because up to this time scale the dominant processes are (i) and (ii), while at higher temperatures the process (iii) gets activated and leads to a faster equilibration. We have found that placing a type-I fracton model prepared in its ground state in contact with a finite-temperature heat bath leads to an exponential in time long equilibration process, typical of quantum glasses [16]. Glasses are characterized by a $\log(t)$ approach to equilibrium, and is exactly what happens to our kinetically constrained three-dimensional, translation invariant model. At long times, the system eventually equilibrates and $T_f = T_b$. This shows that fracton models naturally exhibit a different kind of equilibration dynamics, being unusually robust to thermalization.

Chapter 4

Ergodicity breaking in 1D fracton models

Weather or not the kinetic restrictions inherent of fracton models lead to the breaking of ergodicity is a question which naturally comes to mind. In fact, fracton models where first introduced as stabilizer codes without string logical operators with the purpose of looking for systems stable against perturbations which could serve as recipients for quantum memories. Due to the high dimensionality of the systems where fractons naturally appear, they are numerically difficult to simulate. Another possibility is that of externally induce fractonic behavior in lower-dimensional systems. This is done by considering spin chains with local Hamiltonians featuring both charge and higher moment conservation laws. In this way it is possible to numerically time evolve these systems in order to study the dynamical behavior of single charges (fractons) and dipoles, to see whether the predictions of glassy behavior/non-ergodicity are respected.
This chapter is mostly centered around the numerical simulations implemented on these particular spin systems and the study of their thermal behavior. The simulations rely mostly on exact-diagonalization. In particular, it has been used the "QuSpin" library [49], which is an open source Python package particularly useful for exact-diagonalization and dynamical evolution of many-body systems. This technique has the advantage of being exact also for system with high entanglement, where for example the matrix product state representation of wave-functions fails.
As seen in the previous chapter (Sec. 3.2.2), breaking of ergodicity is usually accompanied by the separation of the Hilbert space into many sub-sectors not associated to any symmetry. This phenomenon is usually dubbed *fragmentation* of the Hilbert space. Let us now see how this happens in a system with fractonic behavior. The restriction in mobility of fracton phases can be traced to the super-selection structure of the underlying theories, like for the X-Cube model of Sec. 1.2. What we observe in this chapter is that in $1D$ spin systems, conservation of charge and dipole moment is enough for the system to undergo an extensive fragmentation of the Hilbert space. In some circumstances that

we will see below, in turn this can lead to breakdown of thermalization [17]. It is found that the thermal behavior strongly depends on the range of the local terms in the model. The chapter is organized as follows. First, in section 4.1 we introduce the two models under study and their symmetries: we consider two dipole conserving Hamiltonians with different range of interactions. Then, in section 4.2 we study the Hilbert space of these models in order to see whether or not fragmentation appears and in which amount. Following, in section 4.3 time evolution is performed to evaluate the long-time expectation values of some characteristic quantities in order to see whether the systems thermalize or not. Further, the Hamiltonians are exactly diagonalized in section 4.4 in order to study the eigenstates of the models and compare them with the predictions of the eigenstate thermalization hypothesis. In section 4.5 we study a possible connection with the PXP model and we identify the equivalent of the Néel state for our dipole-conserving model. In Sec. 4.6 we conclude the discussion with some simulations of the transition between of the two models.

4.1 Dipole-conserving Hamiltonians

Let us introduce the models under study. First, remind that for exact-diagonalization to work for significant system sizes we have to restrict our-self to one-dimensional spin chains. In order for our model to exhibit "fractonic" behavior, we want it to locally conserve both charge and dipole moment, thus it is convenient to consider spin-1 chains where the local Hilbert space has dimension 3: each spin can be either in the state $+$, 0 or $-$.
The operators implementing charge and dipole conservation can be written as

$$Q = \sum_i S_i^z \tag{4.1a}$$

$$P_{i_0} = \sum_i (i - i_0) S_i^z \tag{4.1b}$$

Here i_0 is a reference point which we take to be $i_0 = 0$ for the $2m + 1$-long chain going from $i = -m$ to $i = m$. The eigenvalues (q, p) of these operators will define separated sub-sectors of the Hilbert space. A (q, p) symmetry sector is a subspace of the Hilbert space characterized by states having charge q and dipole moment p. Since the models we consider conserve the total charge and dipole moment, these sectors will be completely decoupled from each other. Sometimes we will undergo simulations within a particular symmetry sector in order to reduce the basis dimension. The distribution of sub-sectors' dimensions is reported in Fig. 4.1. As it is possible to note, the largest sector is the one with quantum numbers $(q, p) = (0, 0)$. Now we can consider the possible Hamiltonians

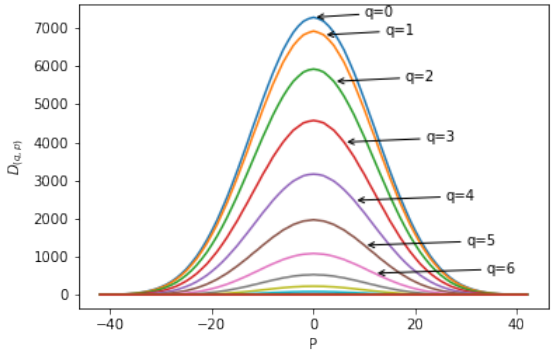

Figure 4.1: *Distribution of sub-sectors' dimensions for the three-term Hamiltonian (4.2) at $L = 13$. The continuous lines are artificial since each sub-sector has a finite dimension. However the distribution fits along the plotted lines.*

which respect these constraints and which will be the focus of our following study

$$H_3 = \sum_i S_i^+ (S_{i+1}^-)^2 S_{i+2}^+ + h.c. \tag{4.2}$$

$$H_{34} = H_3 + \sum_i S_i^+ S_{i+1}^- S_{i+2}^- S_{i+3}^+ + h.c. \tag{4.3}$$

where $S^{+,-}$ are the usual spin raising/lowering operators.
The first is a Hamiltonian where the local terms have maximum range of three sites, thus we will refer to it as *three-term* model. Instead, the second contains (4.2) and has also terms with range of four sites, thus we will call it *four-term* model. As we will see, this difference in the range of the Hamiltonian leads to great differences in the thermal behavior of the models.
Let us look at the symmetries of these two systems. First of all we can readily see that both models display a "parity" symmetry under exchange of the spins ($+ \leftrightarrow -$). Further, the three-term model possesses some additional symmetries. The first one we see is a sub-lattice parity symmetry

$$\mathbb{P}^z_{odd} = exp\left(i\pi \sum_{n\ odd} S^z_n\right) \tag{4.4}$$

This symmetry is readily seen to be fixed by the dipole moment since* $exp\,(i\pi \sum_{n\ odd} S^z_n) = exp\,(i\pi \sum_n n S^z_n) = exp\,(i\pi P)$. This sub-lattice symmetry is emblematic since we can see that the total parity can be obtained through $\mathbb{P}^z = \mathbb{P}^z_{odd}\mathbb{P}^z_{even}$ and will be related to the

*We use here a property of spin-1 systems, namely that a 2π rotation equals to the identity.

total charge through $\mathbb{P}^z = exp\,(i\pi Q)$.
Another important quantity is the operator

$$\mathcal{C} = \prod_n e^{i\pi\left(S^z_{4n}+S^z_{4n+1}\right)} \tag{4.5}$$

This is readily shown to commute with the charge and dipole operators as defined in Eqs. (4.1). Also, it anti-commutes with H_3, thus making its spectrum symmetric around zero in every (q, p) sector.
Instead in the four-term model, the range four terms in the Hamiltonian commute with (4.5) so the spectrum will not be symmetric.

4.2 Fragmentation of the Hilbert space

Let us consider first the three-term Hamiltonian. A chain evolving under this Hamiltonian will have some "frozen" states which are annihilated by all the terms in (4.2) and so which do not evolve at all under Hamiltonian dynamics. These can be explicitly constructed and are reported in Tab. 4.1.
As a first check we can count how many these frozen states are, since this will give us a lower bound on the number of sectors the Hilbert space is fragmented in. Actually, this is an easy calculation since we can reduce it to the problem of diagonalizing a matrix. This can be seen by considering that for each frozen state in a chain of length n it is

Sites	Operators	Frozen states
3-terms	$S^-(S^+)^2S^-$ $S^+(S^-)^2S^+$	000, 00+, 00−, +00, +0+, +0−, −00, −0+, −0−, +++, ++0, ++−, 0++, −++, − − −, −−+, −−0, +−−, 0−−

Table 4.1: *List of frozen states for the three-term Hamiltonian of Eq.* (4.2).

enough to look at the last two sites of the chain to know which frozen states of length $n+1$ we can construct. Let us see this with an example: a chain of length 3 has 19 frozen states, the ones reported in Tab. 4.1. If we consider for example the state 000, it is easy to see that we can attach a spin with arbitrary value to its the end and obtain a length-4 chain which will still be a frozen state (000+, 0000 and 000−). In turn, starting from the state +0+ we can only go to one frozen state: $+0++$. We can define a set of rules to go from one frozen state to another with a length higher by one, as reported in Tab. 4.2. We can now observe that this construction can be equivalently written as a

Last 2 sites	Possible added site
+ +	+,0,−
+ −	+,0,−
+ 0	−
0 +	+
0 0	+,0,−
0 −	−
− +	+
− 0	+,0,−
− −	+,0,−

Table 4.2: *Rules for going from a length n frozen state to another of length $n+1$.*

recursive operation [52]

$$\begin{bmatrix} ++ \\ +0 \\ +- \\ 0+ \\ 00 \\ 0- \\ -+ \\ -0 \\ -- \end{bmatrix}_{L+1} = \begin{bmatrix} 1 & 0 & 0 & 1 & 0 & 0 & 1 & 0 & 0 \\ 1 & 0 & 0 & 0 & 0 & 0 & 0 & 0 & 0 \\ 1 & 0 & 0 & 0 & 0 & 0 & 0 & 0 & 0 \\ 0 & 1 & 0 & 0 & 1 & 0 & 0 & 1 & 0 \\ 0 & 1 & 0 & 0 & 1 & 0 & 0 & 1 & 0 \\ 0 & 1 & 0 & 0 & 1 & 0 & 0 & 1 & 0 \\ 0 & 0 & 0 & 0 & 0 & 0 & 0 & 0 & 1 \\ 0 & 0 & 0 & 0 & 0 & 0 & 0 & 0 & 1 \\ 0 & 0 & 1 & 0 & 0 & 1 & 0 & 0 & 1 \end{bmatrix} \begin{bmatrix} ++ \\ +0 \\ +- \\ 0+ \\ 00 \\ 0- \\ -+ \\ -0 \\ -- \end{bmatrix}_{L} \tag{4.6}$$

where the signs in the two column vectors refer to the last two sites of the chain. Finally, we can evaluate the scaling of these frozen states by diagonalizing this matrix and keeping only the largest eigenvalue which in our case is $\lambda \sim 2.2$. This means that the number of frozen states will scale as 2.2^L in growing system size, which is exponentially large[†]. Frozen states are just the lowest dimensional sub-sectors (dimension 1) of the Hilbert space, bigger ones can be obtained with a bit more work. Intuitively, there will be states

Figure 4.2: *Higher dimensional subspaces can be found by considering an active region bounded by two walls of inert states separating the active region from the frozen one.*

restricted to a sub-sector of the Hilbert space because of the constrained dynamics. As

[†]Keep in mind that the full Hilbert space for a spin-1 chain scales as 3^L.

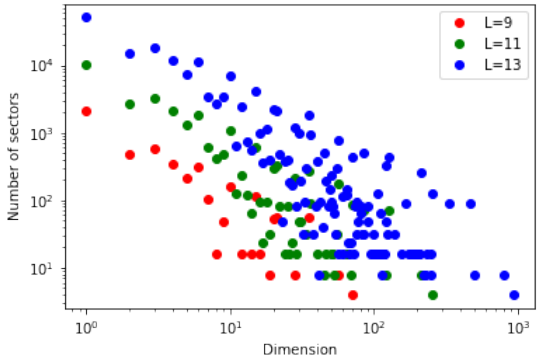

Figure 4.3: *Representation of the fragmentation of the Hilbert space for the three-term Hamiltonian (4.2). Note the great number of low dimensional subspaces, which increases when going up in system size.*

an example, one could think of domain walls of same charge sites, like $++\cdots+$ or $--\cdots-$, surrounding an active region like in Fig. 4.2. The embedded active region will be completely isolated from the rest of chain and so will be constrained to a higher dimensional sub-sector of the Hilbert space. In order to calculate the exact number of separated sectors and their dimension, was used a C++ code exploring all possible states of the Hilbert space and separating them in groups of states which can be obtained by applications of the operators in the Hamiltonian. Since the Hilbert space dimension grows as 3^L the calculation becomes rapidly inaccessible, so we will restrict to small system sizes. We can see from Fig. 4.3 the distribution of sub-sectors with their relative dimension. We can observe that for the three-term model the fragmentation is very extended, with many sectors of small dimension. Fragmentation also happens when

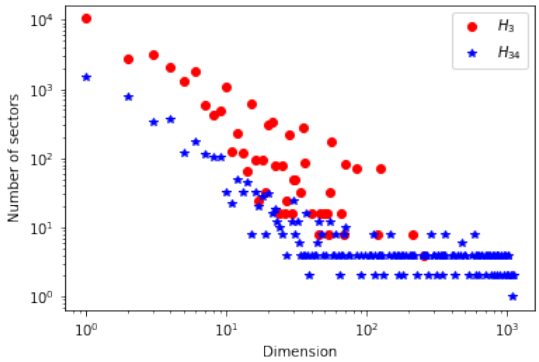

Figure 4.4: *Number of sectors over sectors' dimensions for three (red dots) and four (blue stars) -term Hamiltonians at $L = 11$.*

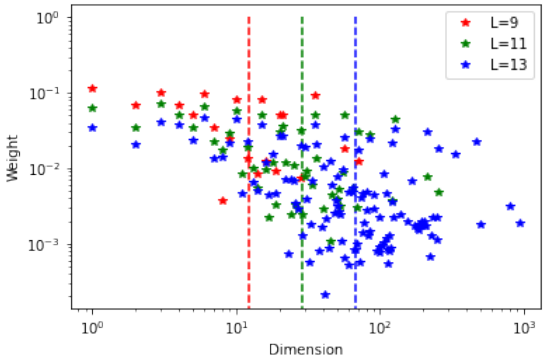

Figure 4.5: *Weights* (4.7) *for three-term Hamiltonian at different system sizes. The vertical line represents the mean of the distribution, and it is possible to see that it is located closer to the lower dimensional sub-spaces.*

considering the four-term Hamiltonian (blue stars in Fig. 4.4) but in a fundamentally different way. The Hilbert space gets still fragmented in an exponentially large number of subspaces, but much less than in the previous case. In fact, if we confront the subspaces in the two models we consider, we see that for H_{34} there are many more sub-sectors of high dimensions.
In order to distinguish better the two cases it is useful to define a weight for each sub-sector's dimension D

$$W_D = \sum_{D_i=D} \frac{\mathrm{tr}(Z_i^2)}{\mathrm{tr}\left[(S_0^z)^2\right]} \tag{4.7}$$

Here $Z_n \equiv \mathcal{P}_n S_0^z \mathcal{P}_n = \mathcal{P}_n S_0^z$ is the projection of S_0^z in the sub-sector $\mathcal{H}_n$. This weight essentially assigns a value to each dimension depending on how many sub-sectors fall in that category. For a highly fragmented space the weights' mean will point towards lower dimensions, while for the weakly fragmented case it will be larger. Its value for the three-term Hamiltonian at different system sizes is reported in Fig. 4.5 while the comparison with the H_{34} case is reported in Fig. 4.6. The high number of sub-sectors seen in the three-term model is referred to as *strong* fragmentation. In the case of the four-term Hamiltonian there are still an exponentially large number of sectors but still much less than for H_3 and so is called *weak* fragmentation. As we will see below analyzing the dynamical behavior and the properties of the spectrum of these models, this difference plays a central role in their thermal behavior. In fact, strong fragmentation will lead to a strong violation of the ETH, with all eigenstates being non thermal, while in the weak case the system will violate ETH only in a weaker form, with a vanishing fraction of eigenstates failing in thermalizing.
Let us end the section by noticing that additional terms in the Hamiltonian that are diagonal in the z basis do not alter the fragmentation of the Hilbert space but only lift

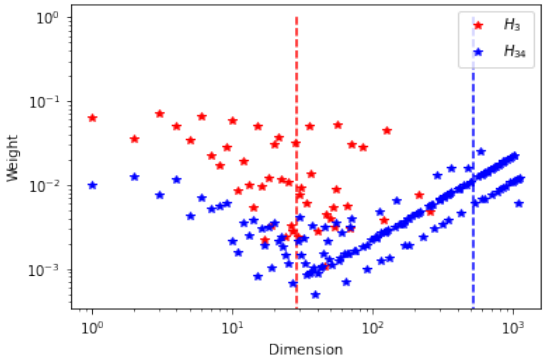

Figure 4.6: *Weights (4.7) for three and four -term Hamiltonians at $L = 11$. The mean of the three-term Hamiltonian is clearly displaced towards lower dimensions, while for the four-term model the mean is towards the higher dimensions.*

the energy of the eigenstates. However, in the presence of such terms the spectrum of H_3 would no-longer be symmetric around 0 since they do not anti-commute with (4.5).

4.3 Time evolution

There are many observables which can be used to determine whether the system thermalizes at long times or not. In this section we analyze the dynamical properties of the systems under study. We adopt open boundary conditions throughout all the simulations.
A particularly useful observable is the so-called auto-correlator [17]

$$C_0(t) = \langle S_0^z(t) S_0^z(0) \rangle \tag{4.8}$$

where the subscript 0 indicates we are considering operators acting on the central cite of the chain and S^z represent the usual spin operator

$$S^z = \begin{pmatrix} 1 & 0 & 0 \\ 0 & 0 & 0 \\ 0 & 0 & -1 \end{pmatrix} \tag{4.9}$$

We evaluate this quantity at infinite temperature, meaning that the expectation value of an observable $\hat{O}$ is evaluated using an identity Boltzmann factor $\rho = e^{-\beta H}$. So,[‡]

$$\langle \hat{O} \rangle = \mathrm{Tr}\, \rho \hat{O} = \mathrm{Tr} \exp(-\beta H) \hat{O} \simeq \mathrm{Tr}\, \hat{O} \tag{4.10}$$

[‡]This actually means that all the states in the Hilbert space have the same importance.

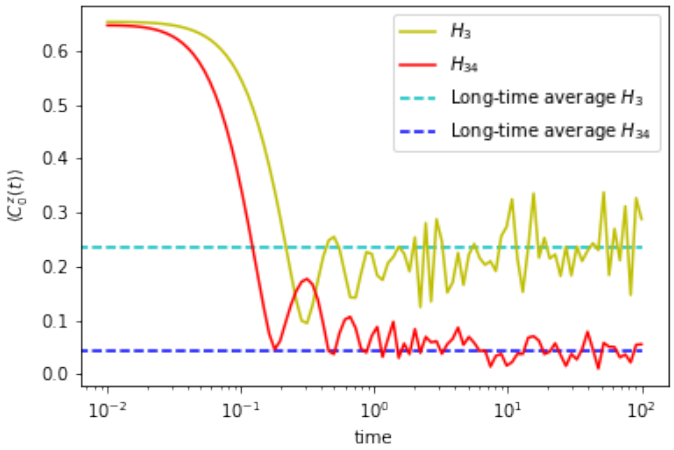

Figure 4.7: *Auto-correlator (4.8) for $L = 13$ in the sector $(q, p) = (0, 0)$. We observe a long time saturation value different from the expected thermal one for the three-term Hamiltonian.*

The initial state is taken randomly from the Hilbert space. We can do this because of "quantum typicality" [53]. This means that for a macroscopic and isolated quantum system in an unknown pure state the expectation value of any observable is close to the ensemble average. The initial state thus has the form

$$|\psi\rangle = \mathcal{N} \sum_{l=1}^{L} c_l |l\rangle \tag{4.11}$$

with $\{|l\rangle\}$ an orthonormal basis, the coefficients $c_l \in \mathbb{C}$ taken randomly and $\mathcal{N}$ a normalization factor. The basis is taken to be the one along the z axis, with states made of $+$, 0 and $-$.
The initial value of the auto-correlator will be $C_0(0) = 2/3$[§] and for a thermalizing systems we expect at long times to see the system distribute homogeneously over the whole chain and thus that the auto-correlator saturates to $2/(3L)$ for a length L chain. What we observe for the three-term Hamiltonian is instead pretty different, with the long time value of the auto-correlator saturating to a constant value, as shown in Fig. 4.7. Instead, for the four-term Hamiltonian the expectation value decreases like for a thermalizing system, but with a saturation value still different from 0. This offset can be observed to be a finite size effect. In fact, from Fig. 4.9 the long-time expectation values of the auto-correlator are plotted as a function of the system size and we can see how for the three-term model it tends to a constant while for the four-term model it decreases to small values close to 0 in the thermodynamic limit.

[§]This can be seen by noticing that for the site $l = 0$ in the $|+\rangle$ or $|-\rangle$ state it takes the value $+1$ while if it is in the state $|0\rangle$ it takes value 0. Thus, for a random state the expectation value will be $2/3$.

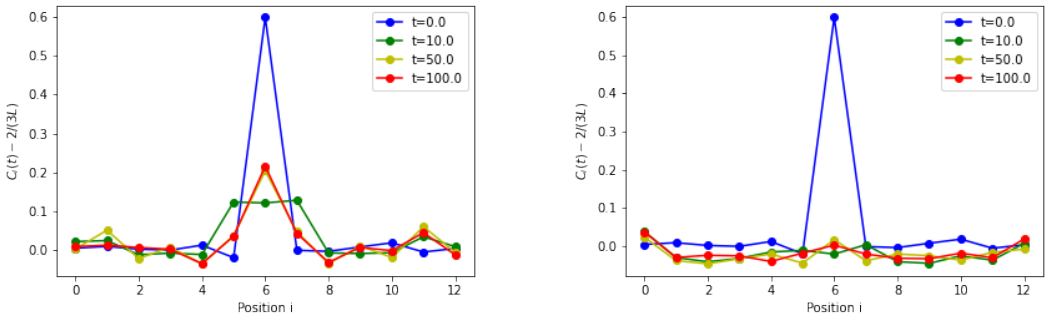

Figure 4.8: *Spatially-resolved auto-correlator* (4.12) *for an* $L = 13$ *chain in the sector* $(q, p) = (0, 0)$. *Panel (a): in the case of the three-term Hamiltonian it shows a long-time localized behavior. Panel (b) for the* H_{34} *model it saturates to a thermal value.*

Another observable which is useful to show this behavior is the spatially-resolved auto-correlator, plotted in Fig. 4.8

$$C_i(t) = \langle S_i^z(t) S_0^z(0) \rangle \tag{4.12}$$

This observable shows how for the three-term model the state remains localized at long times while for the four-term Hamiltonian it distributes over the chain with no memory of the initial state.
The long-time saturation value of the auto-correlator can be explained through the previously studied (Sec. 4.2) fragmentation of the Hilbert space. Let us consider $\mathcal{P}_n$ the projectors into the connected Hilbert subspaces $\mathcal{H}_n$ of dimensions $\mathcal{D}_n$. The projectors form an orthogonal set of conserved quantities $\mathcal{P}_n \mathcal{P}_m = \delta_{nm} \mathcal{P}_n$. We can use Mazur's inequality [54] to get a lower bound on the value of the auto-correlator. Mazur's inequality states that in the presence of a set of constants of motion (in our case the projectors), the long-time average correlation of an operator is lower bounded by the projection of the operator on the single charges[¶]. Thus, we can write

$$\lim_{T\to\infty} \frac{1}{T} \int_0^T dt \langle S_0^z(t) S_0^z(0) \rangle \geq \sum_n \frac{[\mathrm{tr}(Z_n)]^2}{3^L \mathcal{D}_n} \equiv C_0^z(\infty) \tag{4.13}$$

with Z_n defined as in (4.7). This lower bound is calculated through the fragmentation of the Hilbert space and is in great agreement with the long-time value of the auto-correlator evaluated dynamically evolving the state. As can be seen from Fig. 4.9, $C_0^z(\infty)$ acts as a lower bound for the auto-correlator, indicating that the main cause of the non-ergodicity is indeed the fragmentation of the Hilbert space.

[¶]An operator thus is ergodic if it is orthogonal to all the conserved charges.

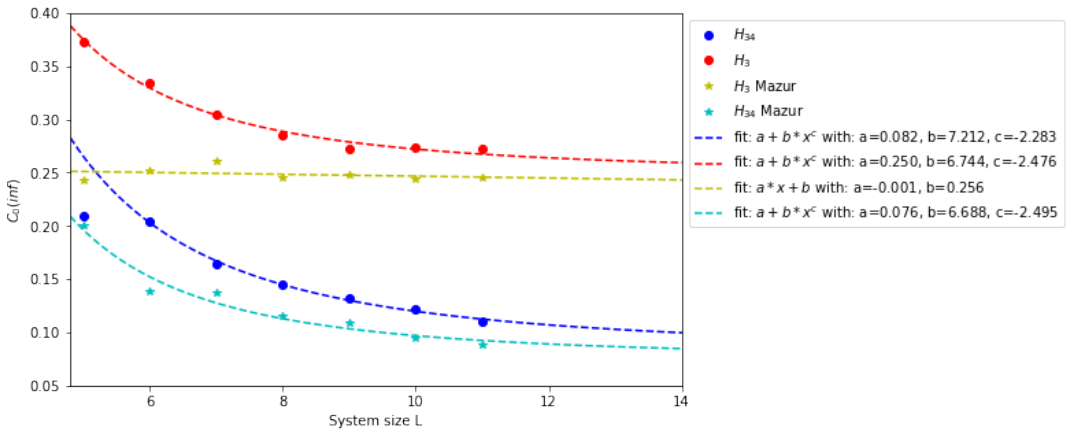

Figure 4.9: *Scaling in system size of long-time averages of the auto-correlator. The fits are power laws with parameters reported in the legend. We can see how the values obtained from the Mazur's inequality are a lower bound for the systems under consideration.*

4.4 Other observables

Let us pass now to the study of the spectrum and of the eigenfunctions of the systems by considering different observables.

Expectation value of $(S_0^z)^2$
An observable which is useful in the characterization of the thermal properties of a system is the expectation value of an operator on all the eigenstates. From ETH these expectation values should be close to the canonical ones, with a distribution becoming narrower increasing the system size. In particular, here we consider the operator $(S_0^z)^2$, evaluated on all energy eigenstates and plotted in Fig. 4.10 as a function of energy. We see that for the three-term model (Fig. 4.10a) the distribution of expectation values is extremely wide and does not broaden increasing the system size, thus implying a strong violation of ETH. Instead, in the four-term model, plotted in Fig. 4.10b, we recover the expected thermal behavior, seen also by the fact that the computed expectation values are interpolated by the canonical ones. The canonical prediction is calculated from the Gibbs' states defined by the density matrix

$$\rho_{can} \propto \exp(-\beta H) \tag{4.14}$$

with $\beta \in (-\infty, \infty)$ [47].
From Fig. 4.10b we also see that there is a small number of states with expectation values lying far from the canonical prediction. This agrees with the situation of a system exhibiting a weak violation of ETH, with a small number of non-thermal eigenstates.

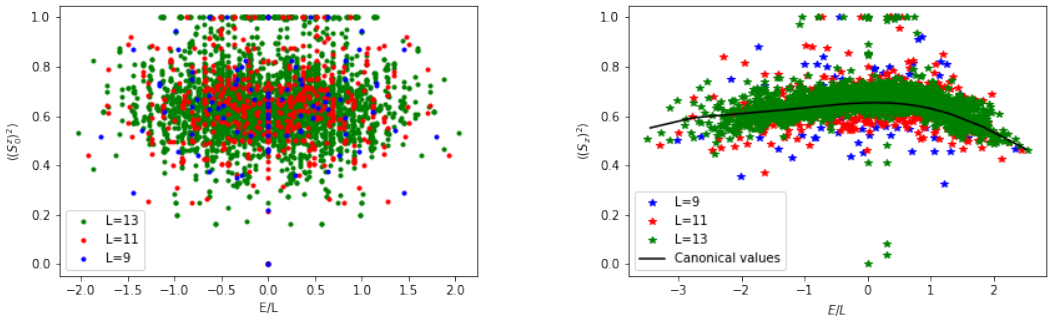

(a) **(b)**

Figure 4.10: *Expectation value of the operator* $(S_0^z)^2$ *evaluated over all eigenstates in the* $(q,p) = (0,0)$ *sector for different system's size. In (a) we consider the three-term model and we note a wide distribution of expectation values which remains wide increasing the length of the chain. In (b) instead we consider the four-term model and the situation is quite different. First we note that, as expected, the spectrum is not symmetric around* 0*. Second, we see that the points are distributed around the canonical expectation values (black line) with a width of the distribution that decreases increasing the system's size.*

Inverse Participation Ratio

Another quantity often used in the study of the thermal properties of a system is the so-called Inverse Participation Ratio (IPR). This gives information on the localization properties of the states [55]. In order to define it let us recall that we can expand each (energy) eigenstate in a set of basis states $|l\rangle$ as

$$|\epsilon_i\rangle = \sum_l c_{l,i} \, |l\rangle \tag{4.15}$$

where as basis states we use the same as in eq. (4.11). Then, we can define the probability of finding an eigenstate of energy ϵ_i in a particular basis element $|l\rangle$ through $p_l(\epsilon_k) = |c_{l,k}|^2$. Finally, the IPR is defined as

$$IPR(\epsilon_k) = \sum_l p_l(\epsilon_k)^2 \tag{4.16}$$

The IPR will be large (close to 1) for localized states and small ($\sim 1/\mathcal{N}$ where $\mathcal{N}$ is the Hilbert space dimension) for states equally distributed on all sites. The results for our model Hamiltonians are reported in Fig. 4.11 for the $(q,p) = (0,0)$ sector. As we can see, for the three-term model the values of the IPR are not all close to 0, indicating a strong fragmentation of the Hilbert space with a large number of states which are not thermal. Instead, for H_{34} almost all IPR values are concentrated close to 0, with a small number of states whose IPR lies above this value. Notice that such states tend to have an energy close to zero.

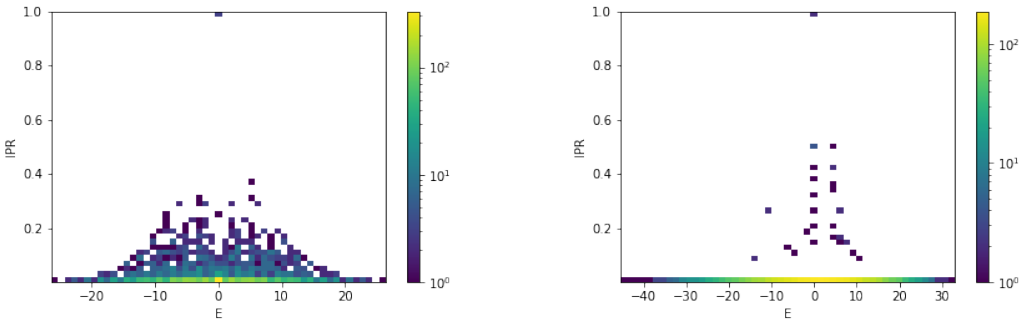

(a) **(b)**

Figure 4.11: *IPR value for eigenstates in* $(q, p) = (0, 0)$ *sector for* $L = 13$*. The color-bars indicate the number of states in the bin. In (a) we see that it distributes over many values while in (b) it concentrates around* 0 *with a small number of outlying states. These latter states show peculiar thermalizing behavior, and are the same found in Fig. 4.10.*

Entanglement entropy

An additional observable is the entanglement entropy (EE). For a system in the state $|\psi\rangle$, we can define the density matrix $\rho = |\psi\rangle \langle\psi|$. Then, by considering a sub-system A and its complementary B we can define the reduced density matrix $\rho_A = \mathrm{Tr}_B\, \rho$ by tracing out the degrees of freedom of B. Finally, the entanglement entropy of the sub-system A is defined as

$$S_A = -\,\mathrm{Tr}\, \rho_A \ln(\rho_A) \tag{4.17}$$

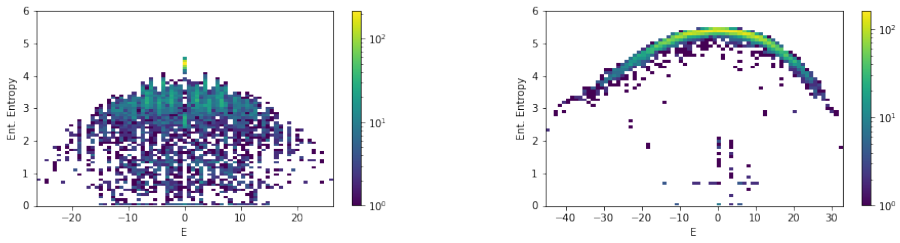

(a) **(b)**

Figure 4.12: *Half-chain entanglement entropy of* H_3 *(a) and* H_{34} *(b) eigenstates in the* $(0, 0)$*-sector as a function of energy for* $L = 13$*. For the three-term model we observe low and spread values of entanglement entropy while for the four-term model these values follow the ETH predictions except for a few states at low entanglement.*

We evaluate the entanglement entropy taking as subsystem A half of the chain for all the

energy eigenstates of the two models. This is plotted in Fig. 4.12. To obtain the plots of EE, both here and in the plots below, we forced QuSpin to use an orthonormal basis of eigenvectors without imposing parity symmetry, so that the obtained set of eigenvectors contains both a state $|e\rangle$ and its symmetric $|e'\rangle$ obtained by changing all $+$'s in $-$ and vice-versa[‖]. The half-chain entanglement entropy for a thermalizing system is expected

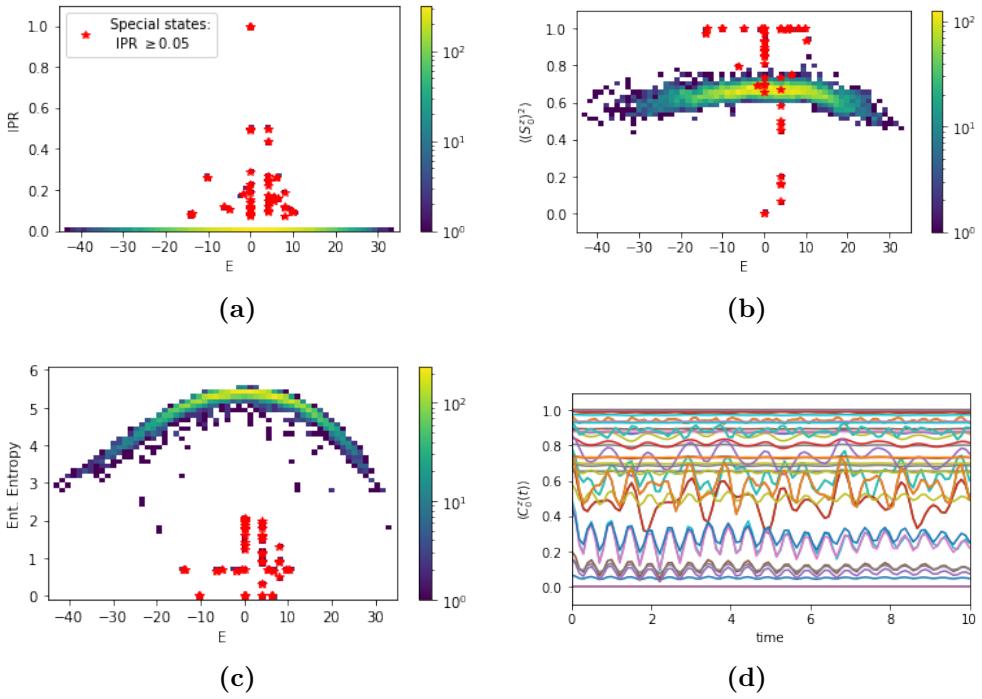

Figure 4.13: *Panel (a): IPR values for all eigenstates of an $L = 13$ chain in the $(0, 0)$-sector where the more localized $IPR > 0.05$ states are highlighted by a red star. Panel (b): Expectation values of the operator $\langle (S^z_0)^2 \rangle$ with the same states highlighted by a red star. Panel (c): Half-chain entanglement entropy with special states marked by a red star. In the various observables the the states exhibiting the non-thermal behavior are always the same. Panel (d): Auto-correlator evaluated on these special states. These states are either frozen and thus constant or oscillate without reaching a thermal value at long times.*

to have "high" values for all eigenstates [45], as for the PXP model in Fig. 3.3. What we observe for the three-term model are instead "low" values of EE, in great disagreement with ETH. Differently, in the four-term case we observe a situation quite analogue to the PXP model, with a small number of states exhibiting low entanglement.
By studying the states with IPR different from 0 it is possible to show that these are

[‖]If we impose the symmetry restricted basis, the two degenerate eigenstates are taken as a linear superposition of the symmetric partners. This alters the actual final value of EE, but we verified that the shape of the distribution is nevertheless the same.

the same found having a different behavior both in the expectation values of S_z^2 and also in the half-chain entanglement entropy. Here were consider the states having an IPR$\geq$ 0.05, so only the most localized states clearly visible in Fig. 4.11b**. Then, we evaluate the entanglement entropy and the expectation value of $(S_0^z)^2$ on these same states, highlighting the results in panels (a), (b) and (c) of Fig. 4.13. Finally, we compute the expectation value of the auto-correlator on these special states and we show in Fig. 4.13d that these states do not relax to thermal values of the auto-correlator even at long times.

Level statistic

Finally, as we did for the PXP model in Sec. 3.2.1 we can study the statistical properties of the spectrum of the models under consideration. Since we are not able to simulate systems with a high number of sites, our data might be strongly affected by finite size effects and therefore we might only give qualitative results. What we observe in this case is reported in Fig. 4.14. We consider here both the energy level spacing distribution as

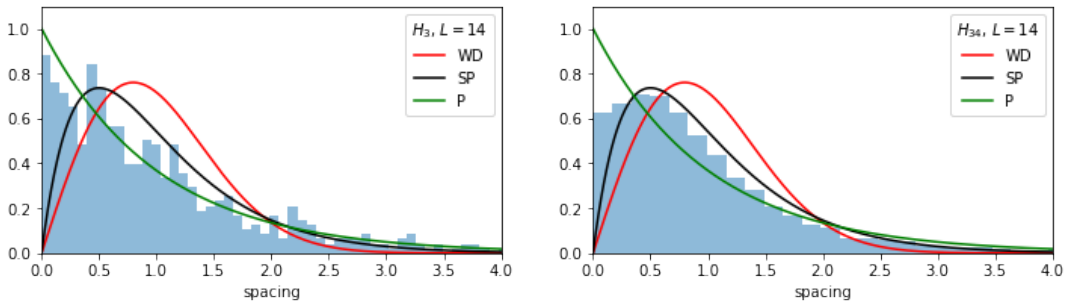

(a)

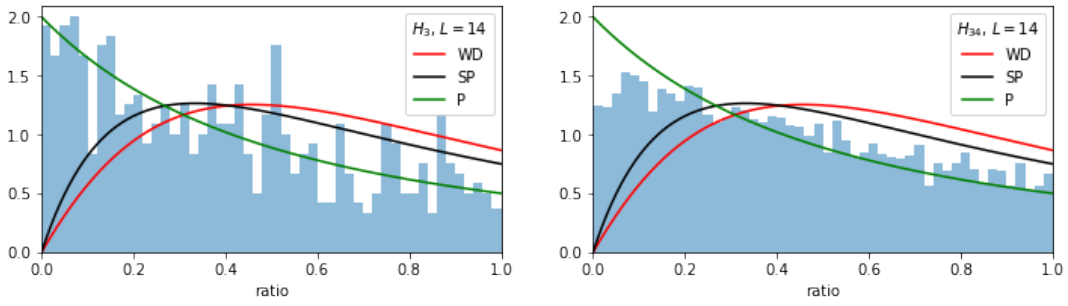

(b)

Figure 4.14: *Panel (a): energy level spacings for three (left) and four (right) -term models. Panel (b): ratio of consecutive spacings statistic for for three (left) and four (right) -term models. In all graphs are shown the values expected from WD, SP and P distributions.*

**These are about 35 states for an $L = 13$ chain.

defined in (3.5) and the consecutive spacings' ratio (3.9). We can observe that for the three-term model the level statistics is close to the Poisson distribution. However, the high degeneracy encountered in this model makes it difficult to evaluate the statistical behavior of its levels as can be seen from the highly nonuniform behavior of the levels. Instead, for the four-term model the distribution of spacings and ratios follows a behavior which seems to be intermediate between the Poisson and Semi-Poisson behaviors. This can be seen better by looking at Fig. 4.15. Here the ratios mean is evaluated for values of the normalized spectrum (3.15) $\epsilon \in [0.3, 0.7]$ with 20 steps in order to not consider local fluctuations. For the four-term model we observe a behavior intermediate between the P and the SP distributions. Instead, for the three-term model the mean value of spacings indicates a Poisson statistics.

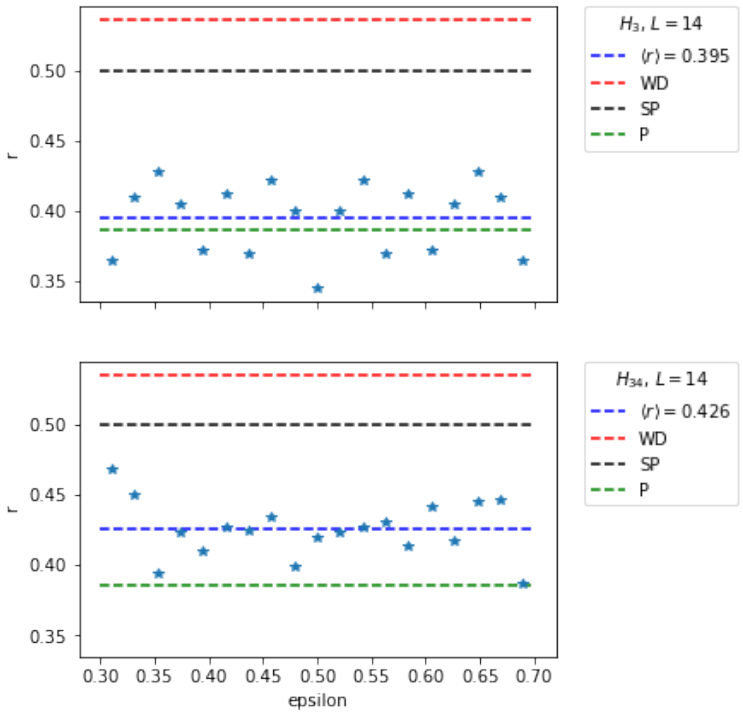

Figure 4.15: *Ratios of consecutive level spacings for three (upper panel) and four (lower panel) -term models. The ratios are plotted in function of the normalized spectrum ϵ in the range $\epsilon \in [0.3, 0.7]$ with 20 steps. We can see that for the four-term model the ratios fall in the mid region between the Poisson and Semi-Poisson distribution. Instead, for the three-term model it seems that the level statistics follows a Poisson behavior.*

4.5 Relation with PXP model

There is an interesting connection between the PXP model encountered in the context of many-body scars and the dipole-conserving three-term Hamiltonian H_3. Let us recall that the PXP model describes a chain of spin-1/2s with the characteristic that an excited state can exist only if its neighbors are in the ground state, and is described by the Hamiltonian

$$H_{PXP} = \sum_n \mathcal{P}_{n-1}\sigma_n^x\mathcal{P}_{n+1} \tag{4.18}$$

with $\mathcal{P}_n = (1-\sigma_n^z)/2$ the projectors imposing the Rydberg blockade. In finding an analog in the context of dipole-conserving Hamiltonians, let us focus on the form of the Néel states $|\mathbb{Z}_2\rangle$ and $|\mathbb{Z}_2'\rangle$ which we know exhibit the strange behavior of QMBS.
Now, we will show that some sub-sectors of the Hilbert space of the H_3 model are governed by the PXP Hamiltonian. These will constitute the analogue of the Néel state in the fracton language. There is no known analytical way of finding these states, just a good guessing which can be verified a posteriori. Our guess is the state

$$|\mathbb{F}_2\rangle = |\cdots - + - - - + - - - + - - - + - \ldots\rangle \tag{4.19}$$

with a $+$ state every 4 sites and all $-$ background. This chain can be divided into blocks of $-+-$ separated by a single $-$. Let us consider a multiple of 4 length chain in order to have an integer number of blocks. In this kind of state the dipole moment will be given by $P(n_+) = L/2(1 - L/2 + n_+)$ with n_+ the location of the first $+$ in the chain (from the left). Because of the periodicity, there will be 4 different dipole moments with this pattern. Let us now recall the form of the local terms of H_3 (4.2): the only non-trivial action of such operators on our chain will be on the blocks $-+-$, since consecutive $--$ are always annihilated. By applying the operator $S^+S^{-^2}S^+$ on two consecutive blocks, the result will be

$$|\mathbb{F}_2\rangle \to \left|\tilde{\mathbb{F}}_2\right\rangle = |\cdots - + - -0 - 0 - 0 - 0 - - + - \ldots\rangle \tag{4.20}$$

This transforms the state in a form such that it is no more trivial to apply an operator on the central site (applying $S^-S^{+^2}S^-$ on the same sites just takes us back to the original state). In particular by applying $S^-S^{+^2}S^-$ on the three central spins results in the state

$$\left|\tilde{\mathbb{F}}_2\right\rangle \to \left|\hat{\mathbb{F}}_2\right\rangle = |\cdots - + - -0 - - + - - 0 - - + - \ldots\rangle \tag{4.21}$$

That behavior is reminiscent of the PXP model. What we have found is that the action of a local operator of H_3 is non-trivial when centered on even sites depending on the states on odd near sites. We can thus restrict the Hamiltonian to a subspace made of the possible configurations of (4.19)

$$H_3|_{PXP} = 4\sum_{k=1}^{L/2} |- +_{2k} -\rangle\langle 0 -_{2k} 0| + h.c. \tag{4.22}$$

This Hamiltonian effectively implements a Rydberg blockade since a configuration with neighboring + states is prohibited by the dynamics. Also, we can identify a map translating from spin-1 configurations centered on even sites to spin-1/2 states centered on even sites in the PXP model through

$$\begin{aligned} &|0-0\rangle \leftrightarrow |\downarrow\downarrow\downarrow\rangle \qquad |-+-\rangle \leftrightarrow |\downarrow\uparrow\downarrow\rangle \qquad |0--\rangle \leftrightarrow |\downarrow\downarrow\uparrow\rangle \\ &|--0\rangle \leftrightarrow |\uparrow\downarrow\downarrow\rangle \qquad |---\rangle \leftrightarrow |\uparrow\downarrow\uparrow\rangle \end{aligned} \tag{4.23}$$

With this map in mind we can rewrite (4.22) in a more PXP-explicit way

$$\begin{aligned} H_3|_{PXP} &= 4\sum_{k=1}^{L/2} |\downarrow\uparrow\downarrow\rangle\langle\downarrow\downarrow\downarrow| + h.c. = \\ &= 4\sum_{k=1}^{L/2} |\downarrow\rangle\langle\downarrow|_{2(k-1)} \otimes |\uparrow\rangle\langle\downarrow|_{2k} \otimes |\downarrow\rangle\langle\downarrow|_{2(k+1)} + h.c. = 4H_{PXP} \end{aligned} \tag{4.24}$$

Thus the restriction of H_3 to this family of connected subspaces is equivalent to a PXP model on a chain of length $L/2$ up to a factor of 4. By applying a parity transformation on $|\mathbb{F}_2\rangle$ we obtain an analogue state with $+ \leftrightarrow -$, thus there are eight[††] different symmetry sectors governed by the PXP Hamiltonian. This is another hint that the special states found in our dipole-conserving Hamiltonian could be scar states.

4.6 Final remarks

The comparison between the three and four -term models suggests that the dipole moment conservation in the latter is no-longer enough to strongly violate ergodicity even though the model still exhibits many non-thermal eigenstates, disconnected from the bulk of the spectrum and co-existing with thermal eigenstates at the same temperatures. The strong fragmentation of the three-term model has been observed to impose a strong violation of ETH and thus leads to non-ergodicity. On the other hand with the weak fragmentation of the four-term model we saw that there still exist non-thermal eigenstates but these are no more sufficient to avoid thermalization for typical initial states. In conclusion, the range of the local terms seems to be of fundamental relevance in the thermal behavior of dipole conserving Hamiltonians. A longer range furnishes more connections through the various states of the Hilbert space, causing a smaller fragmentation. A precise definition of the fragmentation strength needed to obtain a non-ergodic behavior is still missing.
Another thing which can be analyzed is the kind of transition which happens passing

[††] There are 4 different $|\mathbb{F}_2\rangle$ states, which with the parity transformation become eight.

from the three-term model to the four-term one slowly introducing the higher range local terms. This can be done by considering an Hamiltonian

$$H_{trans}(\lambda_4) = H_3 + \lambda_4 H_4 \tag{4.25}$$

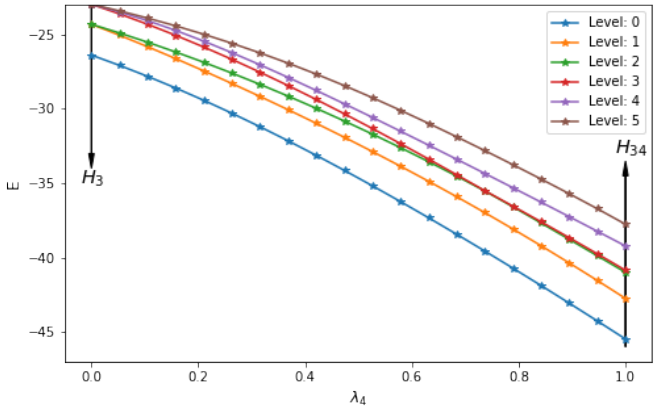

Figure 4.16: *First* 6 *energy levels of* H_{trans} *at different values of* λ_4*. Here was considered an* $L = 13$ *chain in the* $(0, 0)$*-symmetry sector. For* $\lambda_4 = 0$ *we recover the three-term model while for* $\lambda_4 = 1$ *we obtain the four-term Hamiltonian. We can observe that the gap with the ground state remains open and also that the degeneracy of the three-term spectrum is lifted turning on the longer-range term.*

where H_3 and H_4 contain only the range three and four terms respectively. Evaluating the lowest energy levels for H_{trans} at different values of λ_4 we obtain the plots in Fig. 4.16. One thing that can be observed is that the ground state remains separated from the first excited one. From this we can conclude that the two models belong to the same universality class. Also, we can see how the effect of the range-four terms is that of spreading the degenerate energy levels of the three-term model.
We also evaluated the various observables seen till now for intermediate values of λ_4. In particular, in Fig. 4.17a are plotted the IPR values for all eigenstates, in Fig. 4.17b the time evolution of the auto-correlator and in Fig. 4.17c the values of the entanglement entropy for all eigenstates. The general behavior we can observe is that by turning on the interaction, the various observables rapidly tend to reach thermal values. This is particularly clear in the entanglement entropy plots.

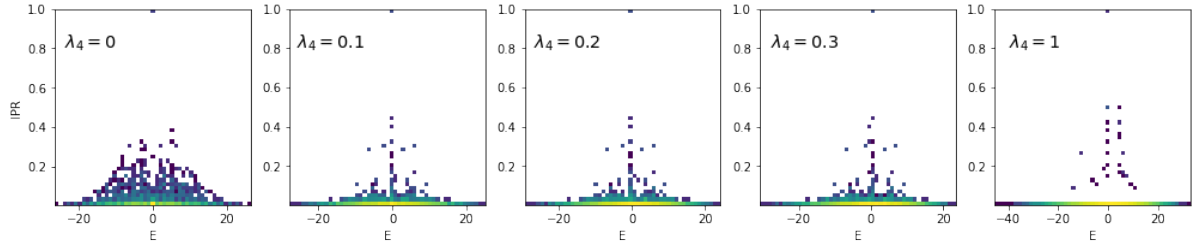

(a)

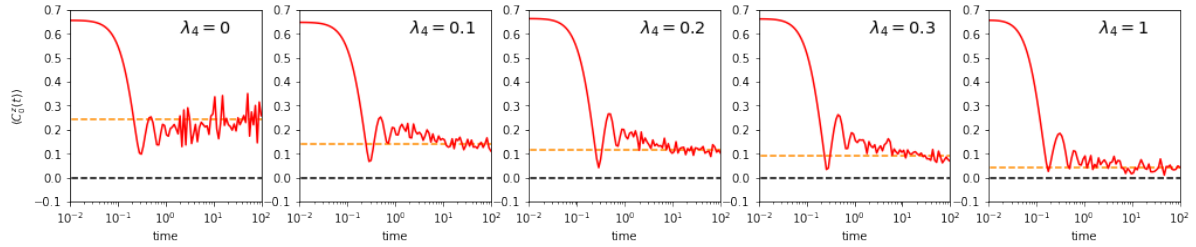

(b)

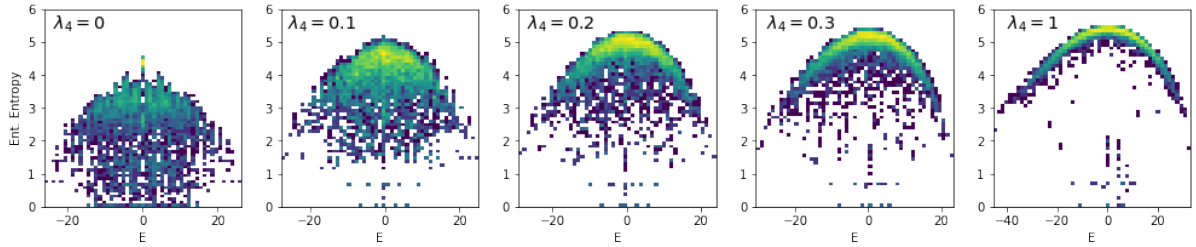

(c)

Figure 4.17: *Various observables evaluated at different values of λ_4. In (a) the variation in the IPR values of the eigenstates passing from H_3 (leftmost panel) to H_{34} (rightmost panel) is showed. In (b) the time evolution of the auto-correlator $C_0^z(t)$ on random initial states is considered. Finally, in (c) the entanglement entropies of the eigenstates for the various steps are plotted.*

Chapter 5

Conclusions

In this thesis we introduced the vast field of fracton phases of matter. Fractons are emergent quasi-particle excitations featuring a restriction in their motion. We found and described these particles in exactly solvable quantum spin models and we showed that fractonic order constitutes a new kind of ordering with substantial differences with respect to usual topological order. We also described fracton phases from a more field-theoretic point of view, that of gauge theory. It has been shown how such phases can be obtained by considering rank-2 symmetric tensor gauge theories. The theory with scalar charges was studied in deep showing that the constrictions in motion arise as a consequence of a generalized Gauss' law which imposes the conservation of higher order momenta. Then, we showed that such theory constitutes a stable phase of matter in $3D$ and that it features a set of generalized Maxwell's equations as usual electromagnetism. A review of some possible phases appearing considering finite densities of excitations was then given, focusing on examples of particular interest from the theoretical point of view: Fermi liquids in $3D$ and the quantum Hall effect in $2D$.
The characteristic constraints in the motion of charges in fracton models has then led the subject of this thesis towards the analysis of the thermalizing capabilities of such phases. Many numerical simulations were performed to study the dynamical behavior of $1D$ spin-1 chains featuring fractonic characteristics. In particular, local Hamiltonian models respecting the conservation of charge and dipole moment (in analogy with scalar charge theory of Sec. 2.2) were considered in order to impose "by hand" the kinetic constraints. We found that these two conservation laws indeed restrict considerably the dynamics. For dipole conserving Hamiltonians with a range of three sites was seen a clear non-ergodic behavior. This is observed both from the non-thermal distribution of the expectation values of physical observables in the energy eigenstates and also from the finite long-time average value of the auto-correlator function. This thermal behavior is explained in terms of the found strong fragmentation of the Hilbert space in an exponentially large number of separated sectors. Instead, for dipole conserving Hamiltonians with a larger range of the interactions a behavior more similar to systems weakly breaking ergodicity

is observed, in a way analogue to the PXP model. In this case a thermal behavior for almost all eigenstates in the system was observed, except for a small fraction of "special" states. These are found to have strongly non-thermal characteristics, thus being very similar to the scar states of the PXP model. Also in this case a fragmentation of the Hilbert space is observed, but this time it seems to be not sufficient to prevent the system from thermalizing from random initial states. Finally, the transition between the two models was also analyzed and has been observed that there is no gap closure, thus ruling out the possibility of a phase transition.
The open directions for future works are multiple. From a more theoretic point of view it could be interesting to analyze the relation between the dipole-conserving systems analyzed in this thesis and the type-I fracton models. Also, the role of the fragmentation of the Hilbert space concerning the thermal properties of the system has to be clarified. In particular, what kind of conserved operators can be defined to label the different sectors is still unknown. Considering the scar states, there is still much to be unraveled concerning their role in the thermalizing behavior of the systems they are part of. Finally, a connection with many-body localized (MBL) systems is to be expected but is still missing.
From the point of view of experimental applications we mention that recent point of views on Bloch [55] and Stark [56] many-body localization could lead the way to a possible verification of these dipole conserving systems. For what concerns the analysis performed in this thesis, new calculations could be performed extending the system to a $2D$ layer in order to verify if the thermal properties change increasing the spatial dimension, where new routes to thermalization are possible.
Concluding, the field of fractons is rapidly growing in interest in the physics community because of the various fields of applicability and the promising results obtained till now. Of particular interest is the application of such phases of matter to the construction of reliable quantum memories. There are still many open questions regarding fracton phases and their description is just at the beginning, exciting developments are surely to be expected.

Appendix A

Cluster state as SPT phase

Cluster states [57–60] are a particular class of interacting spin states which are especially useful as sources of entanglement in the so-called Measurement Based Quantum Computation [61]. In particular, a cluster state on the lattice is defined as the common eigenstate of the stabilizers

$$S_i = X_i \prod_{j \in \mathcal{N}(i)} Z_j \tag{A.1}$$

where $\mathcal{N}(i)$ represents the nearest neighbors to the spin on the i-th site. A cluster state is the non-degenerate ground state of the Hamiltonian $\mathcal{H}_C = -\sum_i S_i$. A cluster state can be constructed via the application to the starting state $|+\rangle^{\otimes N}$ of controlled-phase gates. In one dimension the resulting cluster state can be written as

$$|\phi_N\rangle \propto \left(|0\rangle_1 Z^{(2)} + |1\rangle_1\right)\left(|0\rangle_2 Z^{(3)} + |1\rangle_2\right)\ldots\left(|0\rangle_N + |1\rangle_N\right) \tag{A.2}$$

In a more compact form we can write it as

$$|\phi_N\rangle = \frac{1}{2^{N/2}} \bigotimes_{a=1}^{N} \left(|0\rangle_a Z^{(a+1)} + |1\rangle_a\right) \tag{A.3}$$

with the convention that $Z^{N+1} = \mathbb{1}$.
Cluster states are different from other entangled states in that they are maximally entangled. For $N > 3$ they are different from N-qubit GHZ states. It is harder to destroy entanglement in cluster states than in GHZ ones by local operations [58]. In order to classify different entangled states we can introduce the notion of *maximum connectedness* and *persistency*. The former refers to the fact that any two qubits of the state can be projected into a pure Bell state by local measurement on a subset of the other qubits. The latter refers to the minimum number of local measurements to be performed such that the final state is completely disentangled. In particular, cluster states are maximally

connected and their persistency is $P(|\phi_N\rangle) = \lfloor N/2 \rfloor$*.
It is possible to generalize the construction of cluster states to higher dimensions. A cluster in a d-dimensional lattice is defined as a set of spins on a lattice which are all connected to each other via other spins of the cluster. In this set of qubits the cluster state can be written as

$$|\Phi\rangle_C = \bigotimes_{c\in C} \left(|0\rangle_c \left[\otimes_{\gamma\in\Gamma} Z^{(c+\gamma)}\right] + |1\rangle_c\right) \tag{A.4}$$

where Γ is the set of links connecting to nearest-neighboring sites. For a square lattice in $2D$ it is $\Gamma = \{(1,0),(0,1)\}$. The state (A.3) is recovered for $\Gamma = \{1\}$.
Let us now pass to the classification of this model in terms of symmetries. In fact, symmetries are the usual way to look at phases in matter. Different phases exhibit different symmetries and in the standard paradigm when there is a phase transition a symmetry is broken. However, this is not always the case, in fact it has been found that different phases with the same unbroken symmetries can exist. These new phases are known as symmetry protected topological (SPT) phases of matter [62–64]. Such phases are characterized by symmetry protected boundary gapless modes under open boundary conditions whose existence is guaranteed as long as the symmetry is unbroken.
Symmetry protected topological phases (SPTs) are fundamentally different from usual topological phases (Ts). SPTs are protected only from symmetry-preserving perturbations, while Ts endure any perturbation since are protected by the topology of the manifold. Further, Ts exhibit long range entanglement while SPTs only short range entanglement. Finally, Ts are allowed to have fractional excitations, differently from SPTs. Examples of Ts are fractional quantum hall states, quantum spin liquids, toric code and Kitaev's honeycomb model. Examples of SPTs instead are the Haldane chain, topological insulators (quantum spin Hall effect) and topological superconductors.
Cluster states fit naturally into this context, in fact a $1D$ cluster chain is a $\mathbb{Z}_2 \times \mathbb{Z}_2$ SPT phase. To see this let us consider a chain divided into two sub-lattices A and B with a spin for each site. The $1D$ cluster Hamiltonian is given by

$$H_{1d} = -\sum_{i\in A} \tau^z_{i-1}\sigma^x_i\tau^z_{i+1} - \sum_{i\in B} \sigma^z_{i-1}\tau^x_i\sigma^z_{i+1} \tag{A.5}$$

This model posses a $\mathbb{Z}_2 \times \mathbb{Z}_2$ global symmetry obtained by flipping all spins on one sub-lattice, and is generated by the operators $\prod_{i\in A}\sigma^x_i$ and $\prod_{i\in B}\tau^x_i$. The ground state is $\mathbb{Z}_2 \times \mathbb{Z}_2$ symmetric and, in the $\{\sigma^z_i, \tau^x_i\}$ basis, it is an equal weight superposition of of all possible σ^z_i with domain walls $\sigma^z_{i-1}\sigma^z_{i+1} = -1$ decorated by a $\tau^x_i = -1$, otherwise $\tau^x_i = 1$.
Let us first note that this system is in a topological phase, since introducing a boundary would result in a twofold degeneracy which cannot be broken conserving the symmetry. Here we also see a general property of SPTs, namely that the global symmetries realize

*$\lfloor x \rfloor$ denotes the integer part of a positive number x. It is also called *floor* function

projective representations of the symmetry group at the boundary [62]. In particular, consider an open chain of length L terminating with two σ spins as in Fig. (A.1). Let

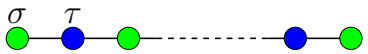

Figure A.1: *Lattice spin chain divided into two sub-lattices. The sub-lattice A (B) contains the σ (τ) spins, denoted in green (blue).*

us exclude from the Hamiltonian any term that is not fully contained in the system, to ensure no symmetry is broken. In this case these terms will be the two exceeding elements of the Hamiltonian (A.5): $\tau^z_{-1}\sigma^x_0\tau^z_1$ and $\tau^z_{L-1}\sigma^x_L\tau^z_{L+1}$. Thus, the remaining terms will be $L-2$, leaving a 2^2-fold degeneracy. We may now define two sets of Pauli matrices located at the left and right edges

$$\pi^z_l = \sigma^z_1, \quad \pi^{x,y}_l = \sigma^{x,y}_1\tau^z_2 \tag{A.6a}$$

$$\pi^z_r = \sigma^z_L, \quad \pi^{x,y}_r = \tau^z_{L-1}\sigma^{x,y}_L \tag{A.6b}$$

These obey the Pauli algebra and satisfy the relation

$$\prod_{i\in A}\sigma^x_i = \pi^x_l\pi^x_r \tag{A.7a}$$

$$\prod_{i\in B}\tau^x_i = \pi^z_l\pi^z_r \tag{A.7b}$$

on the ground state manifold. Thus, the action of symmetries can be factored into operations acting on the left and right edges separately. When the global symmetry factors in this way, the symmetry at the boundary can act projectively, so with phases that are not present in the action of the global symmetry. For example consider to change the action at the left boundary by a phase α (and at the right one by -α): this factor tells nothing about the underlying physics. Instead, eqs. (A.7) exhibit a different kind of phase, since the two operators at the edges anticommute. This anticommutation indicates that the symmetry group is realized projectively at each edge.

Bibliography

[1]L. Savary and L. Balents, "Quantum spin liquids: a review", Reports on Progress in Physics **80**, 016502 (2016).

[2]A. Kitaev, "Fault-tolerant quantum computation by anyons", Annals of Physics **303**, 2–30 (2003).

[3]E. Fradkin, *Field theories of condensed matter physics*, 2nd ed. (Cambridge University Press, 2013).

[4]M. Pretko, X. Chen, and Y. You, "Fracton phases of matter", International Journal of Modern Physics A **35**, 2030003 (2020).

[5]R. M. Nandkishore and M. Hermele, "Fractons", Annual Review of Condensed Matter Physics **10**, 295–313 (2019).

[6]C. Chamon, "Quantum glassiness in strongly correlated clean systems: an example of topological overprotection", Physical Review Letters **94** (2005).

[7]J. Haah, "Local stabilizer codes in three dimensions without string logical operators", Physical Review A **83** (2011).

[8]S. Vijay, J. Haah, and L. Fu, "Fracton topological order, generalized lattice gauge theory, and duality", Physical Review B **94** (2016).

[9]D. J. Williamson, "Fractal symmetries: ungauging the cubic code", Physical Review B **94** (2016).

[10]M. Pretko, "Subdimensional particle structure of higher rank u(1) spin liquids", Physical Review B **95** (2017).

[11]P. Orland, "Instantons and disorder in antisymmetric tensor gauge fields", Nuclear Physics B **205**, Volume B205 [FS5] No. 2 to follow in approximately one month, 107–118 (1982).

[12]A. Prem, M. Pretko, and R. M. Nandkishore, "Emergent phases of fractonic matter", Physical Review B **97** (2018).

[13]M. Pretko, "Emergent gravity of fractons: mach's principle revisited", Physical Review D **96** (2017).

[14]M. Pretko and L. Radzihovsky, "Fracton-elasticity duality", Physical Review Letters **120** (2018).

[15]A. Prem, J. Haah, and R. Nandkishore, "Glassy quantum dynamics in translation invariant fracton models", Physical Review B **95** (2017).

[16]A. Amir, Y. Oreg, and Y. Imry, "Electron glass dynamics", Annual Review of Condensed Matter Physics **2**, 235–262 (2011).

[17]P. Sala, T. Rakovszky, R. Verresen, M. Knap, and F. Pollmann, "Ergodicity breaking arising from hilbert space fragmentation in dipole-conserving hamiltonians", Physical Review X **10** (2020).

[18]H. Bernien, S. Schwartz, A. Keesling, H. Levine, A. Omran, H. Pichler, S. Choi, A. S. Zibrov, M. Endres, M. Greiner, and et al., "Probing many-body dynamics on a 51-atom quantum simulator", Nature **551**, 579–584 (2017).

[19]D. Bulmash and M. Barkeshli, "Higgs mechanism in higher-rank symmetric u(1) gauge theories", Physical Review B **97** (2018).

[20]H. Ma, M. Hermele, and X. Chen, "Fracton topological order from the higgs and partial-confinement mechanisms of rank-two gauge theory", Physical Review B **98** (2018).

[21]B. Zeng, X. Chen, D.-L. Zhou, and X.-G. Wen, *Quantum information meets quantum matter – from quantum entanglement to topological phase in many-body systems*, 2018.

[22]A. G. Fowler, M. Mariantoni, J. M. Martinis, and A. N. Cleland, "Surface codes: towards practical large-scale quantum computation", Physical Review A **86** (2012).

[23]H. Ma, E. Lake, X. Chen, and M. Hermele, "Fracton topological order via coupled layers", Physical Review B **95** (2017).

[24]Z.-C. Gu and X.-G. Wen, "Emergence of helicity ±2 modes (gravitons) from qubit models", Nuclear Physics B **863**, 90–129 (2012).

[25]S. Sachdev, *Quantum phase transitions* (Cambridge University Press, 2011).

[26]A. M. Polyakov, "Compact gauge fields and the infrared catastrophe", Physics Letters B, Vol. 59, Issue 1 (1975).

[27]C. X. A. Rasmussen Y.-Z. You, "Stable gapless bose liquid phases without any symmetry", eprint arXiv:1601.08235 (2016).

[28]C. Xu, "Gapless bosonic excitation without symmetry breaking: an algebraic spin liquid with soft gravitons", Physical Review B **74** (2006).

[29]M. Pretko, "The fracton gauge principle", Physical Review B **98** (2018).

[30]M. Pretko, "Generalized electromagnetism of subdimensional particles: a spin liquid story", Physical Review B **96** (2017).

[31]Z.-C. Gu and X.-G. Wen, "A lattice bosonic model as a quantum theory of gravity", arXiv preprint gr-qc/0606100 (2006).

[32]B. Spivak and S. Kivelson, "Transport in two dimensional electronic micro-emulsions", Journal de Physique IV (Proceedings) **131**, 255–256 (2005).

[33]E. Wigner, "On the interaction of electrons in metals", Phys. Rev. **46**, 1002–1011 (1934).

[34]M. Pretko, "Finite-temperature screening of u(1) fractons", Physical Review B **96** (2017).

[35]P. M. Chaikin and T. C. Lubensky, *Principles of condensed matter physics* (Cambridge University Press, 1995).

[36]M. Pretko, "Higher-spin witten effect and two-dimensional fracton phases", Physical Review B **96** (2017).

[37]D. A. Abanin, E. Altman, I. Bloch, and M. Serbyn, "Colloquium: many-body localization, thermalization, and entanglement", Reviews of Modern Physics **91** (2019).

[38]J. M. Deutsch, "Eigenstate thermalization hypothesis", Reports on Progress in Physics **81**, 082001 (2018).

[39]L. D'Alessio, Y. Kafri, A. Polkovnikov, and M. Rigol, "From quantum chaos and eigenstate thermalization to statistical mechanics and thermodynamics", Advances in Physics **65**, 239–362 (2016).

[40]S. Goldstein, J. L. Lebowitz, R. Tumulka, and N. Zanghí, "Long-time behavior of macroscopic quantum systems", The European Physical Journal H **35**, 173–200 (2010).

[41]Y. Y. Atas, E. Bogomolny, O. Giraud, and G. Roux, "Distribution of the ratio of consecutive level spacings in random matrix ensembles", Physical Review Letters **110** (2013).

[42]M. V. Berry and M. Tabor, "Level clustering in the regular spectrum", (1977).

[43]A. M. García-García and J. Wang, "Semi-poisson statistics in quantum chaos", Physical Review E **73** (2006).

[44]Y. Y. Atas, E. Bogomolny, O. Giraud, P. Vivo, and E. Vivo, "Joint probability densities of level spacing ratios in random matrices", Journal of Physics A: Mathematical and Theoretical **46**, 355204 (2013).

[45]M. Serbyn, D. A. Abanin, and Z. Papić, "Quantum Many-Body Scars and Weak Breaking of Ergodicity", (2020).

[46]E. J. Heller, "Bound-state eigenfunctions of classically chaotic hamiltonian systems: scars of periodic orbits", Phys. Rev. Lett. **53**, 1515–1518 (1984).

[47]C. J. Turner, A. A. Michailidis, D. A. Abanin, M. Serbyn, and Z. Papić, "Quantum scarred eigenstates in a rydberg atom chain: entanglement, breakdown of thermalization, and stability to perturbations", Physical Review B **98** (2018).

[48]C. J. Turner, A. A. Michailidis, D. A. Abanin, M. Serbyn, and Z. Papić, "Weak ergodicity breaking from quantum many-body scars", Nature Physics **14**, 745–749 (2018).

[49]P. Weinberg and M. Bukov, "Quspin: a python package for dynamics and exact diagonalisation of quantum many body systems. part ii: bosons, fermions and higher spins", SciPost Phys. **7**, 20 (2019).

[50]P. Naldesi, E. Ercolessi, and T. Roscilde, *Detecting a many-body mobility edge with quantum quenches*, 2016.

[51]S. Ok, K. Choo, C. Mudry, C. Castelnovo, C. Chamon, and T. Neupert, "Topological many-body scar states in dimensions one, two, and three", Physical Review Research **1** (2019).

[52]V. Khemani, M. Hermele, and R. Nandkishore, "Localization from hilbert space shattering: from theory to physical realizations", Physical Review B **101** (2020).

[53]P. Reimann, "Typicality for generalized microcanonical ensembles", Phys. Rev. Lett. **99**, 160404 (2007).

[54]J.-S. Caux and J. Mossel, "Remarks on the notion of quantum integrability", Journal of Statistical Mechanics: Theory and Experiment **2011**, P02023 (2011).

[55]E. van Nieuwenburg, Y. Baum, and G. Refael, "From bloch oscillations to many-body localization in clean interacting systems", Proceedings of the National Academy of Sciences **116**, 9269–9274 (2019).

[56]M. Schulz, C. A. Hooley, R. Moessner, and F. Pollmann, "Stark many-body localization", Physical Review Letters **122** (2019).

[57]D. J. Williamson and T. Devakul, "Type-ii fractons from coupled spin chains and layers", Physical Review B **103** (2021).

[58]H. J. Briegel and R. Raussendorf, "Persistent entanglement in arrays of interacting particles", Physical Review Letters **86**, 910–913 (2001).

[59]B. J. Brown, W. Son, C. V. Kraus, R. Fazio, and V. Vedral, "Generating topological order from a two-dimensional cluster state using a duality mapping", New Journal of Physics **13**, 065010 (2011).

[60]W. Son, L. Amico, R. Fazio, A. Hamma, S. Pascazio, and V. Vedral, "Quantum phase transition between cluster and antiferromagnetic states", EPL (Europhysics Letters) **95**, 50001 (2011).

[61]R. Raussendorf and H. J. Briegel, "A one-way quantum computer", Phys. Rev. Lett. **86**, 5188–5191 (2001).

[62]Y. You, T. Devakul, F. J. Burnell, and S. L. Sondhi, "Subsystem symmetry protected topological order", Physical Review B **98** (2018).

[63]Y. You, T. Devakul, F. Burnell, and S. Sondhi, "Symmetric fracton matter: twisted and enriched", Annals of Physics **416**, 168140 (2020).

[64]T. Devakul, Y. You, F. J. Burnell, and S. Sondhi, "Fractal symmetric phases of matter", SciPost Physics **6** (2019).